WOOD AND FIBER SCIENCE

The Sustainable Natural Materials Journal

Volume 56, Number 1_2024 *(ISSN 0735-6161)*

Open Access

JOURNAL OF THE

SWST – International Society of Wood Science and Technology

WOOD AND FIBER SCIENCE

WOOD AND FIBER SCIENCE is published quarterly in January, April, July, and October by the Society of Wood Science and Technology, P.O. Box 6155, Monona, WI 53716-6155

There are three classes of membership (electronic only) in the Society: Members – dues $150; Retired Members – dues $75; Student Members – dues $25. We also have membership category for individuals from Emerging Countries where individual members pay $30, individual students pay $10; Emerging Group of 10 pay $290, and Student Groups of 10 pay $90. Institutions and individuals who are not members pay $300 per volume (electronic only). Applications for membership and information about the Society may be obtained from the Executive Director, Society of Wood Science and Technology, P.O. Box 6155, Monona, WI 53716-6155 or found at the website http://www.swst.org.

Site licenses are also available with a charge of:
- $300/yr for single online membership, access by password and email
- $500/yr for institutional subscribers with 2–10 IP addresses
- $750/yr for institutional subscribers with 11–50 IP addresses
- $1000/yr for institutional subscribers with 51–100 IP addresses
- $1500/yr for institution subscribers with 101–200 IP addresses
- $2000/yr for institutions subscribers with over 200 IP addresses.

New subscriptions begin with the first issue of a new volume. All subscriptions are to be ordered through the Executive Director, Society of Wood Science and Technology.

The Executive Director, at the Business Office shown below, should be notified 30 days in advance of a change of email address.

Business Office: Society of Wood Science and Technology, P.O. Box 6155, Monona, WI 53716-6155.
Editorial Office: Jeff Morrell, jmorrell@usc.edu.au

EDITORIAL AND PUBLICATION POLICY

Wood and Fiber Science as the official publication of the Society of Wood Science and Technology publishes papers with both professional and technical content. Original papers of professional concern, or based on research of international interest dealing with the science, processing, and manufacture of wood and composite products of wood or wood fiber origin will be considered.

All manuscripts are to be written in US English, the text should be proofread by a native speaker of English prior to submission. Any manuscript submitted must be unpublished work not being offered for publication elsewhere.

Papers will be reviewed by referees selected by the editor and will be published in approximately the order in which the final version is received. Research papers will be judged on the basis of their contribution of original data, rigor of analysis, and interpretations of results; in the case of reviews, on their relevancy and completeness.

As of January 1, 2022, Wood and Fiber Science will be an online only, Open Access journal. There will be no print copies. Color photos/graphics will be offered at no additional cost to authors. The Open Access fee will be $1800/article for SWST members and $2000/article for nonmembers. The previous five years of articles are still copyright protected (accept those that are identified as Open Access) and can be accessed through member subscriptions. Once a previous article has reached its 5th anniversary date since publication, it becomes Open Access.

Technical Notes

Authors are invited to submit Technical Notes to the Journal. A Technical Note is a concise description of a new research finding, development, procedure, or device. The length should be **no more than two printed pages** in WFS, which would be five pages or less of double-spaced text (TNR12) with normal margins on 8.5 x 11 paper, including space for figures and tables. In order to meet the limitation on space, figures and tables should be minimized, as should be the introduction, literature review and references. The Journal will attempt to expedite the review and publication process. As with research papers, Technical Notes must be original and go through a similar double-blind, peer review process.

On-line Access to *Wood and Fiber Science* Back Issues

SWST is providing readers with a means of searching all articles in *Wood and Fiber Science* from 1968 to present Articles from 1968 to 2017 are available to anyone, but in order to see 2017 to 2021 articles you must have an SWST membership or subscription. SWST members and subscribers have full search capability and can download PDF versions of the papers If you do not have a membership or subscription, you will not be able to view the full-text pdf.

Visit the SWST website at http://www.swst.org and go to Wood & Fiber Science Online. Click on either SWST Member Publication access (SWST members) or Subscriber Publication access (Institution Access). All must login with their email and password on the HYPERLINK "http://www.swst.org" www.swst.org site, or use their ip authentication if they have a site license.

As an added benefit to our current subscribers, you can now access the electronic version of every printed article along with exciting enhancements that include:

- IP authentication for institutions (only with site license)
- Enhanced search capabilities
- Email alerting of new issues
- Custom links to your favorite titles

(ISSN 0735-6161)
CODEN WOOFAJ

WOOD AND FIBER SCIENCE

JOURNAL OF THE SOCIETY OF WOOD SCIENCE AND TECHNOLOGY

VOLUME 56 MARCH 2024 NUMBER 1

CONTENTS

Articles

THE EFFECTS OF WOODEN DOWEL SPECIES AND THE END DISTANCE OF MINIFIX FASTENER ON THE SHEAR FORCE CAPACITY FOR H-TYPE FURNITURE JOINTS

*Abdurrahman Karaman**†*

Associate Professor Doctor
Foresty and Forest Products Program
Forestry Department
Banaz Vocational School
Usak University
Banaz, Usak 64500, Turkey
E-mail: abdurrahman.karaman@usak.edu.tr

(Received February 2023)

Abstract. Effects of the wooden dowel species and edge distances were studied relative to the shear force capacities of H-type furniture joints with minifix fastener under loadings. Melamine-coated medium-density fiberboard (MDF-Lam), minifix fasteners, and wooden dowels were used for specimens as used in the furniture industry. H-type joint specimens were tested in shear force. These compression tests were applied to 60 pieces of test samples prepared for this study based on the principles of ASTM D 1037-06 (2010). According to the results, the highest shear force capacities were obtained for the beech dowel. According to edge distances from end distances, the highest shear force capacities were obtained at 72 mm distance from the edge. In the manufacturing of wood composite based H type furniture, the highest shear force capacity values were obtained with the edge distance of 72 mm with an oak dowel combination (1649 N), while the edge distance of 90 mm with a beech dowel combination (1405 N) gave the lowest shear force capacity values. Furthermore, it was concluded that oak dowel as a substance and the distance 72 mm from the edge as distance could be recommended.

Keywords: Shear force capacity, H-type joint, end distance, minifix fastener, wooden dowel.

INTRODUCTION

Ready-to-assemble (RTA)-type furniture is an important product and is used extensively in offices, homes, and other rooms for essential elements of home furnishings. The furniture typically is constructed from particleboard and medium-density fiberboard coated with colored melamine or wood veneers (Pepke 1988). Melamine-coated medium-density fiberboard (MDF-Lam) is the most common wood-based panel product used in the construction of RTA cabinet furniture (Karaman 2020).

RTA-type furniture has been used for almost half a century (Zhang et al 2005). Minifix fasteners are placed near the ends of the members that are connected to provide mechanical strength with intermediate unglued dowels spaced along the edge of the members to help locate and permanently position them. To obtain a visually tight closing of the ends of the joints, it is important to locate the connectors near the ends of the members. Placing the minifix fastener too close to the ends; however, can seriously affect the structural integrity of the joint. Therefore, it is important to determine the minimum end distance for the placement that allows the development of maximum joint strength (Simek et al 2010).

Liu and Eckelman's (1998) study on corner joints clearly demonstrated that for either glued dowels or screws, the bending moment capacity of the joints decreased as the spacing between the fasteners decreased below 60 mm. Tankut (2005) similarly claimed that the maximum moment capacity per dowel was obtained in the joints when the spacing between the dowels was at least 96 mm. Norvydas et al (2005) investigated the effect of the distances between the dowel and the edge of the piece in glued joints with dowels. They chose distances between the dowel and the

* Corresponding author
† SWST member

edge of the piece of 20, 25, 30, 35, 40, 45, 50, 55, and 60 mm and reported that joint resistance was highest when the distance between the dowel and the part edges was 55 mm. Simek et al (2008) investigated the effect of the end distance of cam-lock fasteners on the bending moment resistance of knock-down corner joints and found that an end distance of 60 mm from the member edges performed best. Simek et al (2010) investigated the effect of the end distance of cam-lock fasteners and nonglued wooden dowels on the splitting and bending moment resistance, respectively, of RTA corner joints. The tests showed that cam connectors located 60 mm from the edge of the joint had the highest moment capacity. Malkocoglu et al (2013) investigated the effects of the number and distance between the dowels of RTA furniture on bending moment resistance. Their results showed that bending moment capacity increased when dowel spacing increased from 96 to 160 mm. Malkocoglu et al. (2014) observed that strength was increased by decreasing end distances and that 50 and 60 mm end distances were stronger than 70 and 80 mm. As a result, the front and rear stop values were recommended as equal and 60 mm.

Karaman (2020) examined the effects of different wood species of dowels and the end distance of catch connectors (Clamex P14) on the bending moment resistance of L-type corner joints under diagonal compression. The highest bending moment resistance was obtained from an end distance of 60 mm.

Limited information is available on the effects of loading type and wooden dowel species on the shear force performance of minifix-connected H-type furniture joints.

The shear strength performance of box furniture H-type joining elements indicates that plastic dowels in box furniture assemblies are not suitable for strength (Kasal et al 2012). Yıldırım et al (2020) studied the performance of H-type furniture joints prepared using wood-based materials (MDF-Lam and YL-Lam) and demountable type connectors against shear forces. Karaman (2019) determined the shear strength performance of H-type furniture joints with disassembled type connectors (Clamex P14 and Tenso P14).

Hypothesis of this Research

1. H0: There is a significant relationship between wooden dowel species and the end distance of minifix fasteners on the shear force performance of H-type furniture joints.
2. H1: There is no significant relationship between wooden dowel species and the end distance of minifix fasteners on the shear force performance of H-type furniture joints.

The objective of this study was to investigate the effects of different wood species of dowels and the end distance of minifix fasteners on the shear force performance of H-type furniture joints. This study will be beneficial for the users of minifix fasteners.

MATERIALS AND METHODS

All joint specimens were prepared from 18-mm-thick MDF-Lam which is used extensively in the furniture industry and was purchased from a local merchant in Usak, Turkey.

In this study, Minifix fasteners were obtained from a local dealer at the Häfele Concept Design Center, Istanbul, Turkey. Dowels (8 mm in diameter and 36 mm long) were chosen to be used with the Minifix fasteners. The dowels were prepared from beech (*Fagus orientalis* Lipsky) and oak (*Quercus petraea* Lieble) as shown in Fig 1.

MDF-Lam panels were tested for MC, density, MOR, and MOE according to TS EN 323 (1999), TS EN 322 (1999), TS EN 310 (1999), and ASTM D1037 (2006), respectively. Wood materials were tested for MC, density, MOR, and MOE according to TS 2471 (1976), TS 2472 (1976), TS 2474 (1976), and TS 2478 (1976) standards, respectively. The determined physical and mechanical properties are shown in Table 1.

Preparation of H-Type Furniture Joints

The wooden dowel materials were conditioned at $20 \pm 2°C$ and $65 \pm 3\%$ RH until their weight

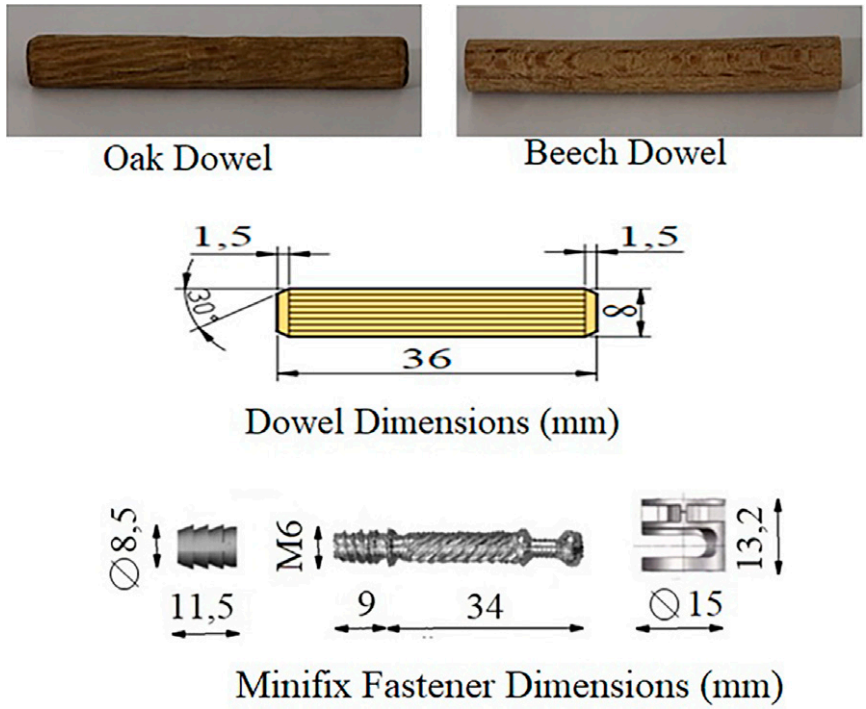

Figure 1. Wooden dowel species and Minifix fastener used in this study (dimensions in mm).

became stable. For making dowels, 1000 × 10 × 10 mm pieces were cut from beech and oak to produce 8-mm diameter and 36-mm long dowels using a dowel machine. The configuration of the H-type joint specimens used for this study is shown in Fig 2. The test specimens consisted of three members: two vertical and one horizontal. The vertical members were 270 × 300 mm and the horizontal element was 270 × 400 mm, which were joined together by specified connectors. Based on the findings from assembly plans, the minifix fasteners were placed close to the end of the joint members. Specimens with three minifix end distances (54, 72, and 90 mm) from the end of members were tested. Holes 15 mm in diameter and 14.5 mm in depth were drilled into the horizontal members for the minifix fastener housings. Connecting holes for the metal bolts 8 mm in diameter were drilled into the horizontal members. Holes 8 mm in diameter and 22 mm in depth were drilled into the horizontal members for the dowels. Corresponding holes (8 mm in diameter and 14 mm deep) were drilled into the vertical members for dowels. Holes (5 mm in diameter and 12 mm deep) were drilled into the vertical members for the threaded part of the metal bolts.

A total of 60 test specimens were prepared at three end distances (54, 72, and 90 mm), two different wooden dowel species (Beech and Oak), one loading format and 10 replicates from each

Table 1. Physical and mechanical properties of materials used in this study.

Materials	MC (%)	Average dry density (g/cm^3)	Air dry density (g/cm^3)	MOE (N/mm^2)	MOR (N/mm^2)	Shear strength (N/mm^2)
Oak	8.6	0.740	0.760	12,161.30	118.50	19.41
Beech	8.5	0.690	0.710	12,462.60	122.90	15.23
MDF-Lam	6.8	0.750	0.760	3465	26.02	5.54

MDF-Lam, medium-density fiberboard.

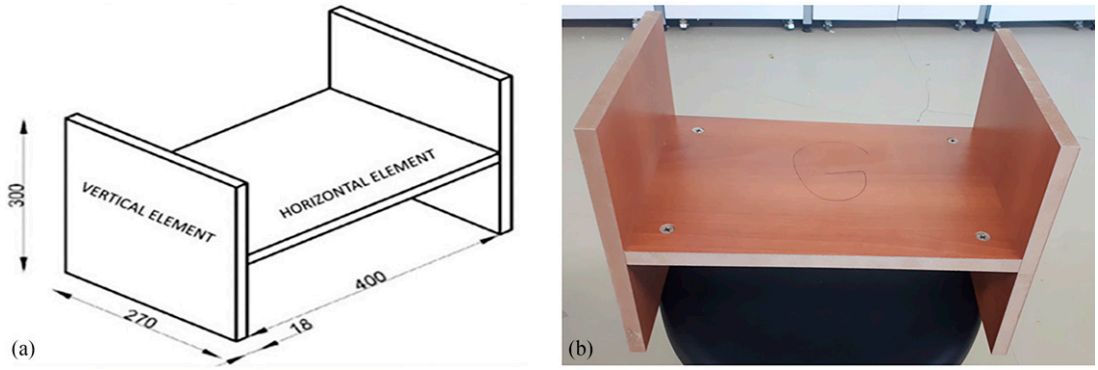

Figure 2. H-type joining test sample (a) and produce test sample (b) (dimensions in mm).

sample. Before the experiment, the samples were equilibrated at 20 ± 2°C and 65 ± 3% RH until they reached constant mass.

Method of Testing

The tests were carried out on a BMT E series universal testing machine, with a 10-kN capacity, in the mechanical testing laboratory at Usak University, Mechanical Engineering Department (Turkey). The test load was applied with a special arrangement prepared with a gap of 20 mm from the edges. The loading rate was 6 mm/min. Maximum loads read from the test machine were recorded in Newton's. There is no standard for the experimental setup, but some researchers have used similar strategies to determine the shear force capacities of both frame and box-type furniture assemblies with such arrangements (Deniz 2010; Kasal et al 2012; Yıldırım et al 2020). The shear force test set-up is shown in Fig 3.

Joint failure modes and maximum failure loads were recorded in Newton's (N). Shear force (*Fk*) corresponds to a joint for maximum (F_{max}) at failure modes where shear force (N) and F_{max} = max load at failure (N).

The shear force (F_k) was calculated by the following formula:

$$F_k = \frac{F_{max}}{2},$$

where F_k is the shear force (N) and F_{max} is the max load at failure (N).

Statistical Analyses

The data were analyzed using Minitab® 18 software (Minitab, Ltd., Coventry, UK). Analysis of variance (ANOVA) was performed to quantify the differences between variables at the 0.05 significance level for the individual data to examine the main factors (wooden dowel species and the

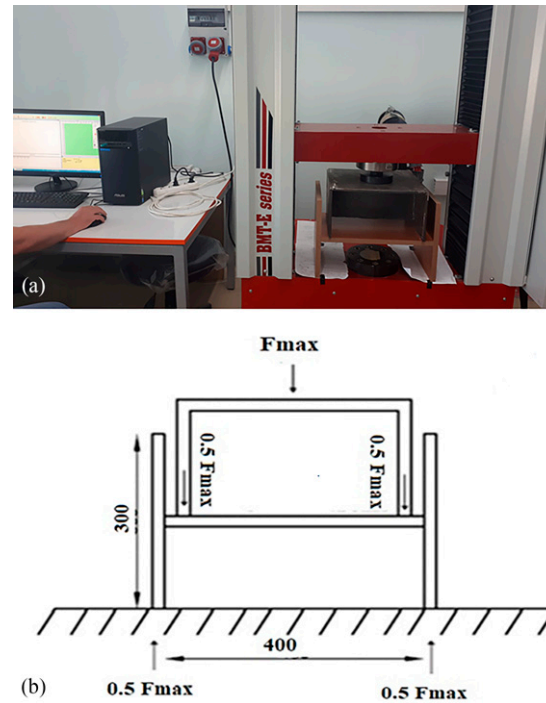

Figure 3. Universal test machine and testing device (a) and shear test points (b) (dimensions in mm).

Table 2. Descriptive statistical values of shear force capacity.

Wooden dowel species	End distances (mm)	Shear force (N)				
		X_{min}	$X_{ort.}$	X_{max}	SD	COV (%)
Oak	54	1536	1591	1630	26.1	1.64
	72	1506	1649	1712	56.1	3.41
	90	1489	1514	1563	25.2	1.66
Beech	54	1339	1454	1536	51.5	3.54
	72	1506	1567	1676	58.6	3.74
	90	1344	1405	1499	45.4	3.23

X_{min}, minimum; X_{max}, maximum; X_{ort}, mean; COV, coefficient of variation.

end distances from the end) and their interactions on the shear force capacity of H-type joints. Statistically significant differences were compared using Duncan's modified least significant difference test ($p < 0.05$).

RESULTS AND DISCUSSION

The mean, minimum, maximum, SD, and coefficient of variation (%) values of the shear force capacity of the H-type joints under load are given in Table 2. The ANOVA results for the shear force capacity values of the tested joints are given in Table 3.

Shear force capacities of joints with oak dowels and the minifix fastener (72-mm the end distance) were approximately 4% and 9% higher than for joints with end distances of 54 and 90 mm, respectively (Table 2).

When oak dowels were used, the shear force capacities of the joints with the minifix fastener (72-mm the end distance) were approximately 8% and 12% higher than for joints with end distances of 54 and 90 mm, respectively.

Table 3. ANOVA of results for shear force capacity.

Source	DF	Adj. SS	Adj. MS	F-value	*p*-value
Wooden dowel species (A)	1	178,952	178,952	82.81	0.000*
End distances (B)	2	220,362	110,181	50.98	0.000*
A × B	2	7506	3753	1.79	0.177
Error	56	121,022	2161	—	—
Pure error	54	113,516	2102	—	—
Total	59	520,336	—	—	—

* *p*-value <0.05 is a significant difference.
SS: Sum of Square; MS: Mean of Square.
ANOVA, analysis of variance.

Table 4. Mean comparison results of shear force capacity for wooden dowel species.

Wooden dowel species	Shear force capacity (N)	HG
Oak	1585	A
Beech	1475	B

HG, homogeneous groups.

Mean shear force capacities for the wooden dowel species and the end distances for the minifix fastener in H-type furniture joints were highest (1649 N) in samples prepared with the end distance of 72 mm and an oak dowel, while the lowest value was obtained in the samples prepared with the end distances of 72 mm (1405 N) and beech dowels (Table 2).

Summary ANOVA results for the shear force capacity values of the tested joints are given in Table 3.

The effect of wooden dowel species and end distances on the shear force capacity of H-type furniture joints under shear load was statistically significant ($\alpha = 0.05$). The wooden dowel species and bilateral interactions were not statistically significant. When the calculated F values indicated that shear force capacity was most affected by the wooden dowel species, then the end distances from the end of minifix fastener, and the least from the interactions.

Comparisons between wooden dowel species indicated that the highest shear force capacity values were obtained for oak (1585 N) (Table 4). These indicated that the direct withdrawal force of single multigroove oak dowels was affected by the wood species of the joints, i.e. the shear bond strength between dowels and joint members was

Table 5. Comparison results of the shear force capacity for end distances the end.

End distances (mm)	Mean bending moment (N)	HG
72	1608	A
54	1523	B
90	1460	C

HG, homogeneous groups.

Figure 4. Types of deformation of H-type furniture joints resulting from the compression test: 54 mm end distance + oak dowel (a), 90 mm end distance + oak dowel (b), 72 mm end distance + oak dowel (c), 54 mm end distance + beech dowel (d), 72 mm end distance + beech dowel (e), and 90 mm end distance + beech dowel (f).

affected by the wood species of the joint members. The mean comparisons of bending moment capacity values of H-type furniture joints for the end distances are shown in Table 5.

The highest shear force capacity values were obtained with an end distance of 72 mm, and the lowest was with an end distance of 90 mm. The mean of shear force capacities of the end distance of 72 mm were 6% and 10% higher than in joints with the end distances of 54 and 90 mm, respectively. The maximum shear force capacity was reached at the end distance of 72 mm. When the end distance increased from 54 to 72 mm, shear force capacity increased while increasing end distance from 72 to 90 mm was associated with reduced shear force capacity.

Failure Modes

After testing, all experimental samples were visually inspected to identify the failure mode of the minifix fastener and dowels. There was no deformation in the connecting elements. The MDF-Lam was fractured due to the compression force on the fastener. Deformations were similar in all experimental specimens. Cracks formed toward the plate end around the minifix and dowel in all H-type furniture joints (Fig 4). As a result, the highest rates of deformation were in Beech dowels + an end distance of 90 mm test samples (see Fig 4[f]). Oak dowels + an end distance of 90 mm, oak dowel + an end distance of 72 mm, and beech dowels + an end distance of 54 mm samples followed, respectively (see Fig 4[a]-[e]).

CONCLUSIONS

This study presents the bending moment resistance of dowels of two wood species used in H-type furniture joints with minifix fasteners under shear load. The effect of end distance (54, 72, and 90 mm) was also considered. In general, the shear force capacity of H-type furniture joints with minifix fasteners under shear loads was significantly affected by dowel species, the end distances, and the interaction of these two factors.

In particular, the tests showed the following:

1. Minifix fasteners with an end distance of 72 mm had the highest shear force capacity of the three end distances tested followed by 54 and 90 mm, respectively.
2. Oak dowels showed the best performance and beech had the lowest performance.
3. Minifix fasteners with an end distance of 72 mm along with oak dowels appeared to provide the best performance. The use of connectors with an end distance of 90 mm with beech dowels appears to be the least ideal.
4. The highest shear force capacity was obtained at an end distance of 72 mm in the samples with oak dowels. The lowest shear force capacity was obtained with a distance of 90 mm in samples with oak dowels.

As a result, an end distance of 72 mm from the edge of the joint combined with the oak dowel provided the best results in constructions requiring high shear force strength. The results of this study provided fundamental information on the strength properties of the selected minifix fastener as an RTA fastener, which will be useful for the disassembled furniture manufacturers and the engineering design of furniture constructions. However, further studies are recommended to examine other materials and combinations.

REFERENCES

ASTM D1037 (2006) Standard test methods for evaluating properties of wood-base fiber and particle panel materials. American Society for Testing and Materials, West Conshohocken, PA.

Deniz E (2010) Strength properties of case furniture joints constructed with solid wood and plastic dowels. MS thesis, Gazi University Institute of Science and Technology, Ankara, IN. 54 pp.

Karaman A (2019) Determination of shear strength performance of H-type furniture joints with disassembled type connectors (Clamex P14 and Tenso P14). Academic Studies on Natural and Health Sciences, Chapter 4, Gece Akademi, Ankara (In English), Turkey. Pages 47-56.

Karaman A (2020) An investigation on the effects of wood species of dowels and the end distance of catch connectors (Clamex P14) on the bending moment of

L-type corner joınts for RTA (ready-to-assemble) furniture. Wood Fiber Sci 53(1):48-61.

Kasal A, Efe H, Deniz E, Kuskun T (2012) Shear force capacity of H-type case furniture joints connected with solid wood and plastic dowels. Kastamonu Univ J Forest Faculty 12(2):209-217.

Liu WQ, Eckelman CA (1998) Effect of number of fasteners on the strength of corner joints for cases. Forest Prod J 48(1):93-95.

Malkocoglu A, Yerlikaya NC, Cakıroglu FL (2013) Effects of number and distance between dowels of ready-to assemble furniture on bending moment resistance of corner joints. Wood Res 58(4):671-680.

Malkocoglu A, Yerlikaya NC, Ozsahin S (2014) Evaluation and optimization of bending moment capacity of corner joints with different boring plans in cabinet construction. Wood Research 59(1):201-216.

Norvydas V, Juodeikiene I, Minelga D (2005) The influence of glued dowel joints construction on the bending moment resistance. Materials science 11(1):36-39.

Pepke E (1988) Ready-to-assemble furniture manufacturing: A business plan for the Northeastern Area. NA-TP-1 2. Radnor, PA: U.S. Department of Agriculture, Forest Service, Northeastern Area, State and Private Forestry. 23 p.

Simek M, Haviarova E, Eckelman CA (2008) The end distance effect of knockdown furniture fasteners on bending moment resistance of corner joints. Acta Univ Agric Silvic Mendel Brun 56:203-209.

Simek M, Haviarova E, Eckelman CA (2010) The effect of end distance and number of ready-to-assemble furniture fasteners on bending moment resistance of corner joints. Wood Fiber Sci 42(1):92-98.

Tankut AN (2005) Optimum dowel spacing for corner joints in 32-mm cabinet construction. Forest Prod J 55(12): 100-104.

TS 2471 (1976) Wood-determination of moisture content for physical and mechanical tests. Institute of Turkish Standards, Ankara, Turkey.

TS 2472 (1976) Wood-determination of density for physical and mechanical tests. Institute of Turkish Standards, Ankara, Turkey.

TS 2474 (1976) Wood-determination of ultimate strength in static bending. Institute of Turkish Standards, Ankara, Turkey.

TS 2478 (1976) Wood-determination of modulus of elasticity in static bending. Institute of Turkish Standards, Ankara, Turkey.

TS EN 310 (1999) Wood-based panels-determination of modulus of elasticity in bending and of bending strength. Turkish Standards Institution, Ankara, Turkey.

TS EN 322 (1999) Wood-based panels-determination of moisture content. Institute of Turkish Standards, Ankara, Turkey.

TS EN 323 (1999) Wood-based panels-determination of density. Institute of Turkish Standards, Ankara, Turkey.

Yıldırım MN, Karaman A, Uslu E (2020) Determination of shear force capacity of H-type box furniture joints connected with different demountable type of connection elements. J Adhes Sci Technol 34(8):867-876.

Zhang JL, Efe H, Erdil YZ, Kasal A, Han N (2005) Moment resistance of multiscrew L-type corner joints. Forest Prod J 55(10):56-63.

EVALUATION OF WITHDRAWAL STRENGTH OF SELF-TAPPING SCREW INSERTED INTO CROSS-LAMINATED TIMBER WITH DIFFERENT ANATOMICAL ASPECTS

Sarah Amira

Doctoral Student
Department of Bioresource Sciences
United Graduate School of Agricultural Science
Gifu University (placement at Shizuoka University)
836 Ohya, Suruga Ward, Shizuoka 422-8529, Japan
E-mail: sarah.amira.19@shizuoka.ac.jp

*Kenji Kobayashi**

Associate Professor
E-mail: kobayashi.kenji.b@shizuoka.ac.jp

Keita Ogawa

Assistant Professor
Department of Bioresource Sciences
Faculty of Agriculture
Shizuoka University
836 Ohya, Suruga Ward, Shizuoka 422-8529, Japan
E-mail: ogawa.keita@shizuoka.ac.jp

(Received September 2023)

Abstract. The use of cross-laminated timber (CLT) technology is witnessing an upsurge in Japan because of its satisfactory performance under seismic conditions. The withdrawal strength (f_{ax}) of a single self-tapping screw (STS) inserted into the CLT was observed using a withdrawal test. The experimental results showed that f_{ax} of the partially threaded STS was higher than that of the fully threaded STS when inserted perpendicular to the grain. The empirical model used to predict f_{ax} provided in the European standard for the design of timber structures was evaluated by comparing the predicted values with the experimental results, which showed that the empirical model was only suitable for predicting the withdrawal strength of specimens with STSs inserted perpendicular to the grain. Therefore, a new probabilistic model was proposed for specimens inserted with STSs inserted parallel to the grain. The failure modes with respect to the orthotropic anatomy of wood materials were observed.

Keywords: Withdrawal strength, probabilistic model, failure mode.

INTRODUCTION

Timber construction techniques have been used to construct temples and shrines in Japan since ancient times. Most residential houses in Japan are constructed using wood. Cross-laminated timber (CLT) is an engineered wood product used in wooden houses to achieve environmental sustainability in Europe, Australia, and North America. Interest in CLT as a newly developed technology has increased in Japan. Izzi et al (2018) stated that CLT structures exhibit satisfactory performance under seismic conditions because of the high strength-to-weight ratio and in-plane stiffness of the CLT panels and the capacity of connections to resist loads with ductile deformations and limited strength impairment.

Self-tapping screws (STSs) optimized mainly for axial load represent a state-of-the-art fastening and reinforcement technique in CLT construction. STSs are highly recommended by CLT manufacturers and designers, both overseas and in Japan, owing to their economic benefits and easy handling (Mohammad et al 2013; Dietsch and Brandner 2015; Kobayashi 2015). Recently, the Japanese

* Corresponding author

Industrial Standard for STSs for timber joints (JIS A 1503) has been published. However, this standard does not include withdrawal strength and head pull-through properties because their inclusion requires the consideration of the properties of the adjacent wood; the JIS is primarily focused on the fastener property (Goto et al 2018). CLT buildings are primarily constructed for residential use and restricted to three stories because of the limited local wood sources, which results in costly and unaffordable CLT production (Passarelli and Koshihara 2018). The lack of standards for CLT structures in Japan renders it difficult to assess the mechanical strength of wood panels and the capacity of connectors to resist loads. An analytical approach for CLT connections is necessary to precisely design CLT constructions and reduce the excessive use of wood in the future.

The raw material for CLT structures should be potentially sourced from species that are readily available in sufficient quantities. Indonesia, in Southeast Asia, has a topography similar to that of Japan and faces the common problem of being an earthquake-prone area. Southeast Asia has one of the oldest tropical forests in the world and supplies large volumes of wood-based products to the world (Okuda et al 2018). The growth of trees as the source of raw wood materials from the tropical natural forest, particularly trees of large diameter with high-quality wood, took a long time to be harvested, one that has seen reckless exploitation in the past. In response to this challenge, Indonesia has planted fast-growing tree species to reduce the use of natural forest trees. Some plantation species in the tropics may grow faster than those in temperate climates because of year-round sunlight exposure. Fast-growing plantation species, such as jabon (*Neolamarckia cadamba* (Roxb.) Bosser), show a relatively high mean annual increment, with a growth of 7-10 cm/yr in diameter and 3-6 m/yr in height within 5 yr (Mansur and Tuheteru 2010).

Neolamarckia cadamba, commonly known in English as bur flower-tree and locally known as kadam or jabon, demonstrates high prospects for industrial plantations and reforestation plants in Indonesia. This species is also expected to become increasingly important for the timber industry in the future, particularly when woodworking raw materials from natural forests are estimated to decrease in the coming years (Krisnawati et al 2011). The wood from this species is typically easy to work on with hand and machine tools. It can be easily resawed, crosscut, and honed and the honed surface produced is smooth. However, its use is mostly limited to furniture, plywood, pulps, and chips, and it is not yet a major structural timber component in the construction sector (Okuda et al 2018). Moreover, CLT reference standards for wood species properties and connections performance are lacking. To ascertain the prospects of this species for CLT construction, its properties are supposed to be investigated against those of several common commercial species used as CLT materials.

The connection geometry, which mainly influences the fastener behavior, includes the axial strengths of the fastener, the density of the wood in which it is inserted, and the direction of loading with respect to the grain orientation (Mahdavifar et al 2018). Previously, studies were conducted on the withdrawal capacity of an STS in a single layer and CLT using a probabilistic approach covering the entire density and diameter bandwidths (Ringhofer et al 2015; Brandner et al 2018; Brandner 2019). However, the length of the inserted STS threaded part was not considered.

The present study investigates the withdrawal performance of the STSs inserted into a CLT with respect to the density of the timber species, the effective insertion length of the STS threaded part, and the CLT side with the STS insertion. The experimental results were evaluated using the authorized prediction equation in EN 1995-1-1:2004/A1 (2008), and a probabilistic model approach was proposed. Moreover, the types of failures that occurred in the withdrawal test were also observed.

MATERIALS AND METHODS

Materials

The withdrawal strength of a single STS inserted into a CLT was measured using a withdrawal-loaded test. The test materials used in this study

were composed of small pieces of CLT and glue-laminated timber (GLT) with two types of STSs (fully threaded and partially threaded). Jabon (*Neolamarckia cadamba* (Roxb.)), sourced from Medan, Indonesia, was used as a representative Indonesian fast-growing hardwood. Sugi (*Cryptomeria japonica* D. Don), hinoki (*Chamaecyparis obtusa*), and karamatsu (*Larix kaempferi*) wood species were used as the representative commercial Japanese softwood samples.

Lamina selection is a prerequisite of the CLT manufacturing process that prevents defects and substandard quality in the final product. Once the lamina materials were visually selected to prevent knots, decay, and finger joints (on jabon materials), they were classified physically and mechanically. The lamina density ρ (kg/m^3) was calculated using the gravimetry method, as depicted in Eq 1.

$$\rho = \frac{m}{V}, \tag{1}$$

where m is the lamina mass (kg) and V is the lamina volume (m^3). The lamina materials were selected according to the Japanese Agricultural Standard for CLT (JAS 3079-2013) by determining the grade of their Young's moduli of bending. Static bending tests were conducted according to JIS Z 2101 (2009), and the Young's modulus of bending E_b (GPa) was calculated using the following expressions:

$$E_b = \frac{l^3 \Delta P}{48 I \Delta y}, \tag{2}$$

$$I = \frac{bh^3}{12}, \tag{3}$$

where l is the bending span (mm), I is the moment inertia of area (mm^4), ΔP is the change in load in the proportional limit area (kN), Δy is the deflection at the center of the span corresponding to ΔP (mm), b is the width of the cross section (mm), and h is the thickness (mm). $\Delta P/\Delta y$ is the slope of load and deflection changes in the elastic range.

The obtained mean Young's modulus of the jabon lamina was 6.614 GPa, with minimum and maximum values of 2.516 and 16.034 GPa, respectively. Therefore, according to JAS 3079-2013, jabon laminas were classified into the M 30A ($E_b \geq 2.5$ GPa) to M 60A grades ($E_b \geq 5$ GPa), which satisfied the minimum grade for structural purposes as CLT materials. Sugi laminas are classified into the M 60A to M 120A ($E_b \geq 10$ GPa) grades, whereas hinoki and karamatsu laminas are classified into the M 90A ($E_b \geq 7.5$ GPa) to M 120A grades. Lamina grading is used as a reference for CLT assembly configuration. Laminas with lower grades were configured for the inner layers, and the higher-graded laminas were configured for the outer layers in this study.

The test specimens were manufactured as five-layer CLT and GLT, yielding an approach model for solid wood. The laminas were adhered to using the aqueous polymer isocyanate (API) adhesive TP-111 at a ratio of 100:15 to a cross-linking agent. The glue spread rate was 250 g/m^2, with a double glue line for face and edge bonding. Using a compressive machine, the assemblies were adjusted with pressures of 1 MPa and retained under pressure at 20°C for 30 min. The API-bonded specimens were produced and conditioned at 65 ± 5% RH and 20 ± 2°C for 2 wk to reach a MC close to 12%.

Three parts of the CLT were available for STS insertion: A, the outermost surface of the CLT; B, parallel to the grain of the CLT core layer; and C, perpendicular to the grain of the CLT core layer. Type A was composed of five layers, whereas types B and C were composed of three layers as the expected effective layers. Ten replicates were used for each combination series. The design of specimen dimensions and STS insertion points are shown in Fig 1. The insertion point of the STS on the CLT was determined according to the European standards for the design of timber structures (EN 1995-1-1 2004 and EN 1995-1-1:2004/A1 2008). Two types of connector, fully threaded STS (PX8-260) and partially threaded STS (PS8-260), manufactured by Synegic Co., Ltd., with a thread diameter of 8 mm and total length L of 260 mm, as illustrated in Fig 2, were considered and distinguished by the effective length of the STS threaded part inserted into the specimen (the shapes of the screw head and screw tip

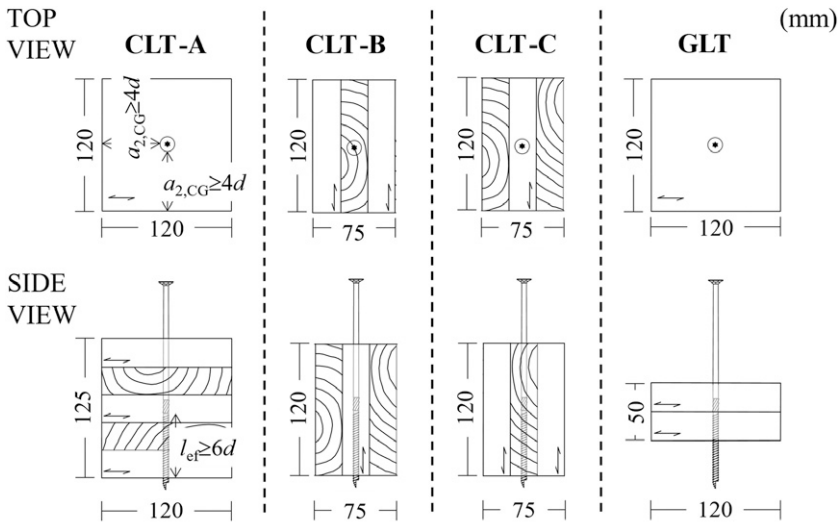

Figure 1. The design of specimen dimensions and self-tapping screw insertion point.

were ignored). The nomenclature of the specimens includes the first letter of the wood species (S for sugi, J for jabon, H for hinoki, and K for karamatsu), followed by the first letter of the STS type (P for partially threaded STS and F for fully threaded STS), and the last character indicating the type of specimen and its STS insertion point (GLT, CLT-A, CLT-B, and CLT-C). Table 1 lists the mean values of the lamina material density (ρ) and the effective length of the fully threaded STS (l_{ef}) for each series.

Withdrawal Test

The STS was driven through the entire test specimen to avoid the tip influencing the layer orientation, as shown in Fig 1. A turned washer with a diameter of 8 mm was used to fix the screw head to the screw grip. A screw grip shaped to fit the head of the STS was attached to the load head of a universal testing machine (UTM) (AG-I 250 kN; Shimadzu Co.). Two displacement gauges (CDP-25) with a capacity of 25 mm (manufactured

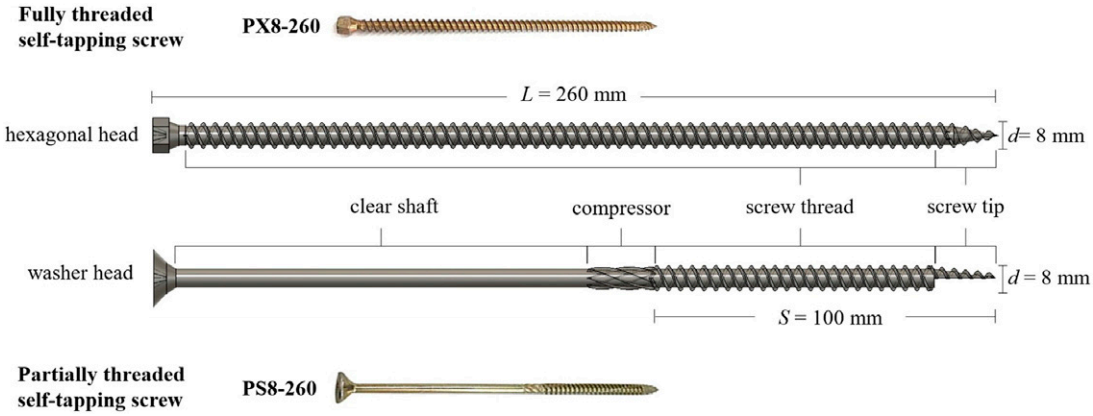

Figure 2. Connector properties: fully threaded self-tapping screw (above) and partially threaded self-tapping screw (below).

Table 1. The mean value of lamina density (ρ) and effective insertion length of self-tapping screw threaded part (l_{ef}) for each series.

	n	ρ		l_{ef}	
Series	#	Mean (kg/m^3)	CoV (%)	Mean (mm)	CoV (%)
S.P.GLT	10	366.7	5.8	32	—
S.P.CLT-A	10	349.2	2.9	80	—
S.P.CLT-B	10	373.0	2.8	80	—
S.P.CLT-C	10	367.3	2.5	80	—
S.F.GLT	10	369.9	4.8	50.9	0.2
S.F.CLT-A	10	376.9	5.7	127.1	0.2
S.F.CLT-B	10	372.4	2.8	120.4	0.7
S.F.CLT-C	10	363.0	5.3	120.3	1.1
J.P.GLT	10	402.7	2.3	32	—
J.P.CLT-A	10	448.3	3.6	80	—
J.P.CLT-B	10	411.5	4.2	80	—
J.P.CLT-C	10	410.4	3.5	80	—
J.F.GLT	10	425.3	7.5	49.5	0.1
J.F.CLT-A	10	426.7	2.9	123.7	0.1
J.F.CLT-B	10	414.2	4.8	118.3	1.4
J.F.CLT-C	10	411.1	3.9	121.5	0.4
H.P.GLT	10	409.2	2.0	32	—
H.P.CLT-A	10	432.6	3.8	80	—
H.P.CLT-B	10	439.2	4.0	80	—
H.P.CLT-C	10	473.9	5.1	80	—
H.F.GLT	10	409.6	2.0	50.8	0.2
H.F.CLT-A	10	432.8	2.2	126.7	1.7
H.F.CLT-B	10	455.7	2.1	120.3	0.4
H.F.CLT-C	10	448.7	2.2	118.9	0.5
K.P.GLT	10	515.3	5.2	32	—
K.P.CLT-A	10	524.4	1.4	80	—
K.P.CLT-B	10	524.5	2.5	80	—
K.P.CLT-C	10	525.9	2.2	80	—
K.F.GLT	10	548.3	4.0	50.5	5.2
K.F.CLT-A	10	530.6	4.4	126.0	2.5
K.F.CLT-B	10	541.7	2.8	120.8	0.3
K.F.CLT-C	10	539.2	1.2	120.4	0.3

by the Tokyo Instrument Research Institute) were attached to record the displacement during the withdrawal test. The withdrawal test apparatus is illustrated in Fig 3.

Monotonic static loading was performed at a constant rate of 1 mm/min. The maximum load, F_{max} was determined, and the f_{ax} (N/mm^2) was calculated using the following equation (Ringhofer et al 2015; Brandner 2019) according to EN 1382 (1999)

$$f_{ax} = \frac{F_{max}}{d\pi l_{ef}}, \tag{4}$$

where F_{max} is the maximum load attained in each test (N), d is the thread diameter (mm), and l_{ef} is the effective insertion length of the threaded part (mm).

According to EN 1995-1-1:2004/A1 (2008), the characteristic withdrawal strength of a single screw $f_{ax,EC5}$ (N/mm^2) is calculated as follows:

$$f_{ax,\ EC5} = 0.52 d^{-0.5} {l_{ef}}^{-0.1} \rho^{0.8}, \tag{5}$$

where d is the thread diameter (mm), l_{ef} is the effective insertion length of the threaded part of the STS (mm), and ρ is the density (kg/m^3). This equation should be divided by π such that the result can be compared with the experimental value obtained from Eq 4. Thus, a comparative equation is generated as follows:

$$f_{ax,\ EC5}/\pi = \frac{0.52 d^{-0.5} {l_{ef}}^{-0.1} \rho_k^{0.8}}{\pi}, \tag{6}$$

Furthermore, the lower 5%-quantile value, assuming a normal distribution of the experimental results, was calculated using the following equation.

$$5\%-\text{quantile value} = \overline{x}(1 - kCV), \tag{7}$$

where $\overline{x}$ is the mean value; k is the coefficient for obtaining the 95% lower tolerance limit at the 75% confidence level, which is 2.104 for 10 specimens of each series (AIJ, 2006); and CV denotes the coefficient of variation, obtained from the ratio of the standard deviation to the mean value.

RESULTS AND DISCUSSION

Relationship between Withdrawal Load and Displacement

The differences in f_{ax} for each specimen series are shown in Fig 4, and the average value is listed in Table 2. The lowest average f_{ax} was obtained for the partially threaded STS on the jabon CLT-B specimen with a value of 3.4 N/mm^2, and the highest average value was obtained from the partially threaded STS on the karamatsu CLT-A specimen (9.15 N/mm^2). The f_{ax} values of the partially threaded STSs were higher than those of the fully threaded STSs for the CLT-A, CLT-C, and

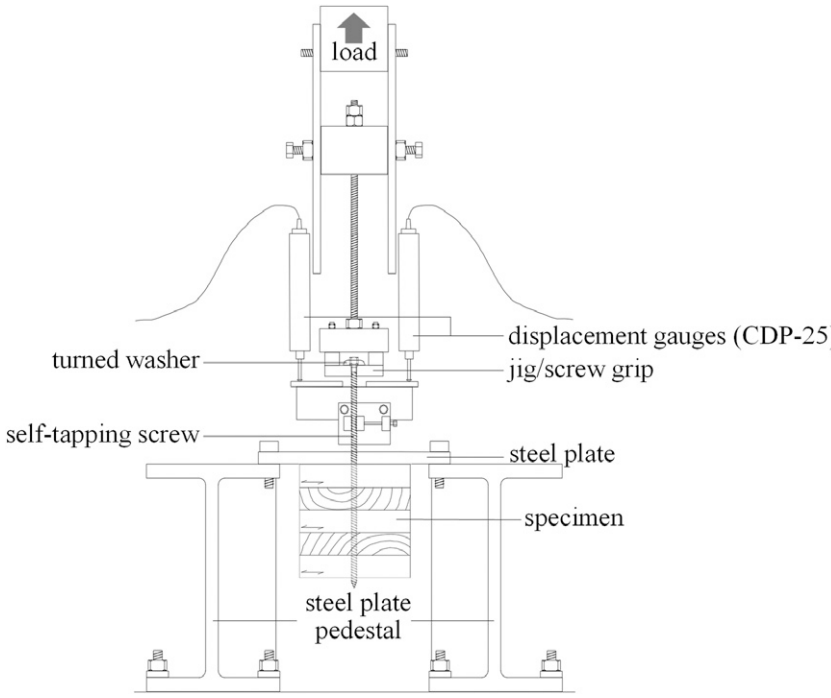

Figure 3. Withdrawal test apparatus.

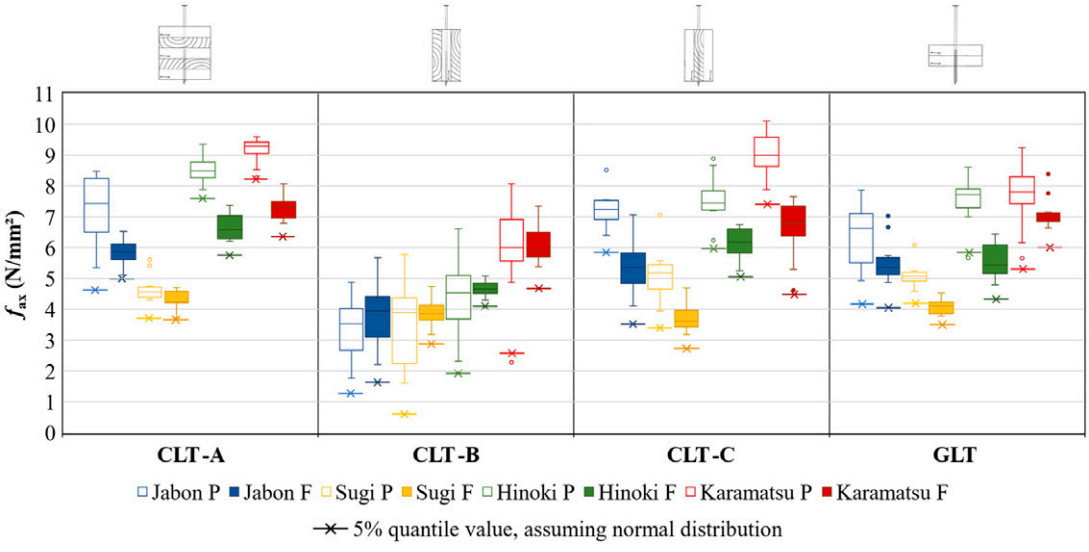

Figure 4. Boxplot of withdrawal strength regarding the lamina species, effective insertion length of self-tapping screw threaded part, and insertion points.

Table 2. The mean value of F_{ax} and f_{ax} for each series.

	n	F_{max}		f_{ax}	
Series	#	Mean (kN)	CoV (%)	mean (N/mm^2)	CoV (%)
S.P.GLT	10	4.09	8.15	5.09	8.15
S.P.CLT-A	10	9.44	9.69	4.70	9.69
S.P.CLT-B	10	7.04	38.83	3.50	38.83
S.P.CLT-C	10	10.42	16.11	5.18	16.11
S.F.GLT	10	5.24	6.69	4.10	6.66
S.F.CLT-A	10	13.79	6.90	4.32	6.84
S.F.CLT-B	10	11.82	12.24	3.91	12.14
S.F.CLT-C	10	11.29	12.47	3.74	12.43
J.P.GLT	10	5.15	16.44	6.41	16.44
J.P.CLT-A	10	14.44	16.80	7.18	16.80
J.P.CLT-B	10	6.84	29.15	3.40	29.15
J.P.CLT-C	10	14.79	9.69	7.36	9.69
J.F.GLT	10	6.94	12.84	5.58	12.82
J.F.CLT-A	10	18.20	6.91	5.85	6.83
J.F.CLT-B	10	11.35	27.29	3.82	26.73
J.F.CLT-C	10	16.39	16.01	5.37	16.10
H.P.GLT	10	6.06	10.62	7.54	10.62
H.P.CLT-A	10	17.13	5.16	8.52	5.16
H.P.CLT-B	10	8.95	26.57	4.45	26.57
H.P.CLT-C	9	15.25	10.04	7.59	10.04
H.F.GLT	10	7.13	10.59	5.59	10.56
H.F.CLT-A	10	21.23	6.01	6.67	6.45
H.F.CLT-B	10	14.15	5.80	4.68	5.64
H.F.CLT-C	10	18.37	8.22	6.15	8.34
K.P.GLT	10	6.19	14.69	7.70	14.69
K.P.CLT-A	10	18.39	4.82	9.15	4.82
K.P.CLT-B	10	11.90	26.58	5.92	26.58
K.P.CLT-C	10	18.07	8.18	8.99	8.18
K.F.GLT	10	9.06	7.73	7.14	7.49
K.F.CLT-A	10	23.18	5.06	7.33	6.21
K.F.CLT-B	10	18.69	11.17	6.16	11.30
K.F.CLT-C	10	19.97	15.13	6.60	15.14

GLT specimens. However, the differences were found less significant for the CLT-B specimens. Within a uniform thread diameter, when the withdrawal load is applied perpendicular to the grain, the shorter the l_{ef}, the smaller the f_{ax}, which is a consequence of the divisor variable in Eq 4. Claus et al (2022) investigated the force distribution along the STSs using fiber Bragg grating measurements and found that the force distribution on an STS insertion of length 270 mm into a GLT material was relatively constant when the screw axis to the grain angle was 0°. When the screw axis to the grain angle was 90°, the withdrawal force tended to be higher at the uppermost screw thread, which then gradually decreased to the lower end of the inserted screw thread. In other words, the length of the inserted threaded part of the STS did not significantly affect the withdrawal force when it was inserted parallel to the grain.

Similar patterns were observed in the CLT-A, CLT-C, and GLT specimens when the angle between the STS axis and wood grain was 90°. However, the withdrawal load was applied in the radial direction of the wood in the CLT-A and GLT specimens, whereas in the CLT-C specimens, the withdrawal load was applied in the tangential direction of the adjacent wood, which in some way altered the difference to the failure occurrences, as discussed later.

Evaluation of the Prediction Model of Withdrawal Strength

The characteristic withdrawal strength of a single screw in EN 1995-1-1:2004/A1 (2008) is basically described by the characteristic density values for European solid timber (EN 338, 2016) and GLT provided in the Eurocode standards (EN 1194, 1999). For the materials used in this study, the withdrawal strength values were to be evaluated for each specimen, along with the mean and 5%-quantile of the experimental series results to the predicted value calculated by Eq 6.

Significant correlations between the experimental results and predicted values are found for GLT, CLT-A, and CLT-C when each specimen within the series is analyzed, as shown in Fig 5. The wide range of density distributions in the experimental results disintegrates the withdrawal strength values predicted using Eq 6. When the mean values are projected onto both the experimental results and predicted values obtained using Eq 6, as shown in Fig 6, a significant correlation is noted for each specimen within the series. Figure 7 shows a comparison of the 5% quantile values of the experimental results and those predicted using Eq 6. Significant correlations can be observed for the GLT and CLT-A specimens; however, the correlations diminish in the remaining specimens. The values predicted using the empirical model in EN 1995-1-1:2004/A1 (2008), except for CLT-B

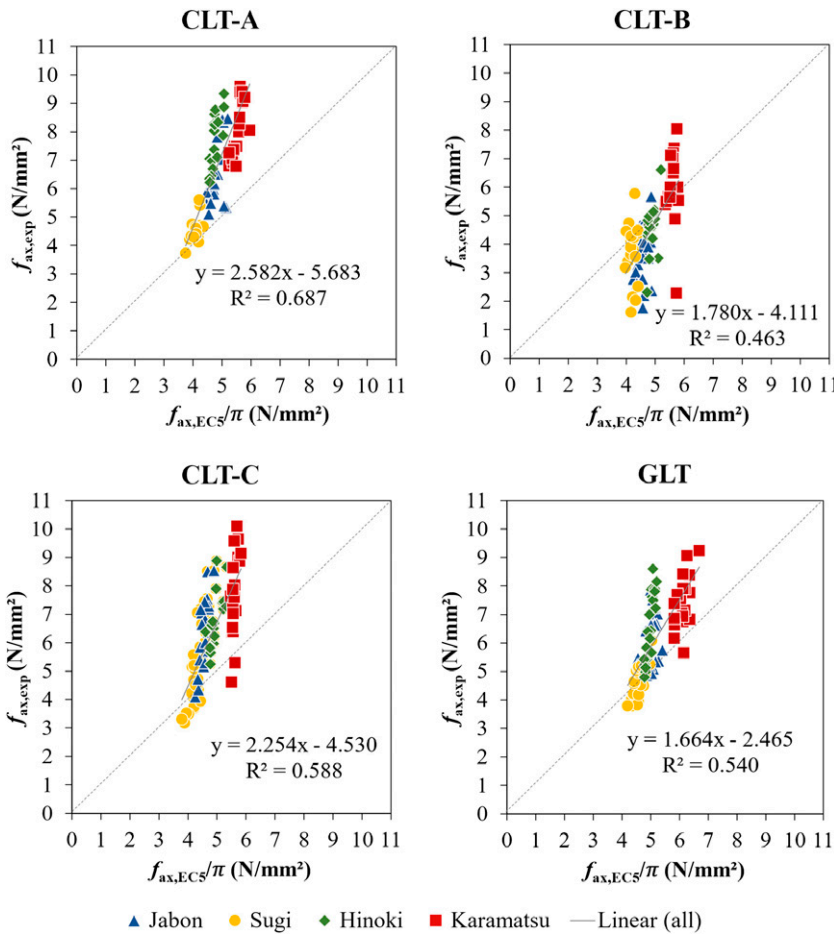

Figure 5. The comparison of experimental results and predicted values by Eq 6.

specimens, did not overestimate the experimental results, which was the expected anticipation for structural designing. Based on the comparison of the values predicted using the empirical model in EN 1995-1-1:2004/A1 (2008) with the calculated experimental values, it can be deduced that the empirical model (Eq 6) is only suitable for the specimens with STSs perpendicular to the grain (90°) if each specimen and 5%-quantile values are considered.

Even though the low withdrawal strength values of STSs inserted parallel to the grain (CLT-B) from experimental results implicitly remind us that the installation of STS in the narrow edge parallel to the grain is recommended to be avoided (Uibel and Blaß 2013), the author proposed the new probabilistic model approach for CLT-B specimens for the anticipatory step in any circumstances. The relationship between f_{ax} and density is usually described by a power regression model of the form $f_{ax} = a\rho^b\varepsilon$, where a and b are the regression parameters, with a as the scaling parameter and b as the power parameter, and ε is the error/randomness in the regression model (Brandner 2019). According to Eq 5 in EN 1995-1-1:2004/A1 (2008), the effective insertion length of the STS threaded part, l_{ef} is also described by a power model. Therefore, the predicted withdrawal strength regarding the wood density and effective insertion length of STS was described in the following form, with a as the scaling parameter and b and c as the power parameters.

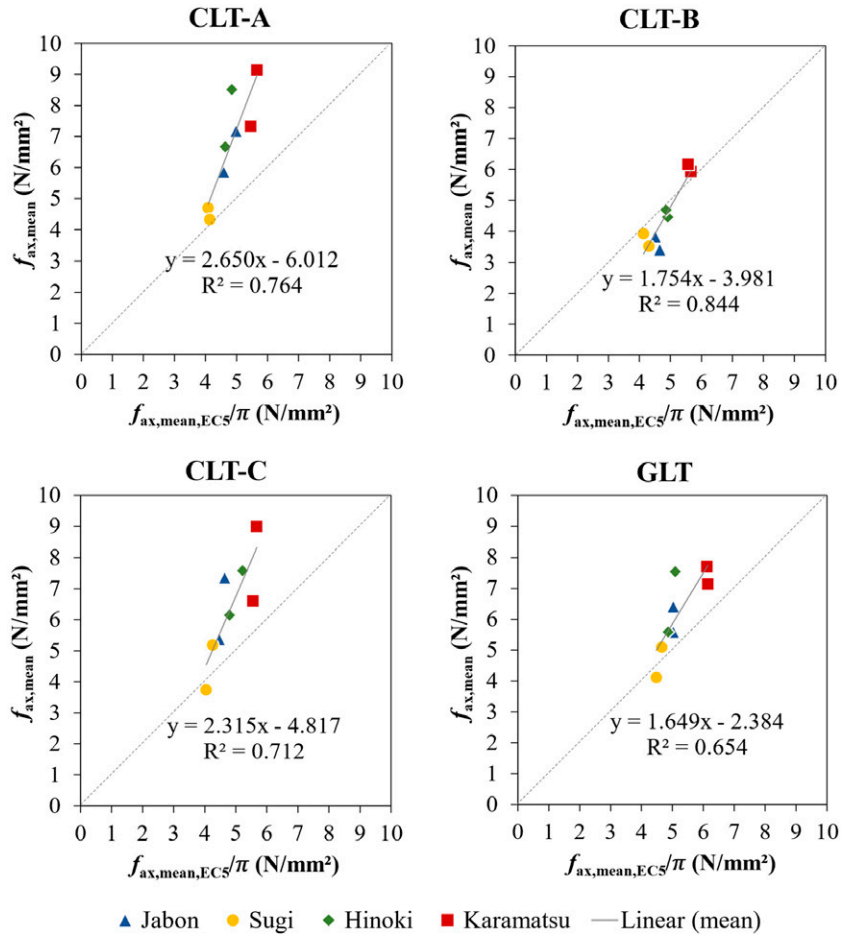

Figure 6. The comparison of mean experimental results and predicted values by Eq 6.

$$f_{ax,\,pred} = a\rho^{b} l_{ef}{}^{c} \tag{8}$$

The substitution variables for the equation above were obtained to make the sum of quadratic differences between the whole experimental results and the proposed prediction model at the minimum. Therefore, the new prediction model for CLT-B specimens with the uniform STS thread diameter at 8 mm was reformed as follows. This proposed model included the π division factor in the equation.

$$f_{ax,\,pred} = 0.0002 l_{ef}{}^{0.08} \rho^{1.6} \tag{9}$$

The proposed prediction model for CLT-B was evaluated by linear regressive analysis with each specimen, mean, and 5%-quantile values of the experimental series results as projected in Fig 8(a), (b), and (c), respectively. When the overall values of the experimental results and the predicted values calculated from the proposed Eq 9 were compared, the linearity was obtained. A more significant linearity was found if the mean withdrawal strength of each series was compared. The 5%-quantile of predicted values from the proposed model in Eq 9 overestimated the 5%-quantile values of experimental results at the near-threshold significance level within the limited parameters in this study. There might also be other wood anatomical parameters that possibly have an influence on the withdrawal strength (Brandner 2019).

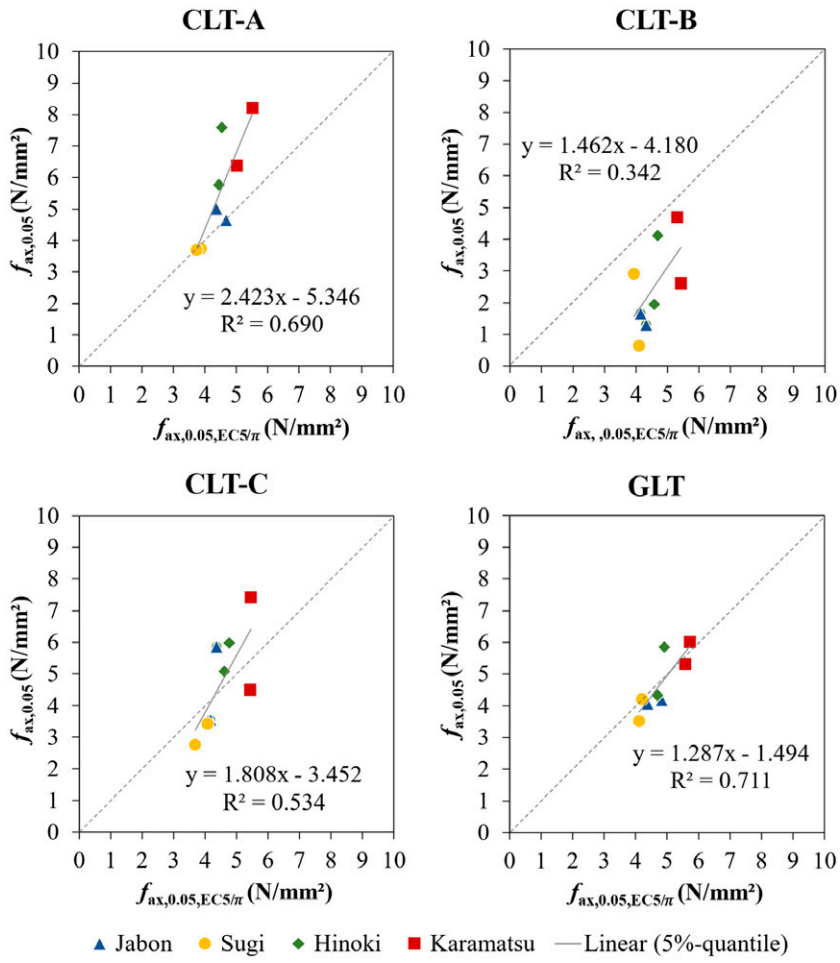

Figure 7. The comparison of 5%-quantile experimental results and predicted values by Eq 6.

However, the projected ρ values to both Eqs 6 and 9 generated a disproportionate distribution on $f_{ax,EC5}/\pi$ and $f_{ax,pred}$ of CLT-B and CLT-C. This is possibly the causative effect of the unspecific value of ρ, which is the mean value of the density of the whole lamina used for CLT layers instead of the STS-adjacent CLT layer density.

Influence of Parameters to Withdrawal Strength

Density, ρ, was the only wood characteristic that considerably influenced the withdrawal strength in this study, and the effective insertion length of the STS threaded part, l_{ef}, was the representative geometrical aspect of STS. Within the limited range of the above parameters, the significance of influencing the withdrawal strength of STS was analyzed through linear regression indicated by the coefficient of determination, R^2. As shown in Fig 9, the significant influence of lamina density within species on the withdrawal strength was indicated by the surrounded regression equations that were found on S.F.CLT-A, S.F.CLT-C, H.F.GLT, H.F.CLT-A, H.F.CLT-B, K.F.CLT-A, S.P.GLT, and S.P.CLT-A. None of the jabon specimens showed a significant effect of the density on the withdrawal strength. Brandner (2019) found out that the withdrawal strength of screws inserted in hardwood increased disharmonious

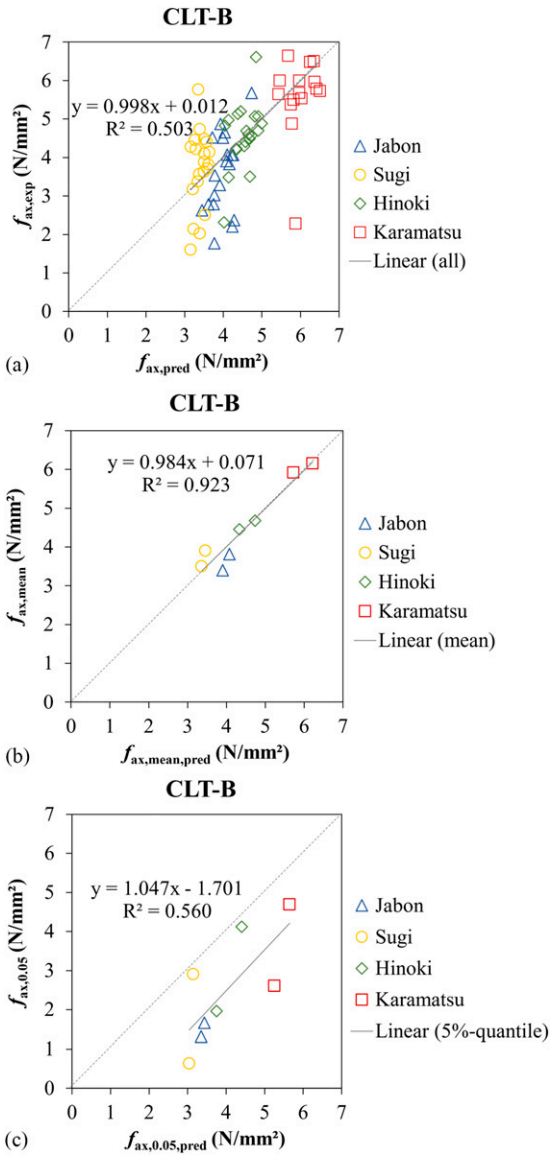

Figure 8. Correlation of the experimental results and the proposed predicted values by Eq 9: (a) each specimen values, (b) mean values, and (c) 5%-quantile values.

with increasing density, which was not the case in softwood (Uibel and Blaß 2007).

Regarding the two types of STS used in this study, the effective insertion length of the STS threaded part affects the withdrawal strength significantly negative on sugi and hinoki GLT, hinoki and karamatsu CLT-A, and a whole specimen of CLT-C (Fig 10). This negative effect of l_{ef} is also reasonably interpreted by the power value in the empirical model, Eq 5.

Failure Modes

Regarding the angle between the STS axis as well as the withdrawal load direction and the grain direction, they were grouped into 0° and 90°. The CLT-B specimen was the only specimen configuration, which is inserted by the STS parallel to the grain (0°). The CLT-A, CLT-C, and GLT were technically in the same state, which is inserted by the STS perpendicular to the grain (90°). However, the difference was noticed in the orthotropic anatomy of the wood materials. The STS was inserted in the radial direction through the crossed layups configuration in the CLT-A specimen. In unidirectional layups, the STS insertion was subjected to GLT in the same direction as CLT-A. And the direction of the STS insertion to the CLT-C was tangential. According to the mentioned conditions, the typical forms of failure modes were observed.

In this study, the failure modes were distinguished into three categories. First, the withdrawal failure, which is an initial failure in the withdrawal test, was characterized by the shear failure at the wooden members surrounding the STS to the sticking out of the upmost layer of CLT around the STS (Pang et al 2020), depicted in Fig 11. The second failure mode was a crack perpendicular to the withdrawal test direction (Fig 12), and the third failure mode was split as the further impact of the crack represented in Fig 13 was categorized into severe damages.

The withdrawal failures were found all over the series before the continued damage occurred. The crack failures occurred on one specimen of H.F.CLT-C, six K.F.CLT-C, seven K.P.CLT-C, one K.F.GLT, and two K.P.GLT. Four K.F.CLT-C, one K.P.CLT-C, and one K.F.GLT were found with split failure. The severe failures, cracks, and splits mostly occurred on the dense specimens in the tangential direction of the withdrawal force. A similar failure also occurred in the previous study by Xu et al (2021), with splitting and tension cracks

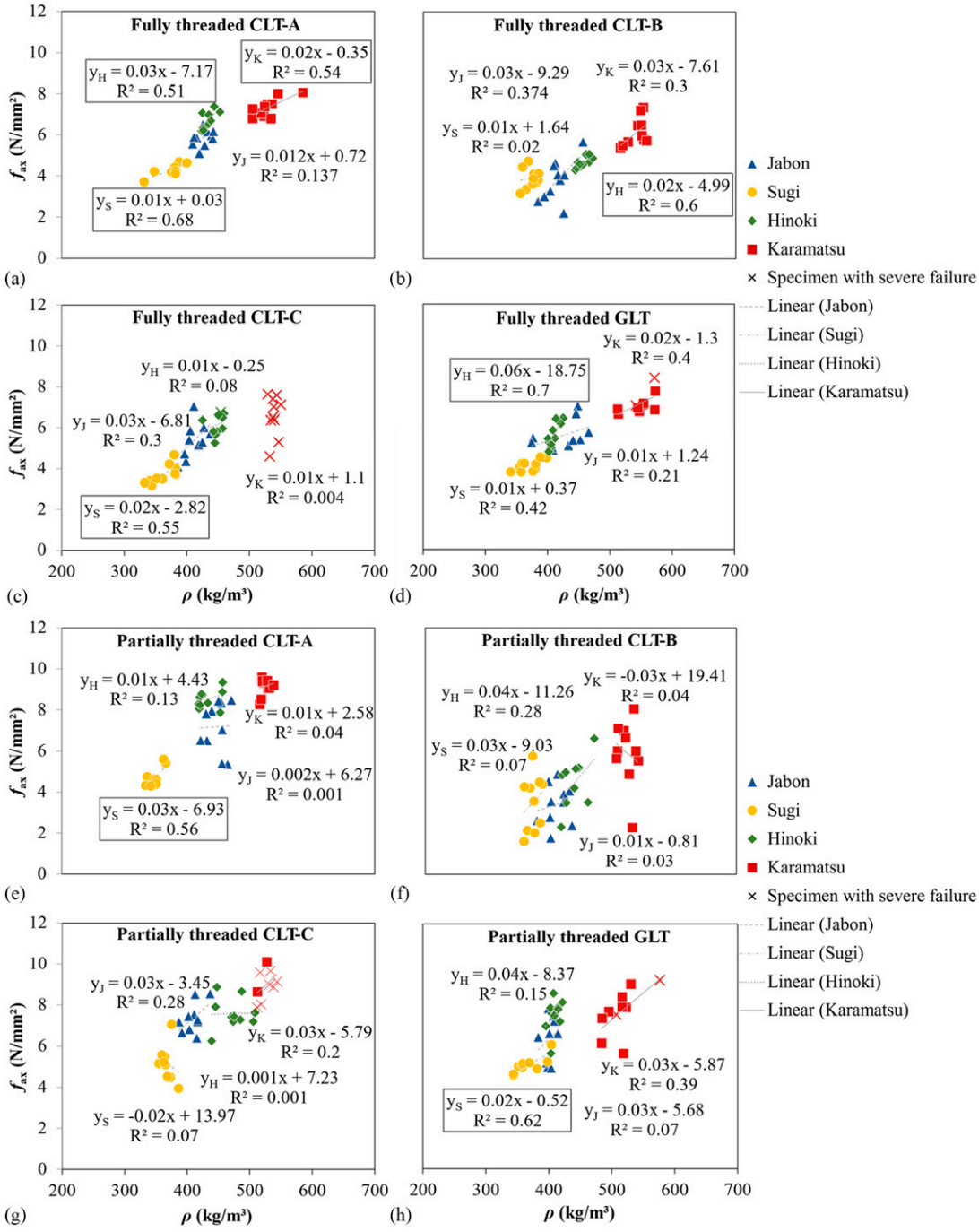

Figure 9. The linear regression graphics analysis of the withdrawal strength depends on the lamina density: (a)-(d) specimens with fully threaded STS and (e)-(h) specimens with partially threaded self-tapping screw.

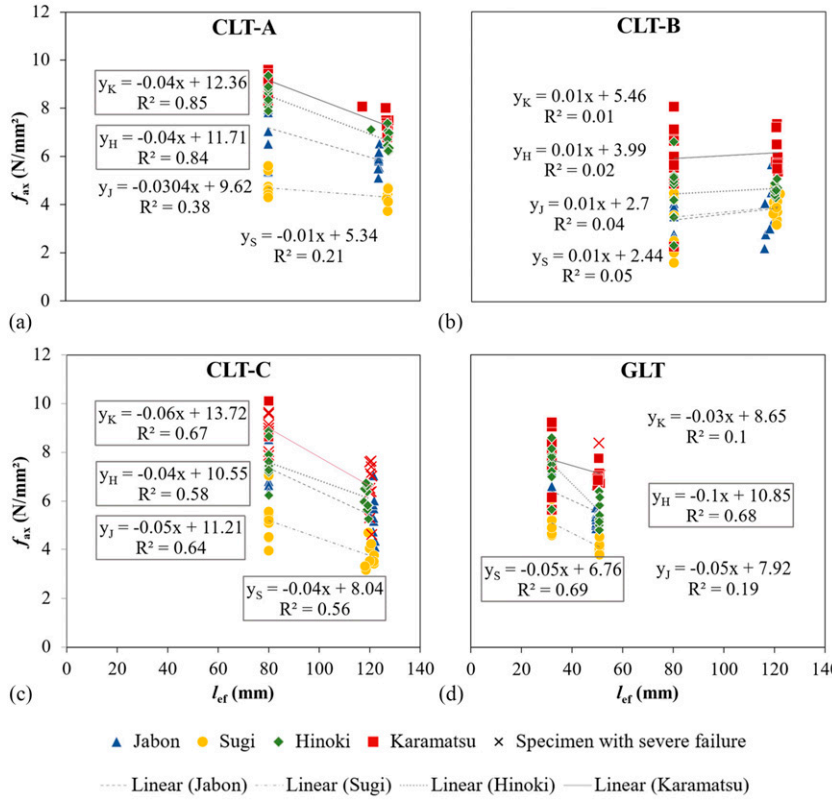

Figure 10. The linear regression graphics analysis of the withdrawal strength depends on the effective insertion length of the self-tapping screw threaded part.

perpendicular to the grain of CLT karamatsu in the first layer. Severe failures were also found on some dense GLT specimens. This would be the important case for the spacing method of STS installment on the narrow edge of the dense wood material in the tangential direction and the dense unidirectional layup material and solid wood in the radial direction. This also proved that the cross-lamination method might enhance the prevention of severe failures.

Figure 11. Typical withdrawal failure mode.

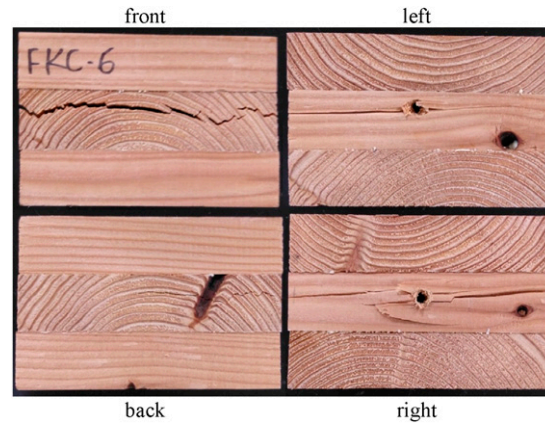

Figure 12. Typical crack failure mode.

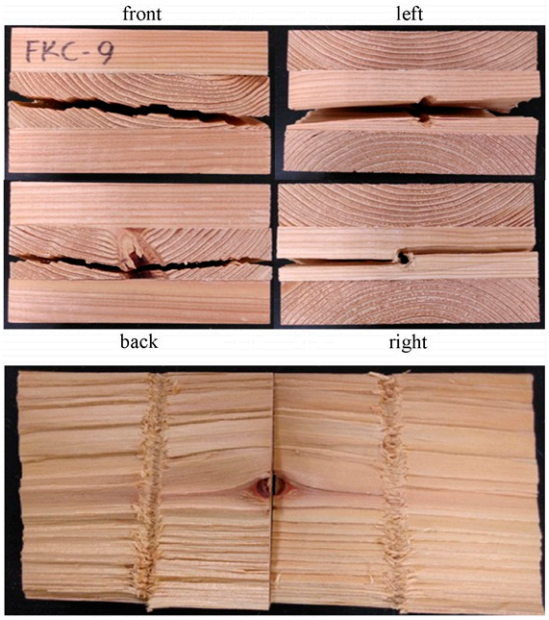

Figure 13. Typical split failure.

CONCLUSIONS

Prior to assessing the prospect of the jabon as a fast-growing-tree species for structural purposes, the preliminary test of the lamina material was performed and proved that the bending Young's modulus E_b passed the minimum grade according to the lamina classification in JAS 3079-2013. Within the density (ρ) and the effective insertion length of the threaded part of STS (l_{ef}) bandwidth in this study, the withdrawal strength of fully threaded and partially threaded STS inserted into the different sides of CLT as well as GLT made of jabon, sugi, hinoki, and karamatsu lamina was evaluated. The result showed that the withdrawal strength of the partially threaded STS was higher than that of fully threaded STS concerning the l_{ef} if it was inserted perpendicular to the grain yet was not the pattern in the STS inserted parallel to the grain of the specimen with respect to the differences on stress distribution along the STS. The compatibility of the probabilistic model given in EN 1995-1-1:2004/A1 (2008) on predicting the withdrawal strength with the limited parameters bandwidth in this study was evaluated. It was found that this probabilistic model was suitable for predicting the withdrawal strength of the STS as long as the predicted values underestimated the experimental results. The significant influence of the lamina density was not found in every wood species and the insertion point of the STS due to the unspecific measurement of density on the STS-inserted wood member. The effective insertion length of the STS threaded part seemed to influence the withdrawal strength if it was inserted in the tangential direction of the wood member. According to the observed failure modes, the spacing design of STS installment on the solid (core layer) and unidirectional layups of dense wood members perpendicular to the grain need to be considered to prevent severe failure caused by the withdrawal force.

ACKNOWLEDGMENTS

The brief results of this experiment have been presented in an online poster presentation at the 71st Japan Wood Society Conference, March 2021. In the preparation of the experiment, the authors were assisted by Tomoki Shinohara, a second year master student in a fiscal year 2020.

CONFLICT OF INTEREST

The authors declare that they have no potential conflict of interest that could have influenced the works reported in this paper.

REFERENCES

AIJ (Architectural Institute of Japan) (2006) Standard for Structural Design of Timber Structure (in Japanese). Page 153. Tokyo: Architectural Institute of Japan.

Brandner R (2019) Properties of axially loaded self-tapping screws with focus on application in hardwood. Wood Mater Sci Eng 14(6):254-268, doi: 10.1080/17480272.2019.1635204.

Brandner R, Ringhofer A, Grabner M (2018) Probabilistic models for the withdrawal behavior of single self-tapping screws in the narrow face of cross laminated timber (CLT). Eur J Wood Prod 76:13-30.

Claus T, Seim W, Küllmer J (2022) Force distribution in self-tapping screws: Experimental investigations with fibre Bragg grating measurement screws. Eur J Wood Prod 80:183-197.

Dietsch P, Brandner R (2015) Self-tapping screws and threaded rods as reinforcement for structural timber

elements—A state-of-the-art report. Constr Build Mater 97:78-89, doi: 10.1016/j.conbuildmat.2015.04.028.

EN 338 (2016) Structural timber - Strength classes. Page 7. European Committee for Standardization (CEN). Brussels, Belgium.

EN 1194 (1999) Timber structures—Glued laminated timber. Strength classes and determination of characteristic values. Page 7. European Committee for Standardization (CEN). Brussels, Belgium.

EN 1382 (1999) Timber structures—Test methods: Withdrawal capacity of timber fasteners. Pages 8-9. European Committee for Standardization (CEN), Brussels, Belgium.

EN 1995-1-1 (2004) Eurocode 5: Design of timber structures—Part 1-1: General—Common rules and rules for buildings. Pages 77-78. European Committee for Standardization (CEN), Brussels, Belgium.

EN 1995-1-1:2004/A1 (2008) Eurocode 5: Design of timber structures—Part 1-1: General—Common rules and rules for buildings. Pages 12-13. European Committee for Standardization (CEN), Brussels, Belgium.

Goto Y, Jockwer R, Kobayashi K, Karube Y, Fukuyama H (2018) Legislative background and building culture for the design of timber structures in Europe and Japan. Pages 8-9 *in* Proceedings, World Conference on Timber Engineering (WCTE 2018), Seoul, Republic of Korea.

Izzi M, Casagrande D, Bezzi S, Pasca D, Follesa M, Tomasi R (2018) Seismic behaviour of cross-laminated timber structures: A state-of-the-art review. Eng Struct 170:42-52.

JIS Z 2101 (2009) Methods of test for woods. Japanese Industrial Standard.

Kobayashi K (2015) Present and future tasks for screw joints in timber structures. Mokuzai Gakkaishi 61(3): 162-168.

Krisnawati H, Kallio M, Kanninen M (2011) *Anthocephalus cadamba Miq.: Ekologi, Silvikultur dan Produktivitas* [*Anthocephalus cadamba Miq.*: Ecology, Silviculture dan Produktivity]. Center for International Forestry Research, Bogor, Indonesia.

Mahdavifar V, Sinha A, Barbosa A R, Muszynski L, Gupta R (2018) Lateral and withdrawal capacity of fasteners on hybrid cross-laminated timber panels. J Mater Civ Eng, 30(9):1-11.

Mansur I, Tuheteru FD (2010) *Kayu Jabon* [Jabon Wood]. Penebar Swadaya, Jakarta.

Mohammad M, Douglas B, Rammer D, Pryor SE (2013) Chapter 5—Connections in cross-laminated timber buildings. Pages 3-44 *in* E Karacabeyli and B Douglas, eds. CLT handbook: Cross-laminated timber. FPInnovations, Pointe-Claire, QC, Canada.

Okuda S, Corpataux L, Muthukrishnan S, Wei KH (2018) Cross-laminated timber with renewable, fast-growing tropical species in Southeast Asia. Pages 1-2 *in* Proceedings, World Conference on Timber Engineering (WCTE 2018), Seoul, Republic of Korea.

Pang S-J, Ahn K-S, Kang SG, Oh J-K (2020) Prediction of withdrawal resistance for a screw in hybrid cross-laminated timber. J Wood Sci 66(79):1-11.

Passarelli RN, Koshihara M (2018) The implementation of Japanese CLT: Current situation and future tasks. *in* Proceedings, World Conference on Timber Engineering (WCTE 2018), Seoul, Republic of Korea.

Ringhofer A, Brandner R, Schickhofer G (2015) Withdrawal resistance of self-tapping screws in unidirectional and orthogonal layered timber products. Mater Struct 48: 1435-1447, doi: 10.1617/s11527-013-0244-9.

Uibel T, Blaß HJ (2007) Edge Joints with Dowel Type Fasteners in Cross Laminated Timber. Pages 6-11 *in* Proceedings, International Council for Research and Innovation in Building and Construction Working Commission W18 - Timber Structures (CIB-W18/40-7-2), Bled, Slovenia.

Uibel T, Blaß HJ (2013). Joints with Dowel type fasteners in CLT structures. Pages 119-134 *in* Proceedings, European Conference on Cross Laminated Timber, Graz, Austria.

Xu J, Zhang S, Wu G, Gong Y, Ren H (2021) Withdrawal properties of self-tapping screws in Japanese larch (*Larix kaempferi* (Lamb.) Carr.) cross laminated timber. Forests 12(524):1-13.

ENGINEERED FLOORING FROM LOW-DENSITY PLANTATION HARDWOOD: EVALUATION OF LONG-TERM IN-SERVICE TRIALS

*Kuluni Millaniyage**

PhD candidate
E-mail: kulunipiumika.millaniyage@utas.edu.au

Nathan Kotlarewski†

Research Fellow in Timber Design and Production
E-mail: nathan.kotlarewski@utas.edu.au

Louise Wallis

Deputy Director
Centre for Sustainable Architecture with Wood
University of Tasmania
Launceston, Tasmania, Australia
E-mail: louise.wallis@utas.edu.au

Assaad Taoum

Senior Lecturer in Civil & Structural Engineering
School of Engineering
College of Sciences and Engineering, University of Tasmania
Hobart, Tasmania, Australia
E-mail: assaad.taoum@utas.edu.au

(Received December 2023)

Abstract. The use of short-rotation hardwood plantation species has been perceived to be unsuitable for flooring until recently, due to the lower densities. This study assesses the performance of a low-density plantation hardwood species, *Eucalyptus nitens* in engineered flooring applications. The selection of a suitable timber species for flooring has conventionally been based on its market acceptance or value and on its hardness to ensure minimal indentations or damages. While both of these reasons have determined flooring species selection, this is becoming more difficult as popular species is less available due to increasing flooring demand, and the diminishing supply of native timbers due to government regulations on harvesting and conservation. Typically, the species hardness is determined by static tests in the laboratory. Although these tests can compare species hardness, they might not reliably indicate an end product's performance, especially with engineered flooring. Despite the global interest in timber flooring manufacturing, investigations on the assessment of alternative testing methods to static hardness, methods to replicate in-service behavior, timber flooring quality determination, and characterization of timber properties for flooring applications are still scarce. In this study, in-service trials were conducted on solid and densified *E. nitens* boards and engineered flooring prototypes with *E. nitens* top layers, to better understand product behavior when exposed to moderate traffic with distinct temperature and RH variations. Dynamic impact hardness tests using the falling ball indentation method adapted from ASTM D 2394 were conducted to assess the surface hardness of the tested prototypes. *E. nitens* engineered prototype performance was comparable to the existing market products used as controls. This demonstrates the potential to use plantation-grown *E. nitens* in engineered flooring applications in domestic dwellings.

Keywords: *Eucalyptus nitens*, *Eucalyptus obliqua*, footprint diameter, dynamic hardness, falling ball indentation, short-rotation, performance evaluation.

INTRODUCTION

Hardwood timber flooring is considered one of the timeless and highly preferred floor covering options by consumers due to its versatility,

* Corresponding author
† SWST member

durability (Uddin 2021), and aesthetics (ATFA 2009a). Although traditional solid timber flooring is still in demand, there is a gradual shift toward multilayer engineered timber flooring products (Sepliarsky et al 2022). While in Europe, 15% of timber floors are made from solid timber and 83% of total production corresponds to engineered parquet (European Parquet Federation 2023), the engineered timber flooring market share in North America, China (Blanchet et al 2002; Chen et al 2015) and Australia are gaining more significance. Engineered timber floor boards generally have multiple layers consisting of thinner top layers made from a hardwood species, placed on a substrate consisting of one or multiple support layers of a lower value species or composite product such as plywood or fiberboard (ATFA 2012; Acuña et al 2020). This facilitates greater product stability (Castro and Zanuttini 2004; Drerup et al 2013) and allows an increase in the square meters of engineered timber boards produced from the hardwood species utilized (Acuña et al 2020).

The selection of timber species for applications are generally governed by traditional convention over availability and technical or aesthetic considerations (Neyses and Sandberg 2015; Millaniyage et al 2023). In Europe, *Quercus robur* and *Quercus petrea* (European Oak) are the most commonly chosen species for parquet (82.1%) (Németh et al 2014; Grześkiewicz et al 2020; European Parquet Federation 2023) although they are moderately hard and dense. In the US, a few species including *Quercus* sp. (Red Oak and White Oak) make up almost 70% of the hardwood market (Uddin 2021; Khademibami et al 2022). Similar observations are made in Australia where the flooring choices are usually made based on a known performance in service for generations, appearance, and cost (ATFA 2009a, 2009b) rather than based on density. A survey conducted on Australian consumers and specifiers reported aesthetic preferences favored Australian hardwoods including *Corymbia* sp. (Spotted Gum), *Eucalyptus microcorys* (Tallowwood), and *Eucalyptus pilularis* (Blackbutt) (Knox 2016). A native forest species mix consisting of *Eucalyptus obliqua*, *Eucalyptus regnans*, and *Eucalyptus delegetensis* is marketed as Tasmanian Oak in Australia and has been widely used in flooring applications for decades (ATFA 2011; Wood Solutions 2020). The predictions on timber supply show that the access to these native species are rapidly decreasing (STT 2022) and native timber harvesting has recently been banned in two states of Australia. Similar observations are made in Europe for Oak.

Globally, commercial timber plantations are becoming an important source of raw material for the timber industry (FAO 2020). In the state of Tasmania (Australia) where the present study is conducted, *Eucalyptus nitens* is the major plantation species grown due to its ability to withstand frost (Onfray et al 2015). There are two types of *E. nitens* plantations present. The majority of the plantations are established to obtain fiber for pulpwood production (ABARES 2022), designed for short rotations of around 15 yr, and do not undergo silvicultural applications such as thinning and pruning (Harwood 2010; Derikvand et al 2019). As a result, the timber from this plantation resource contains many natural features such as knots and do not comply with Australian standards for appearance grading (AS 2796.2 1999, 2082 2007). In contrast, sawlog-managed plantations undergo thinning and pruning and harvested around 21-25 yr of age and are anticipated for future use as a sawlog resource (Washusen et al 2009; Harwood 2010). In this study, these resources are termed fiber *E. nitens* and sawlog *E. nitens* to reflect the silviculture management differences.

To introduce an alternative species for flooring applications that fits outside market conventions, the process is assisted by evaluating the species performance in expected end-use conditions (Németh et al 2014; Millaniyage et al 2023). The authors observed that the global standards commonly used in timber flooring have limitations in benchmarking eight species suitability for end-use applications. Moreover, the current Australian standards do not address the plantation resource base which has distinctive characteristics when compared with native, high-density species. The

conventional technical criterion used in determining the suitability of a species for flooring is hardness (ATFA 2010; Vörös and Németh 2020). Traditional static hardness tests such as Janka hardness (ASTM D 143 2000) and Brinell hardness (EN 1534 2020) methods are commonly used to evaluate species performance. However, as reported by Millaniyage et al (2022) and Grześkiewicz et al (2020), these methods are impacted by the composite structure of engineered flooring and might not always generate reliable observations for engineered flooring products.

The study presented here took place in two stages. Stage one involved the evaluation of the performance of solid *E. nitens* timber boards, hereafter termed the solid flooring trial. Stage two included the development and evaluation of several engineered flooring prototypes with different *E. nitens* top layers. One of the developed engineered flooring prototypes consisted of densified solid *E. nitens* boards to increase the surface hardness of the timber. This in-service trial is hereafter referred to as the engineered flooring trial. To the author's best knowledge neither in-service trials with *E. nitens* has been reported nor has the testing of engineered flooring prototypes. After the in-service trials, each flooring was subjected to dynamic hardness tests using the falling ball indentation method.

In summary, the aim of the study described here was to: 1) evaluate the behavior of the short-rotation hardwood species *E. nitens*, which is not currently used in industrial-scale timber flooring manufacturing, through visual observations obtained from in-service trials and dynamic hardness tests; 2) compare the results with the controls; and 3) determine the suitability of plantation *E. nitens* for an engineered flooring product suitable for domestic/light commercial applications.

MATERIALS AND METHODS

The study used four different sources of *E. nitens* timber. The solid flooring trial included five timber flooring products. In the engineered flooring trial, eight types of timber flooring products including developed prototypes and existing market products were tested (six multilayer products, one solid overlay product, and one solid densified product) as specified in the following section.

Timber Flooring Specimens for the Solid Flooring Trial

The solid timber flooring trial was designed to understand how *E. nitens* would behave in a flooring application when exposed to in-service conditions in comparison with commonly used flooring timber species in Australia.

Two groups of solid timber flooring boards were developed using sawlog and fiber *E. nitens*, to evaluate their performance. *E. obliqua* (Tasmanian Oak species) termed as moderately hard (ATFA 2010), was selected as the main control species based on local industry interest and production. *E. pilularis* (Blackbutt) and *Eucalyptus sieberi* (Silvertop Ash) termed as very hard species (ATFA 2010) were also used for comparison. Based on the common industry practice in Tasmania, it was decided to use 19 mm thickness for solid timber boards used in the trial. From each timber species, ten samples were obtained to determine the MC and oven-dried density as per Australian/New Zealand Standards AS/NZS 1080.1 (2012) and AS/NZS 1080.3 (2000), respectively. The density, MC, and manufacturing details are shown in Table 1.

Timber Flooring Prototypes for the Engineered Flooring Trial

The development of engineered timber flooring prototypes with *E. nitens* top layers was conducted based on the feedback received from interviews conducted with a group of architects, flooring specifiers, and Tasmanian flooring manufacturers familiar with specifying or using Tasmanian Oak in their projects. Specifically for this research, six different prototypes were manufactured aligning with the in-state industry capabilities. Solid 12 mm thick *E. obliqua* overlay and a commercial Tasmanian Oak engineered flooring product processed overseas were used as controls.

Table 1. Solid timber flooring trial: species and properties.

Species	Oven-dried density (kg m^{-3})	MC (%)	Board surface cross section dimensions (mm)	No. of sample boards
Fiber *Eucalyptus nitens*	480 (9.48)	11.5 (8.60)	19 × 105	11
Sawlog *E. nitens*	510 (9.26)	11.1 (9.22)	19 × 105	11
Eucalyptus obliqua	600 (14.23)	10.8 (5.52)	19 × 105	11
Eucalyptus pilularis	815 (5.90)	11.9 (2.22)	19 × 130	10
Eucalyptus sieberi	785 (9.34)	11.4 (5.08)	19 × 130	09

The coefficient of variation percentage for density and MC are shown in the parenthesis.

The materials for the products were supplied from three sawmills in Northern Tasmania:

1. Sawmill A supplied the timber boards for sawlog *E. nitens*, *E. nitens* veneers, and commercially finished *E. obliqua* overlay floor boards;
2. Sawmill B supplied the boards for fiber-managed *E. nitens*;
3. Sawmill C locally manufactured the *E. nitens* plywood used as the substrate used in one of the engineered flooring prototypes;
4. The timber for densified samples was obtained from 26-yr-old sawlog *E. nitens* harvested from plantations located in Ridgely, Tasmania;
5. The marine plywood used as the substrate for other engineered flooring prototypes and Tasmanian Oak engineered flooring products were commercially acquired.

The densification process for sawlog *E. nitens* was conducted at the University of Melbourne. The densification involved three stages adapted from Tenorio and Moya (2019): stage 1 – preheating at 150°C for 10 min; stage 2 – compression perpendicular to the grain until reaching the target thickness of 12 mm (compression ratio of 25%) for 20 min, at the temperature maintained in stage 1; and stage 3 – cooling, the timber was kept compressed but without heat (platens temperature <60°C) for an additional 10 min (Belleville 2021). The compositions of the prototypes used in the trial are presented in Table 2.

The 1.2 mm thick top layers in prototypes $S_{1.2mp}$ and $S_{1.2np}$ were gained by laminating two 0.6 mm veneers together. The veneers were randomly selected from a commercial production line specialized to produce 0.6 mm thick veneers. The development of prototypes was conducted with existing production methods and the top layers of prototypes were laminated to the substrates using polyvinyl acetate using a hot press. All developed prototypes were tongue and groove profiled at the workshop.

Installation of the in-Service Trials

Both trials were installed consecutively at a high school in Launceston, Tasmania, enclosed in a glass-framed bridge linking two buildings. Each trial period was close to 1 yr and involved periodic visual assessments. The school was selected due to the continuity of traffic although moderate levels of traffic exposure and minimal use of stiletto heels were observed. The glass-framed corridor (Fig 1) facilitated dimensional stability and color change observations under extreme environmental conditions.

All timber boards were fixed to 16 mm structural plywood panels using elastomeric glue and secret nailed at the CSAW workshop before installation. This resulted in five panels in the solid flooring trial and eight panels in the engineered flooring trial. Each panel was then manually coated with a two-pack polyurethane waterborne coating system with a clear satin finish replicating industry practices, excluding the commercial Tasmanian Oak engineered flooring product (O_3) which had a prefinished UV-cured coating.

A solid flooring trial was installed on the existing reinforced concrete floor. It was monitored during the period of December 2020 to June 2022. The panels were laid and fixed to the concrete floor

Table 2. Composition of the tested prototypes in the engineered flooring trial.

Specimen codes	Flooring composition	Layer thickness (mm)	Cross section (mm)	Layer density (kg m^{-3})	Average composite density (kg m^{-3})	Layer description
S_{6a}	Sawlog *Eucalyptus nitens*	6.00	12.6 × 85	565 (7.48)	630 (13.59)	Top layer
	Marine plywood	6.00		495 (6.82)		Core layer
	E. nitens veneer	0.60		430 (3.99)		Backing layer
F_6	Fiber *E. nitens*	6.00	12.6 × 85	495 (7.59)	575 (6.96)	Top layer
	Marine plywood	6.00		495 (6.82)		Core layer
	E. nitens veneer	0.60		430 (3.99)		Backing layer
S_{6b}	Sawlog *E. nitens*	6.00	12.0 × 85	565 (7.48)	620 (9.69)	Top layer
	Marine plywood	6.00		495 (6.82)		Core layer
D_{12}	Densified *E. nitens*	12.00	12.0 × 85	670 (13.23)	670 (13.23)	One layer
$S_{1.2mp}$	*E. nitens* veneer	1.20	13.8 × 85	430 (3.99)	555 (3.86)	Top layer
	Marine plywood	12.00		495 (6.82)		Core layer
	E. nitens veneer	0.60		430 (3.99)		Backing layer
$S_{1.2np}$	*E. nitens* veneer	1.20	13.8 × 85	430 (3.99)	750 (6.88)	Top layer
	Local fiber *E. nitens* plywood	12.00		765 (6.65)		Core layer
	E. nitens veneer	0.60		430 (3.99)		Backing layer
O_{12}	Solid *Eucalyptus obliqua*	12.00	12.0 × 85	715 (7.38)	715 (7.38)	One layer
O_3	Prefinished Tasmanian Oak	3.20	14.2 × 165	625 (9.12)	605 (8.16)	Top layer
	Rubberwood (*Hevea*)	11.0		587 (6.02)		Segmented core

Specimen codes signify the top layer whether sawlog, fiber, or densified *E. nitens* followed by top layer thickness in millimeters. The coefficient of variation percentage for density is shown in the parenthesis.

using secret nailing and a clipping system. The trial was visually monitored fortnightly to check if significant shrinkages or indentations occurred. The temperature and RH of the environment was recorded as well as the amount of traffic over the floor. After the solid flooring trial was uninstalled, the engineered flooring panels were installed and monitored during July 2022 to April 2023, replicating the methods used in the solid trial.

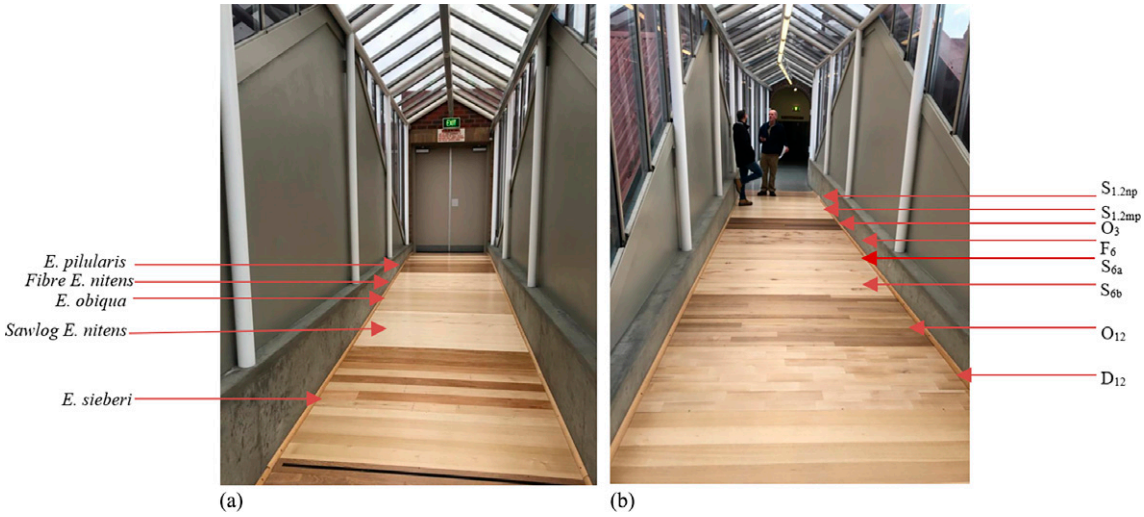

Figure 1. In-service trials (a) solid flooring trial and (b) engineered flooring trial.

Dynamic Hardness Test Using Falling Ball Indentation Method

Dynamic hardness was evaluated on solid and engineered timber flooring panels after they were uninstalled from the school premises. The test was conducted on the panels along with the 16 mm structural plywood backing used for installation in the school and were rested on a flat, reinforced concrete floor at the CSAW workshop to replicate in-service conditions. The test was developed as an adaptation from ASTM D 1037 (1999) and ASTM D 2394 (2017) following the methodology used by Acuña et al (2020) and Sepliarsky et al (2022). The timber hardness was defined by measuring the footprint diameter caused due to the impact from a 536 g and 50 mm diameter steel ball dropped from a determined height.

The steel ball was dropped from each reference height on the test panels using an auxiliary plastic pipe with holes at respective drop heights to guarantee precise height reference. A sheet of carbon paper was placed on the test panel surface to improve the accuracy of the impact reading. The surface deformation was measured using a digital caliper. Since an elliptical deformation was formed on the timber surface due to the differences in compressive strengths in the parallel direction as well as fibers in the perpendicular direction, the footprint diameter was calculated as an average between the highest and lowest observations (Acuña et al 2020; Sepliarsky et al 2022). This method allowed the comparison of both solid and engineered flooring based on the deformation produced by the steel ball. Ten hits per one drop height were conducted on each timber panel making sure that every timber board in the panel was reported once for each drop height. The hits were made at least 50 mm apart resulting in 120 hits per panel (Fig 2).

Statistical Analysis

The statistical analysis was conducted using R software for the data obtained from dynamic hardness tests. Altogether data from approximately 130 timber boards (from 13 panels: the five panels in the solid flooring trial and eight panels in the engineered flooring trial with 10 boards tested from each panel), were analyzed. The assumptions of normality, independence, and equal variances were verified for the data sets. The normality of the data was checked for each sample group at different drop heights using the Shapiro-Wilk test. The assumption of equal variances was contrasted by the Bartlett test on several occasions so that linear statistical methods using ANOVA could not be used. In this regard, Welch's heteroscedastic F test with trimmed means and winsorised variances was used in the analysis (Acuña et al 2020).

RESULTS AND DISCUSSION

In-Service Trials

During the monitored period of the solid flooring trial, no significant stability concerns were observed in the tested panels. The RH and temperature records (Fig 3) show that the environment showed high fluctuations due to the glass roof of the corridor which allowed the sunlight to fall on the timber during daytime. The pedestrian counter located at the entrance to the corridor showed that the solid flooring trial was exposed to 30,000 passes over the tested period (around 50 passes per day). The rationale of the trial was to assess the performance of plantation *E. nitens* in a domestic/light commercial application in comparison with *E. obliqua* (Tasmanian Oak sp.) which is a popular flooring species used for centuries in Australia. Tasmanian Oak is specified by the British Standard *BS EN 8201:2011: Code of practice for installation of flooring of wood and wood-based panels* as suitable for floors with light pedestrian traffic with traffic intensities less than 500 persons per day (BS 8201 2011). Therefore, visual assessments were conducted between plantation *E. nitens* and *E. obliqua* when subjected to similar traffic exposure for comparison. The traffic conditions at the installed site were less than expected due to the COVID-19 lockdowns but were still higher than a typical domestic dwelling.

However, the fiber-managed *E. nitens* panel started to show cracks during the first 3 mo of installation as shown in Fig 4. No such

(a) (b)

Figure 2. Footprint diameter caused by the steel ball on tested panels (a) 6 mm thick *Eucalyptus nitens* top layer and (b) 1.2 mm thick *E. nitens* top layer.

observations were found in sawlog-managed *E. nitens* boards (Fig 4). Visual assessment of all panels after the in-service period showed distinctive lightening of the timbers' original color due to the exposure of sunlight and *E. pilularis* showed the highest visual shrinkage while *E. obliqua* showed the lowest. Few indentation and scuff marks were seen in both *E. obliqua* and

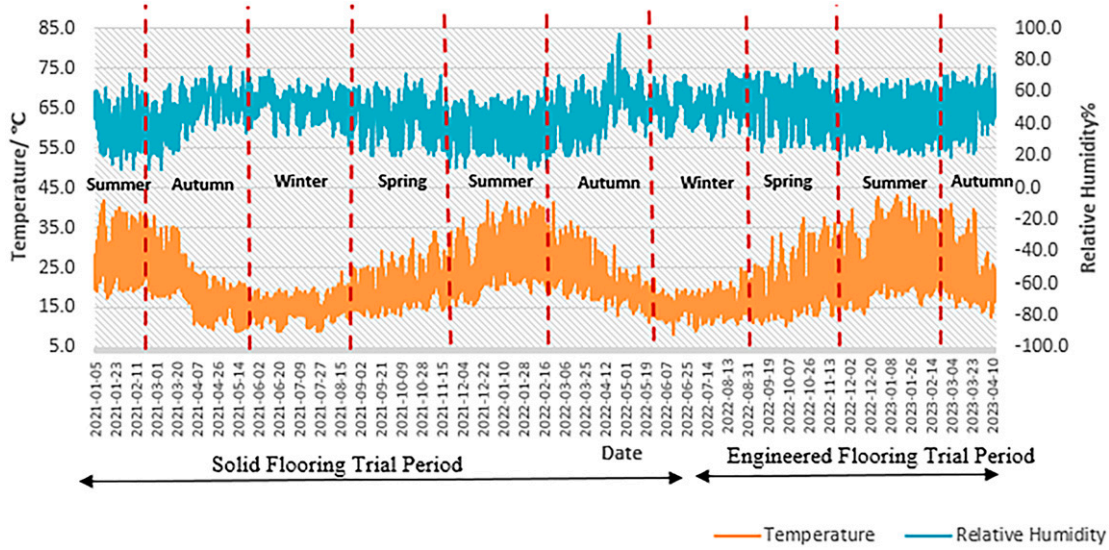

Figure 3. RH and temperature variation during the in-service trials.

(a) (b)

Figure 4. Visual observations of solid *Eucalyptus nitens* after in-service trial (a) fiber *E. nitens* boards showing cracks marked in red and (b) sawlog *E. nitens* panels.

E. nitens panels caused by footwear and cleaning equipment being dragged over the floor.

The consecutive engineered flooring trial was exposed to 11,200 passes of traffic (approximately 37 passes per day). Even the prototypes with 1.2 mm top layers showed no major indentation or scuff marks. The commercial engineered flooring control product (O_3) showed lesser surface color change in comparison with the rest of the panels (Fig 5).

As shown in F_6 of Fig 5, the fiber *E. nitens* panel had a high level of features including knots that impacted the aesthetic acceptance of the product among architects and specifiers. There is no commercial facility in Australia to conduct densification and the densified boards shown in D_{12} of Fig 5 were prepared in a laboratory setting. The densified boards were shorter in length in comparison with other tested prototypes, due to the dimensional restrictions of the laboratory-scale densifier.

Dynamic Hardness Assessment Using Falling Ball Indentation Test

After removing the panels from the installation site, they were subjected to a falling ball indentation test. The solid flooring panels were analyzed first. Residual footprint diameter values (mm) and their coefficient of variation for the tested species in the solid flooring trial are shown in Table 3. All the groups showed $p > 0.05$ in the Shapiro-Wilk normality test allowing the assumption of normality in the data sets.

The footprint diameter showed a clear tendency to increase when the drop height increased as shown in Fig 6 for solid timber flooring. The high-density species *E. pilularis* and *E. sieberi* showed lower footprint diameters in comparison with *E. obliqua* and *E. nitens*.

This was further confirmed by the statistical analysis conducted using Welch's ANOVA test which showed significance between the five tested timber groups in all drop heights. The Posthoc pairwise comparison between groups per each height showed a similar trend, as *E. pilularis* and *E. sieberi* were significantly different from fiber *E. nitens*, solid *E. nitens*, and *E. obliqua* in all drop heights. *E. pilularis* and *E. sieberi* were not statistically significant from each other in any of the tested drop heights (Table 4).

In the next stage, engineered timber flooring prototypes and controls used were subjected to the same test. The footprint diameter and coefficients of variations for the tested panels are shown in Table 5. Similar to the solid flooring data, the data sets in groups showed $p > 0.05$ proving the normality of the data sets but did not have equal variances according to the Bartlett test and showed an increase in footprint diameter with the increase of drop height in all the tested panels.

S_{6a}: 6 mm thick sawlog *E. nitens* glued to marine ply substrate and veneer backing

S_{6b}: 6 mm thick sawlog *E. nitens* glued to marine ply substrate

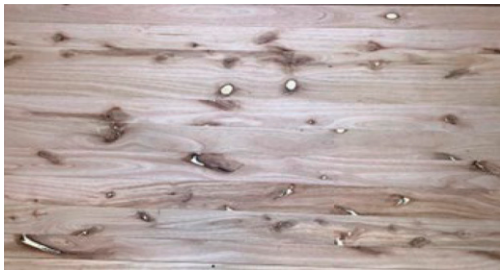

F_6: 6 mm thick fibre *E. nitens* glued to marine ply substrate and veneer backing

D_{12}: 12 mm thick solid, densified *E. nitens*

$S_{1.2mp}$: 1.2 mm thick sawlog *E. nitens* glued to marine ply substrate and veneer backing

$S_{1.2np}$: 1.2 mm thick sawlog *E. nitens* glued to *E. nitens* ply substrate and veneer backing

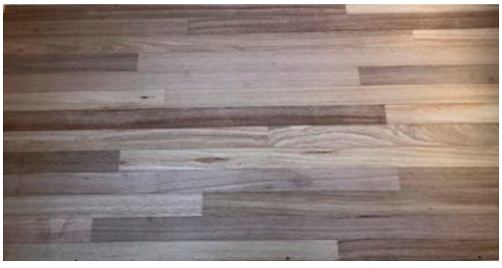

O_{12}: 12 mm thick *E. obliqua* overlay (commercial product used as control)

O_3: 3 mm thick Tasmanian Oak glued to Rubberwood substrate (prefinished, commercial product used as control)

Figure 5. Surface of the tested panels in the engineered flooring in-service trial.

Table 3. Footprint diameter of species in solid flooring trial. Main descriptive statistics.

Height (m)	Fiber *Eucalyptus nitens*	Sawlog *E. nitens*	*Eucalyptus obliqua*	*Eucalyptus sieberi*	*Eucalyptus pilularis*
0.15	**10.39** (6.65)	**9.82** (11.82)	**9.93** (7.18)	**6.96** (11.92)	**7.01** (5.63)
0.30	**12.24** (7.06)	**11.82** (13.10)	**10.94** (8.80)	**8.09** (9.64)	**8.45** (6.29)
0.45	**13.09** (7.23)	**12.86** (14.99)	**12.26** (7.74)	**9.08** (8.55)	**8.99** (8.06)
0.60	**13.64** (8.12)	**13.95** (12.00)	**13.61** (7.42)	**9.82** (8.25)	**9.74** (7.70)
0.75	**14.37** (8.28)	**14.48** (12.78)	**13.78** (8.52)	**10.26** (9.44)	**10.74** (10.31)
0.90	**14.83** (9.26)	**13.94** (13.89)	**14.65** (8.40)	**10.68** (7.38)	**11.47** (6.15)
1.05	**15.13** (10.37)	**15.05** (14.25)	**15.01** (8.00)	**10.91** (7.87)	**11.79** (7.98)
1.20	**15.50** (6.13)	**16.04** (12.26)	**15.03** (6.50)	**11.47** (8.76)	**11.88** (7.00)
1.35	**16.37** (5.02)	**15.74** (5.37)	**15.53** (8.13)	**11.54** (8.47)	**11.70** (7.70)
1.50	**16.24** (4.20)	**16.04** (5.71)	**15.55** (5.74)	**11.79** (10.92)	**11.93** (6.79)
1.65	**16.51** (6.20)	**16.44** (7.13)	**15.66** (8.08)	**11.79** (7.57)	**12.39** (8.61)
1.80	**16.69** (4.45)	**16.64** (7.73)	**16.17** (8.18)	**12.59** (10.15)	**12.30** (6.29)

Mean values in mm appear in bold. The coefficient of variation percentage is shown in the parentheses.

Since S_{6a} and S_{6b} prototypes both showed similar observations, only prototype S_{6a} with 0.6 mm backing layer was used in the statistical analysis as the rest of the designed engineered prototypes had the same design structure. Similar to the observations in the solid flooring trial, the footprint diameter showed a clear tendency to increase with increasing of drop height of the steel ball as shown in Fig 7. Figure 7 also shows the trends observed between the engineered prototypes in comparison with solid sawlog *E. nitens*, solid fiber *E. nitens*, and solid *E. pilularis* boards used in the solid flooring trial.

As shown in Fig 7, prototypes containing 6 mm top layers in sawlog *E. nitens* and fiber *E. nitens* and commercial Tasmanian Oak products with 3 mm thick top layers did not show much variation from the solid boards of the same species. Densified *E. nitens* showed the lowest footprint

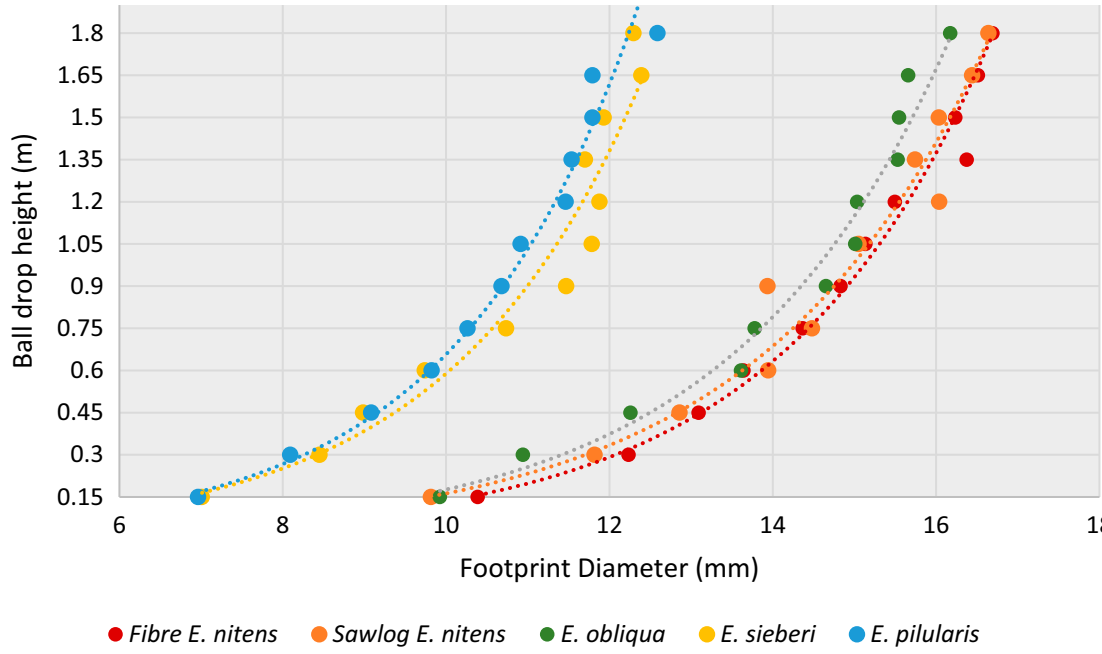

Figure 6. Footprint diameter with different drop heights.

Table 4. Pairwise comparison of solid timber flooring per species and drop height.

		Posthoc pairwise comparison*				
Drop height	*p* value from Welch ANOVA	Sawlog *Eucalyptus nitens*	Fiber *E. nitens*	*Eucalyptus obliqua*	*Eucalyptus pilularis*	*Eucalyptus sieberi*
All heights (0.15-1.8 m)	$p < 0.01$ for all drop heights	a, b	a, c	b, c	d	d

*The same lowercase letter indicates that the pairs are homogenous (ex: a: Sawlog and fibre E. nitens were not statistically significant).

diameter which means the highest impact resistance out of the developed prototypes, followed by 1.2 mm veneer product with *E. nitens* plywood substrate. In contrast, the lowest impact resistance was observed in 1.2 mm *E. nitens* veneer products with marine plywood substrate. It was also observed that the variation of footprint diameter data observed for each drop height was lower in the two veneer products in comparison with the higher-thickness top layers. Solid *E. pilularis* showed the lowest footprint diameter when compared with all products tested in both solid and engineered flooring trials.

Considering the possible deviations from the homoscedasticity of data, Welch's heteroscedastic F test with trimmed means and winsorised variances was used to perform comparisons between the different data groups. The results are presented in Table 6.

To identify the impact of design factors on the impact resistance of tested flooring prototypes, the analysis was conducted on four different categories using the data obtained from both solid and engineered trials. These included four groups evaluating the significance of: a) different top layer material, b) different thicknesses of the same top layer, c) different substrates, and d) comparison with the controls O_{12} and O_3. It should be noted that this experiment is based on a specific experimental design with customized conditions with panels been fixed to structural plywood to replicate in-serve installation, and the results may vary depending on environmental factors, in-service conditions, and installation techniques. Table 6 proves that the pairs compared show statistically significant differences in similar test conditions with the same drop height. Most number of statistically significant differences were observed among the pairs at the 1.8 m drop height of the steel ball. Key observations are as follows:

Impact of different top layers (group a): Other than one pair, all others compared showed significant differences at least for one height. A 6 mm top layers of fiber *E. nitens* (F_6) and sawlog-managed *E. nitens* (S_{6a}) did not show

Table 5. Footprint diameter of prototypes used in engineered flooring trial. Main descriptive statistics (prototype designation as mentioned in Table 2).

Height (m)	D_{12}	S_{6a}	S_{6b}	F_6	$S_{1.2np}$	$S_{1.2mp}$	O_{12}	O_3
0.15	**8.62** (9.68)	**9.20** (11.27)	**9.84** (11.61)	**9.55** (9.57)	**9.80** (11.13)	**9.82** (8.54)	**9.21** (8.84)	**8.74** (10.62)
0.30	**9.86** (8.55)	**10.81** (11.66)	**11.21** (8.18)	**11.27** (17.17)	**11.43** (8.90)	**11.33** (6.73)	**10.67** (8.12)	**11.34** (7.97)
0.45	**11.25** (6.42)	**12.08** (11.94)	**12.14** (8.65)	**12.61** (13.32)	**12.42** (8.59)	**12.88** (6.36)	**11.91** (7.29)	**11.95** (6.17)
0.60	**11.88** (7.72)	**12.72** (8.85)	**12.60** (16.94)	**12.97** (13.46)	**12.92** (8.09)	**13.91** (8.04)	**12.47** (6.13)	**12.83** (8.32)
0.75	**13.15** (6.07)	**13.41** (9.17)	**13.97** (7.99)	**13.99** (13.37)	**13.09** (4.90)	**14.38** (5.42)	**13.43** (11.29)	**13.56** (8.56)
0.90	**13.53** (9.38)	**14.48** (9.33)	**15.06** (10.07)	**15.28** (14.41)	**13.94** (6.10)	**15.07** (5.93)	**13.57** (10.77)	**13.50** (7.02)
1.05	**13.25** (10.00)	**14.21** (8.62)	**15.63** (8.00)	**14.94** (16.80)	**14.36** (6.69)	**15.55** (5.19)	**13.96** (10.39)	**14.55** (7.85)
1.20	**13.63** (8.24)	**15.05** (11.77)	**15.65** (6.54)	**14.52** (22.34)	**14.84** (3.98)	**16.36** (5.82)	**14.60** (8.94)	**14.87** (9.50)
1.35	**14.48** (8.68)	**15.84** (9.54)	**15.90** (7.36)	**15.95** (15.15)	**14.82** (4.09)	**16.83** (5.48)	**14.90** (8.35)	**15.00** (7.54)
1.50	**14.41** (6.83)	**15.79** (7.85)	**16.61** (7.53)	**15.96** (14.96)	**15.28** (4.34)	**17.09** (4.43)	**15.11** (8.41)	**15.33** (5.36)
1.65	**14.61** (7.88)	**16.24** (8.17)	**16.73** (7.54)	**16.88** (14.45)	**15.18** (7.32)	**17.01** (3.98)	**15.35** (7.69)	**15.42** (6.32)
1.80	**14.52** (7.88)	**17.05** (8.73)	**17.24** (10.84)	**17.47** (6.48)	**15.86** (5.30)	**17.57** (5.06)	**15.74** (10.64)	**15.85** (5.67)

Mean values in mm appear in bold. The coefficient of variation percentage is shown in the parentheses.

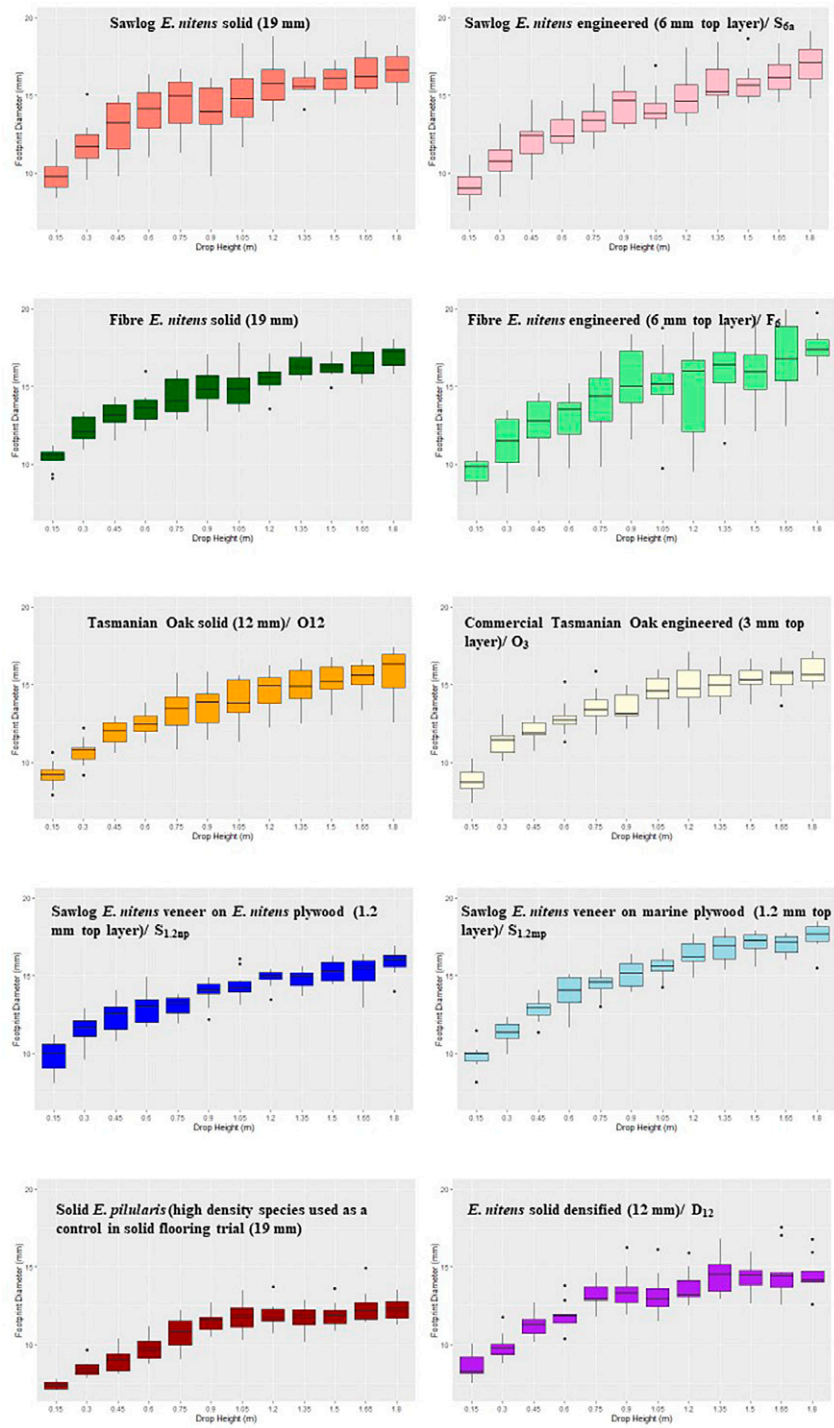

Figure 7. Boxplot graphics: footprint diameter trend against ball drop height for different flooring products.

Table 6. Pairwise comparison of footprint diameter of prototypes.

	Drop height (m)											
Pairs	0.15	0.30	0.45	0.60	0.75	0.90	1.05	1.20	1.35	1.50	1.65	1.80
Group a: different top layers												
F_6 (6mm Fiber *Eucalyptus nitens*) × S_{6a} (6mm Sawlog *E. nitens*)	=	=	=	=	=	=	=	=	=	=	=	=
F_6 (6mm Fiber *E. nitens*) × $S_{1.2np}$ (1.2mm Sawlog *E. nitens* on E. nitens Plywood)	=	=	=	=	=	=	=	=	=	=	=	×
D_{12} (12mm Densified *E. nitens*) × Solid 19 mm Sawlog *E. nitens*	×	×	×	×	=	=	×	×	×	×	×	×
D_{12} (12mm Densified *E. nitens*) × S_{6a} (6mm Sawlog *E. nitens*)	=	×	=	=	=	=	=	=	=	×	×	×
D_{12} (12mm Densified *E. nitens*) × F_6 (6mm Fiber *E. nitens*)	×	=	×	=	=	×	×	=	=	=	×	×
D_{12} (12mm Densified *E. nitens*) × $S_{1.2np}$ (1.2mm Sawlog *E. nitens* on *E. nitens* Plywood)	×	×	×	×	×	=	×	=	=	=	=	×
D_{12} (12mm Densified *E. nitens*) × $S_{1.2mp}$ (1.2 mm Sawlog *E. nitens* on Marine Plywood)	×	×	×	×	×	×	×	×	×	×	×	×
Group b: different top layer thicknesses												
Solid 19 mm Sawlog *E. nitens* × S_{6a} (6 mm Sawlog *E. nitens*)	=	=	=	=	=	=	=	=	=	=	=	=
Solid 19 mm Sawlog *E. nitens* × $S_{1.2np}$ (1.2mm Sawlog *E. nitens* on *E. nitens* ply)	=	=	=	=	=	=	=	=	×	=	=	=
Solid 19 mm Sawlog *E. nitens* × $S_{1.2mp}$ (1.2mm Sawlog *E. nitens* on Marine Plywood)	=	=	=	×	=	=	=	=	×	×	=	×
S_{6a} (6 mm Sawlog *E. nitens*) × $S_{1.2np}$ (1.2mm Sawlog *E. nitens* on *E. nitens* Plywood)	=	=	=	=	=	=	=	=	×	=	=	=
S_{6a} (6 mm Sawlog *E. nitens*) × $S_{1.2mp}$ (1.2mm Sawlog *E. nitens* on Marine Plywood)	=	=	=	×	×	=	×	=	=	×	=	=
Solid 19 mm Fiber *E. nitens* × F_6 (6mm Fiber *E. nitens*)	×	=	=	=	=	=	=	=	=	=	=	=
O_{12} (12mm Solid *Eucalyptus obliqua*) × O_3 (3mm Tasmanian Oak on Rubberwood)	=	=	=	=	=	=	=	=	=	=	=	=
Group c: different substrates												
$S_{1.2np}$ (1.2mm Sawlog *E. nitens* on *E. nitens* Plywood) × $S_{1.2mp}$ (1.2mm Sawlog *E. nitens* on Marine Plywood)	=	=	=	×	×	×	×	×	×	×	×	×
Group d: comparison with controls												
O_{12} (12mm Solid *E. obliqua*) × S_{6a} (6mm Sawlog *E. nitens*)	=	=	=	=	=	=	=	=	=	=	=	=
O_3 (3mm Tasmanian Oak on Rubberwood) × S_{6a} (6mm Sawlog *E. nitens*)	=	=	=	=	=	=	=	=	=	=	=	=
O_{12} (12mm Solid *E. obliqua*) × $S_{1.2np}$ (1.2mm Sawlog *E. nitens* on *E. nitens* Plywood)	=	=	=	=	=	=	=	=	=	=	=	=
O_3 (3mm Tasmanian Oak on Rubberwood) × $S_{1.2np}$ (1.2mm Sawlog *E. nitens* on *E. nitens* Plywood)	=	=	=	=	=	=	=	=	=	=	=	=
O_{12} (12mm Solid *E. obliqua*) × $S_{1.2mp}$ (1.2mm Sawlog *E. nitens* on Marine Plywood)	=	=	×	×	×	×	×	×	×	×	×	×
O_3 (3mm Tasmanian Oak on Rubberwood) × $S_{1.2mp}$ (1.2mm Sawlog *E. nitens* on Marine Plywood)	×	=	×	×	=	×	=	×	×	×	×	×
O_{12} (12mm Solid *E. obliqua*) × F_6 (6mm Fiber *E. nitens*)	=	=	=	=	=	=	=	=	=	=	=	×
O_3 (3mm Tasmanian Oak on Rubberwood) × F_6 (6mm Fiber *E. nitens*)	=	=	=	=	=	×	=	=	=	=	=	×
O_{12} (12mm Solid *E. obliqua*) × D_{12} (12mm Densified *E. nitens*)	=	×	=	=	=	=	=	=	=	=	=	=
O_3 (3mm Tasmanian Oak on Rubberwood) × D_{12} (12mm Densified *E. nitens*)	=	×	×	×	=	=	×	×	=	×	=	×

×, difference is statistically significant ($p < 0.05$); =, difference is not statistically significant ($p > 0.05$).

statistical significance in all tested drop heights. F_6 showed significantly lower impact resistance with veneer product on *E. nitens* plywood substrate ($S_{1.2np}$) only at 1.8 m drop height. Densified *E. nitens* (D_{12}) showed statistically significant higher impact resistance in all tested pairs and was statistically different with 1.2 mm veneer product on marine plywood substrate ($S_{1.2mp}$) at all the considered drop heights.

Impact of different top layer thicknesses (group b): A 19 mm thick solid sawlog *E. nitens* did not show statistical difference with 6 mm top layer of the same species. Similar observations resulted with fiber *E. nitens* where statistical difference was only observed at the lowest drop height of 0.15 m. *E. obliqua* 12 mm thick solid overlay (O_{12}) and 3 mm thick Tasmanian Oak top layer in the commercial engineered product (O_3) also did not show statistical difference at any of the drop heights, suggesting that higher thicknesses in top layers (3-6 mm as observed in the present study) showed similar behavior with solid boards of the same species. However, the two veneer products with 1.2 mm top layers showed significant differences with higher thickness material. $S_{1.2np}$ showed significantly higher impact resistance at 1.35 m drop height with 19 and 6 mm thick sawlog *E. nitens* products. In contrast, $S_{1.2mp}$ showed significantly lower impact resistance with 19 mm sawlog *E. nitens* in four heights (0.6, 1.35, 1.5, and 1.8 m) and with 6 mm sawlog *E. nitens* in four drop heights as well (0.6, 0.75, 1.05, and 1.5 m). This proves that at thinner top-layer thicknesses, the impact resistance is governed by the substrate rather than the top-layer properties.

Impact of different substrates (group c): A comparison was conducted between the two veneer products which had similar structures and designs other than the core layer material. The results showed that $S_{1.2mp}$ with marine plywood (density: 495 kg m^{-3}) was significantly lower in impact resistance measured as footprint diameter in the majority of the tested drop heights (0.6-1.8 m) when compared with $S_{1.2np}$ with *E. nitens* plywood core layer (density: 765 kg m^{-3}) further confirming the observations of group b.

Comparison with controls (group d): All engineered prototypes developed were compared with 12 mm *E. obliqua* overlay (O_{12}) and the prefinished Tasmanian Oak commercial engineered product (O_3). O_{12} and O_3 both did not show significant differences with sawlog *E. nitens* engineered products (S_{6a} and $S_{1.2np}$) in all tested drop heights. O_{12} and O_3 both showed statistically higher impact resistance with F_6 in 1.8 m drop height. Both O_{12} and O_3 showed higher impact resistance in most of the tested drop heights in comparison with 1.2 mm sawlog *E. nitens* with marine ply substrate ($S_{1.2mp}$). O_{12} and densified *E. nitens* (D_{12}) were statistically different only at 0.3 m drop height while O_3 was statistically different with D_{12} in seven drop heights (0.3, 0.45, 0.6, 1.05, 1.2, 1.5, and 1.8 m).

At the start of this research, no published studies were available on how Tasmanian plantation-grown *E. nitens* would behave in a flooring application. An in-service trial conducted at the premises of the University of Tasmania during 2007-2009 indicated that only a few millimeters of resanding was required to remove the indentations caused by stiletto heels during the in-service trial. This was found to be comparable to native *E. obliqua* which was used as a control in the study. However, these findings were from personal communication with the research team, and due to unforeseen circumstances, it had not been reported. To understand how this novel timber resource would behave in flooring applications, it was decided to install a solid flooring trial before designing the engineered flooring prototypes. The observations proved that sawlog-managed *E. nitens* behaved comparable to native *E. obliqua* in stability considerations and had an aesthetic appeal due to its lighter color similar to Scandinavian timbers which is currently in trend in the flooring market. There are few studies reported in the literature on in-service trials, in comparison with studies based on analysis of individual timber properties. Harper (1961) is one of the early literatures mentioning the use of in-service trials

for flooring materials. Harper (1961) suggests that it is an essential requirement in practical trials of materials that they should have usage of equivalent type and need to be as severe as possible to generate quick results. These two requirements have resulted in most researchers selecting places of high traffic exposure and large spaces for a series of finished products to be laid. The study further suggests that if the traffic remains constant or can be counted, several successive series can be compared for the purpose. Although moderate traffic conditions and exposure to sunlight were observed in the premises where the in-service trials were conducted in the present study, it facilitated quick results under extreme environmental conditions and provided higher traffic exposure than expected in an usual domestic application. Since the study is focusing on the potential of using plantation *E. nitens* in domestic or light commercial applications, the conditions herein provide comparable exposure situations.

It was observed that both types of engineered prototypes: consisting of 6 mm thick *E. nitens* top layers and 1.2 mm thick *E. nitens* top layers behaved comparatively as per visual observations. However, further analysis is recommended to understand how the 1.2 mm thick top layers might behave when exposed to the conditions over longer time periods and more traffic exposure. The feedback received on the developed prototypes from several architects and flooring manufacturers had different focuses on the significance of the thickness of top layers of engineered flooring products. The architects preferred 6 mm thick top layers as it gave them confidence in specifying the product with the knowledge of the possibility to resand the product and considered the product to be more sustainable as it ensured longer life spans for the product. However, some flooring manufacturers and experts expressed that most domestic household floors never get resanded and usually get replaced when the installed product gets out of fashion and that both 6 and 1.2 mm products provided the same surface appearance which is the major consideration by many domestic consumers when selecting a product.

Previous research suggests that dynamic hardness tests may more reliably simulate timber flooring performance in-service than static load tests (Oliveira et al 2019; Acuña et al 2020; Sepliarsky et al 2022). In addition, it can be conducted on an installed floor without the need for sophisticated equipment. As per ASTM D 2394 (2017), the falling ball indentation test requires to determine the indentation index by determining the intercept at 1.8 m drop height from the plotted graph between the drop heights and indentation depth. The present study conducted a modified approach to the method as followed by Acuña et al (2020) and Sepliarsky et al (2022), and used indentation diameter instead of the indentation depth as measuring the footprint diameter is more precise than measuring the indentation depth (Sepliarsky et al 2022).

Based on the observations of the falling ball indentation results in the present study, different top layer properties (densification), top layer thicknesses, and substrates had an impact on the residual footprint diameter caused by the steel ball. The observations showed that 6 and 3 mm thick top layers behaved similarly to a 19 mm thick solid timber board of the same species. This observation is different from the observations reported in Sepliarsky et al (2022) where the majority of significant differences were observed between solid timber boards of 25 mm thick *Q. robur* and *Hymenaea courbaril* and 16 mm thick *Eucalyptus globulus* and *Eucalyptus grandis* when compared with 3 mm thick top layer engineered products from each species when subjected to falling ball impact test of three diameter types of steel balls (50, 40, and 30 mm) at five drop heights (0.60, 0.75, 0.90, 1.05, and 1.20 m). The engineered products used in the study had a 9 mm thick high-density fiberboard substrate (density: 850 kg m^{-3}) and an additional 2 mm thick *Pinus radiata* layer (density: 500 kg m^{-3}) backing. *E. globulus* (density: 855 kg m^{-3}) and *E. grandis* (density: 490 kg m^{-3}) used in the study were fast-growing plantation timber from Spain. Figure 8 shows the results obtained in the present study for solid boards of sawlog- and fiber-managed *E. nitens* and *E. obliqua* in

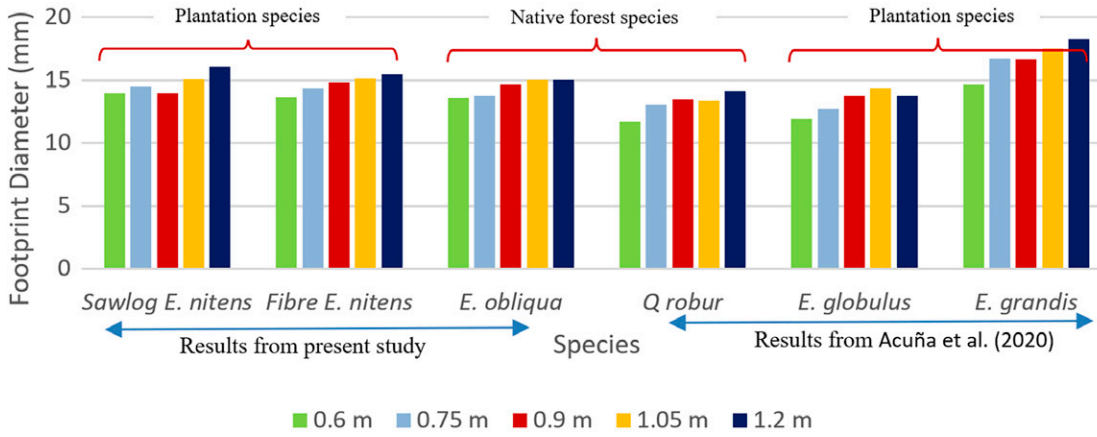

Figure 8. Comparison of the results from the present study with Acuña et al (2020).

comparison with values obtained in Acuña et al (2020) for solid *Q. robur*, *E. globulus*, and *E. grandis* boards subjected to the impact of a 50 mm diameter steel ball when dropped from five height intervals ranging from 0.60 to 1.20 m.

The results for footprint diameter of sawlog *E. nitens* (density: 510 kg m^{-3}), fiber *E. nitens* (density: 480 kg m^{-3}) and *E. obliqua* (density: 600 kg m^{-3}) in the present study were higher than those reported in Acuña et al (2020) for *Q. robur* (density: 685 kg m^{-3}) and *E. globulus* (density: 855 kg m^{-3}) but lower than those reported for plantation *E. grandis* (density: 490 kg m^{-3}). The differences in density of the tested species likely account for these observations. Furthermore, Sepliarsky et al (2022) reported an extension to the results from Acuña et al (2020), where comparisons were conducted between solid boards and 3 mm thick engineered flooring products from *Q. robur, H. courbaril, E. globulus*, and *E. grandis* with engineered products with 0.6 mm veneers from the same species. The top layer consisted of a sliced 0.6 mm veneer, a 9 mm thick HDF panel (density: 850 kg m^{-3}), and a 0. 5 mm thick *P. radiata* backing veneer (density: 500 kg m^{-3}). Similarly, the 1.2 mm *E. nitens* top layers used in the prototypes in the present study consisted of 0.6 mm sliced veneer which was glued together to obtain a 1.2 mm thickness. The results by Sepliarsky et al (2022) suggests lowest footprint diameter for each species was observed in the products with 0.6 mm veneer supporting the lower footprint diameters observed in the 1.2 mm thick top layer product with *E. nitens* plywood substrate in the present study. Similarly, the present study confirms that the design configuration of engineered timber flooring has an impact on its structural performance, especially when thinner top layers are of concern. In lower thinner layers, the substrate layer is responsible for absorbing the impact energy and actively forces the outer layer to recover from the deformation caused by external force on the surface.

CONCLUSIONS

Based on the observations of the in-service trials and results from falling ball indentation tests, the following key outcomes can be highlighted.

Sawlog *E. nitens* solid boards and engineered flooring products with sawlog *E. nitens* top layers showed similar behavior in comparison with *E. obliqua* in the solid flooring trial and dynamic hardness tests. Hence, sawlog *E. nitens*, a short-rotation, low-density species, may hold potential as an alternative species for the domestic and light commercial flooring market, especially in view of the limited access to native, high-density species in the upcoming years. Some boards in the fiber

E. nitens panel showed cracks after 3 mo of installation in the solid flooring in-service trial. Although this reduced the aesthetic acceptance of the product, further assessment with falling ball indentation tests was conducted on the panel to determine the dynamic hardness of the product. Falling ball indentation tests were conducted to generate new knowledge on the resource and as an alternative test for traditional hardness tests, better simulating the in-service conditions of an end product. Fiber *E. nitens* showed lower indentation resistance in comparison with sawlog *E. nitens* and *E. obliqua* but the values were not significantly different. It should be noted that the age, density of the plantation, site productivity, and location were not considered in the present study due to the material having been obtained from commercial facilities. These variables could impact the results but are beyond the scope of this study.

Among the developed engineered flooring prototypes, the highest indentation resistance was reported for densified *E. nitens* based on falling ball indentation tests. However, the densified timber boards showed increased brittleness during the processing stage. Further research on densification techniques for *E. nitens* has been identified as an important future research area. With respect to design aspects, the replacement of the solid timber with 12 mm thick plywood as a substrate showed a significant variation in the resistance to indentation with top layers of 1.2 mm thickness. The footprint diameter caused on the 1.2 mm top layer product with *E. nitens* backing demonstrated performance comparable to (or better than) those of solid timber flooring and engineered flooring with a 6 mm thick top layer. Although both veneer products tested in the study showed similar behavior in-service, the falling ball indentation test showed that the high-density substrate resulted in a significantly lower footprint diameter due to impact energy caused by the dropping of the steel ball. Similar observations were reported in Sepliarsky et al (2022) and Sydor et al (2020, 2022), where high-density substrate improved the behavior of the flooring product in terms of hardness tests, regardless of the hardwood species used in thinner top layers. This implies that using a high-density substrate and thinner top layers (0.6-1.2 mm) of the solid wood may produce a high-quality, low-cost final product with better performance in terms of resistance to denting caused by dynamic impacts. For instance, many producers in Europe produce engineered flooring with veneer top layers with high-density fiberboard in the substrate claiming the resistance to impact is better than the conventional engineered flooring products with 3 mm thick top layers (Sepliarsky et al 2022). However, it is important to note that the technical lifespan of a product is reduced in such circumstances due to the limitations of recoating and resanding. Usually, veneer flooring with top layers less than 0.7 mm might only be subjected to recoating and not resanding (Sepliarsky et al 2022). Therefore, such products should be developed to suit an expected end-use application, so that the consumers understand the expected performance of the product.

ACKNOWLEDGMENTS

National Institute for Forest Product Innovation (NIFPI) and the industry partners associated (including Britton Timbers, Neville Smith Forest Products, and Ta Ann) with the project are acknowledged for funding and support for this research (grant number: NT015/NIF079). Benoit Belleville from the University of Melbourne is acknowledged for conducting densification of timber samples and provision of insight. The authors are grateful for the support given by Launceston College for the in-service trial. Luke Dineen, Stuart Meldrum, and Malcolm Liehr are acknowledged for their technical assistance and support.

REFERENCES

ABARES (2022) Australian plantation statistics 2022 update. Canberra, ABARES. https://doi.org/10.25814/8ghb-em15.

Acuña L, Sepliarsky F, Spavento E, Martínez RD, Balmori J-A (2020) Modelling of impact falling ball test response on solid and engineered wood flooring of two Eucalyptus species. Forests 11(9):933-952.

AS 2082 (2007) Timber—Hardwood—Visually stress graded for structural purposes. Standards Australia, Sydney, Australia.

AS 2796.2 (1999) Timber—Hardwood—Sawn and milled products, part 2: Grade description. Standards Australia, Sydney, Australia.

AS/NZS 1080.1 (2012) Timber—Methods of test—Moisture content. Standards Australia, Sydney, Australia.

AS/NZS 1080.3 (2000) Timber—Methods of test, method 3: Density. Standards Australia, Sydney, Australia.

ASTM D 143 (2000) Standard test methods for small clear specimens of timber. American Society for Testing and Materials (ASTM) International, Conshohocken, PA.

ASTM D 1037 (1999) Standard test methods for evaluating properties of wood-base fiber and particle panel materials. American Society for Testing and Materials (ASTM) International, Conshohocken, PA.

ASTM D 2394 (2017) Standard methods for simulated service testing of wood and wood-base finish flooring. American Society for Testing and Materials (ASTM), Conshohocken, PA.

ATFA (2009a) The final appearance. Australian Timber Flooring Association, Shelly Beach, Queensland, Australia.

ATFA (2009b) Owner expectations for completed floors. Australian Timber Flooring Association, Shelly Beach, Queensland, Australia.

ATFA (2010) Timber flooring hardness. Australian Timber Flooring Association, Shelly Beach, Queensland, Australia.

ATFA (2011) Hardwood species names. Australian Timber Flooring Association, Shelly Beach, QLD, Australia.

ATFA (2012) Engineered flooring industry standards. Australian Timber Flooring Association, Shelly Beach, Queensland, Australia.

Belleville B (2021) Developing a new generation of appearance hardwood products for in-state design and manufacturing: NIF079 milestone #3 report. The University of Melbourne Faculty of Science.

Blanchet P, Beauregard R, Cloutier A, Gendron G, Lefebvre M (2002) Evaluation of various engineered wood flooring constructions. For Prod J 53(5):30-37.

BS 8201 (2011) Code of practice for installation of flooring of wood and wood-based panels. British Standards Institution (BSI), London, UK.

Castro G, Zanuttini R (2004) Multilaminar wood: Manufacturing process and main physical-mechanical properties. For Prod J 54(2):61-67.

Chen Q, Guo X, Ji F, Wang J, Wang J, Cao P (2015) Effects of decorative veneer and structure on the thermal conductivity of engineered wood flooring. BioResources 10(2):2213-2222.

Derikvand M, Kotlarewski N, Lee M, Jiao H, Nolan G (2019) Characterisation of physical and mechanical properties of unthinned and unpruned plantation-grown *Eucalyptus nitens* H. Deane & Maiden lumber. Forests 10(2):194-207.

Drerup MJ, Erdem I, Anthony RW (2013) Trouble underfoot—In situ and laboratory investigation of engineered wood flooring. San Francisco, CA, USA, 31 October–3 November 2012; pp. 621–630 *in* Forensic engineering 2012: Gateway to a safer tomorrow. https://doi.org/10.1061/9780784412640.066.

EN 1534 (2020) Wood flooring and parquet—Determination of resistance to indentation—Test method. European Committee for Standardisation (CEN), Brussels, Belgium.

European Parquet Federation (2023) The European parquet industry in 2022, *Press Release*, Brussels, Belgium. Accessed 30 June 2023.

FAO (2020) Global forest resources assessment 2020: Main report. Rome. Accessed 29 September 2023. https://www.fao.org/documents/card/en/c/ca9825en.

Grześkiewicz M, Kozakiewicz P, Borysiuk P, Romanovski V, Cichy A (2020) Influence of top layer density and thickness on hardness of two-layer floor elements. Drewno 63(205):69-80.

Harper F (1961) The abrasion resistance of flooring materials: A review of methods of testing. Wear 4(6):461-478.

Harwood C (2010) Sawn timber from native forests and plantations in Tasmania. Coop Res Centre For Bull 13. https://www.crcforestry.com.au/publications/downloads/Bulletin-13-Sawn-timber-properties.pdf.

Khademibami L, Shmulsky R, Snow D, Sherrington A, Montague I, Ross RJ, Wang X (2022) Wear resistance and hardness assessment of five US hardwoods for bridge decking and truck flooring. For Prod J 72(s1):8-13.

Knox A (2016) Timber flooring systems market research, project grain. Pollinate. https://fwpa.com.au/timber-flooring-systems-market-research/ (5 May 2023).

Millaniyage K, Kotlarewski N, Taoum A, Wallis L (2023) The role of abrasion resistance in determining suitability of low-density plantation timber for engineered flooring. Forests 14(7):1309-1324.

Millaniyage K, Kotlarewski N, Wallis L, Taoum A, Nolan G (2022) Janka hardness evaluation of plantation-grown *Eucalyptus nitens* for engineered flooring applications. Buildings 12(11):1862-1876.

Németh R, Posch PM, Molnár S, Bak M (2014) Performance evaluation of strip parquet flooring panels after long-term, in-service exposure. Drewno 57(193):119-134.

Neyses B, Sandberg D (2015) A new methodology to select hardwood species for wooden products. Wood Mater Sci Eng 10(4):344-352.

Oliveira MB, Silva JRM, Hein PRG, Lima JT (2019) Establishment of quality classes for hardwood floorings by simulated use. Cerne 25(1):105-109.

Onfray R, Ravenwood I, Dean G, de Little D (2015) Surrey Hills, northwest Tasmania—The birthplace of industrial-scale eucalypt plantations in Australia. Pages 21–24 *in* Ninth National Conference of the Australian Forest History Society Inc, Mount Gambier, South Australia. Accessed 20 September 2023. https://www.foresthistory.org.au/2015_conference_papers/08-Onfray.pdf.

Sepliarsky F, Acuña L, Balmori J-A, Martínez RD, Spavento E, Keil G, Casado M, Martín-Ramos P (2022) Modeling of falling ball impact test response on solid, veneer, and traditional engineered wood floorings of several hardwoods. Forests 13(2):167-181.

STT (2022) Sustainable high quality eucalypt sawlog supply from Tasmania's permanent timber production zone land. Sustainable Timber Tasmania. Accessed 23 September 2023. Online, DOI chrome-extension://efaidnbmnnnibpcajpcglclefindmkaj/https://sttwebdata.blob.core.windows.net/stt-prod/assets/Sustainable_Yield_Report_6_FINAL_ae09c6e8ea.pdf.

Sydor M, Pinkowski G, Jasińska A (2020) The Brinell method for determining hardness of wood flooring materials. Forests 11(8):878-891.

Sydor M, Pinkowski G, Kučerka M, Kminiak R, Antov P, Rogoziński T (2022) Indentation hardness and elastic recovery of some hardwood species. Appl Sci 12(10):5049-5063.

Tenorio C, Moya R (2019) Development of a thermo-hydro-mechanical device for wood densification adaptable to universal testing machines and its evaluation in a tropical species. J Test Eval 49(4):2597-2608.

Uddin MM (2021) Improving product quality and production yield in wood flooring manufacturing using basic quality tools. Ijqr 15(1):155-170.

Vörös Á, Németh R (2020) The history of wood hardness tests. IOP Conf Ser Earth Environ Sci 505. doi:10.1088/1755-1315/505/1/012020.

Washusen R, Harwood C, Morrow A, Northway R, Valencia JC, Volker P, Wood M, Farrell R (2009) Pruned plantation-grown *Eucalyptus nitens*: Effect of thinning and conventional processing practices on sawn board quality and recovery. N Z J For Sci 39(1):39-55.

Wood Solutions (2020) Oak, Tasmanian. Forest and Wood Products Australia Ltd. https://www.woodsolutions.com.au/wood-species/oak-tasmanian (9 April 2021).

EVALUATION OF FLAME RETARDANT IMPREGNATION IN PERFORATED HINOKI (*CHAMAECYPARIS OBTUSA*) PLYWOOD

Eun-Suk Jang
Ph.D.
Research Institute of Human Ecology, College of Human Ecology
Jeonbuk National University
Jeonju 54896, South Korea
and
Sambo Scientific Co. Ltd, R&D Center
Seoul 07258, South Korea
E-mail: esjang@sambosc.com

Woo-Jong Yong
Master
E-mail: yong900305@naver.com

Seok-Un Jo
Ph.D.
E-mail: jo18041@naver.com

Chun-Won Kang†
Professor
E-mail: kcwon@jbnu.ac.kr

*Hee-Jun Park**
Professor
Department of Housing Environmental Design, College of Human Ecology
Jeonbuk National University
Jeonju 54896, South Korea
E-mail: phjun@jbnu.ac.kr

(Received June 2023)

Abstract. Recently, perforated plywood has been widely used as an indoor sound absorber. Flame retardant treatment is essential for the utilization of wood materials as indoor building materials. Among the various flame retardant treatment methods, we focused on pressure impregnation of water-soluble phosphate flame retardant in commercial Hinoki (*Chamaecyparis obtusa*) plywood. Experimental perforation rates were 0.06%, 0.1%, 0.3%, and 1.7%, and impregnation times were 30, 60, and 90 min. Then, we evaluated the impregnation as a function of plywood perforation frequency and impregnation time using Pearson's coefficient correlation analysis and multilinear regression analysis. The greater the perforation frequency and impregnation time, the greater the impregnation. Increasing impregnation correspondingly improved the performance of the flame retardant.

Keywords: Flame retardant, WPFR, Hinoki, *Chamaecyparis obtuse*, impregnation, perforated plywood.

INTRODUCTION

Wood possesses inherent natural characteristics, providing stability, and aesthetic appeal (Shen et al 2021; Jang 2022b). In addition, wood can capture atmospheric carbon dioxide, which can contribute to climate change mitigation (Howard et al 2021; Jang 2022a).

Commercial wood materials are broadly divided into solid wood, fiberboard, particleboard, and

* Corresponding author
† SWST member

plywood. Plywood has been used since ancient Egyptian times, and its use began to expand in the mid-19th century (Fekiač et al 2021). Plywood products rose to prominence in the early 1900s due to two significant advancements: the introduction of synthetic waterproof adhesives and the subsequent development of robust and long-lasting wood composites (Hughes 2015). These products have extensive applications in furniture manufacturing as a versatile decorative element and in residential construction projects (Li et al 2021; Mai et al 2022).

The COVID-19 pandemic greatly increased the time spent indoors (Andargie et al 2021; Jang 2022c), drawing more attention to comfortable indoor environments. Critical factors for creating such an environment are temperature and humidity control, indoor air quality, lighting, and noise control (Ncube & Riffat 2012). In particular, noise can disrupt work and activities and also contribute to stress (Wallenius 2004). The easiest way to overcome these challenges is by introducing sound-absorbing materials into the indoor space (Jang 2023). In Korea, interest in perforated plywood, an eco-friendly sound-absorbing material, is increasing. Perforated plywood can act as a resonant sound-absorbing material when the size and frequency of its perforations and the distance from the back space are adjusted (Song et al 2016; Peng et al 2018; Fekiač et al 2021).

Although perforated plywood has excellent sound absorption performance, it has a dangerous disadvantage of flammability as an interior building material. Therefore, many countries have mandated flame retardant treatment for wood as a building material (Vojta et al 2017; Park et al 2020; Xiong et al 2020). However, the lack of regulation regarding the flame retardancy of wood in various interior applications is a reality in many countries.

Applying flame retardant treatment to wood can significantly improve its fire safety. Flame retardant chemicals often include elements such as halogens, nitrogen, boron, phosphorus, aluminum, iron, magnesium, or their various combinations (Chen et al 2021).

Two methods are commonly employed to apply flame retardants to wood: coating (Hu & Sun 2021; Chu et al 2022) and impregnation (Fu et al 2017; Lu et al 2022). These methods bear similarities to wood preservation treatments. We focused on flame retardant impregnation of perforated plywood.

In a previous study, Jang and Kang (2023b) investigated the impregnation of larch (*Larix kaempferi*) and pine (*Pinus koraiensis*) wood with preservatives. Multiple regression analysis was performed to determine the influence of pressure, temperature, and time on wood impregnation. The results revealed that pressure had the most significant effect on the impregnation process. In addition, Jang and Kang (2023a) introduced a steam explosion treatment to improve the chemical impregnation capacity of wood and reported improved impregnation through the creation of microcracks in the cell walls of the wood, increasing the open pore content.

Based on the results of these previous studies, we investigated the effect of perforation frequency on the impregnation of flame retardants in perforated plywood. We hope that our findings will enable improvements to the flame retardant impregnation of perforated plywood.

MATERIALS AND METHODS

Sample Preparation

In this study, we prepared commercial Hinoki (*Chamaecyparis obtusa*) plywood obtained from Gaonwood in Jeonju, Korea. The plywood was thermoformed using a 1.7-mm veneer with a petroleum resin adhesive, and its dimensions were 1220 mm (W) × 2440 mm (L) × 18 mm (T). The MC (MC) was measured as 10.6 (0.6, standard deviation) % using an electric MC meter.

We cut a piece of plywood to a size of 180 mm (W) × 360 mm (L) and used a computer numerical control to drill 5-mm-diameter holes. Figure 1 shows drawings of the samples with different hole spacing. Sample A represents unperforated plywood, whereas Samples B, C, D, and E have perforation rates of 0.06% (5 mm diameter, hole spacing of 120 mm), 0.1% (5 mm diameter,

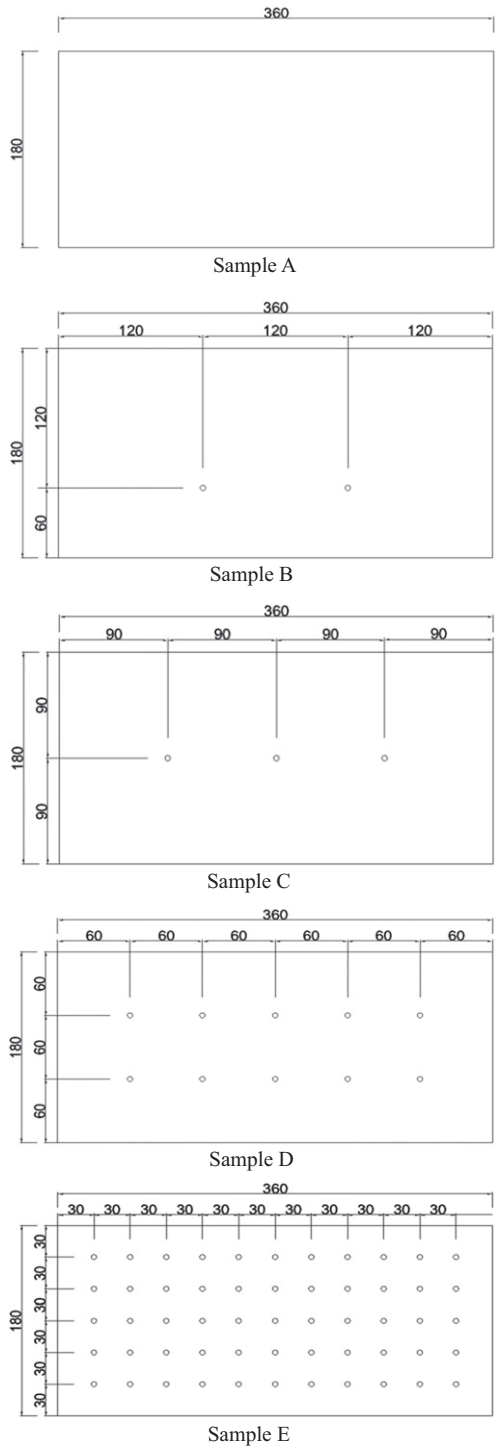

Figure 1. Schematics of Hinoki plywood with different perforation spacings.

hole spacing of 90 mm), 0.3% (5 mm diameter, hole spacing of 60 mm), and 1.7% (5 mm diameter, hole spacing of 30 mm), respectively.

Flame Retardant

We used a water-soluble phosphate flame retardant (WPFR) provided by Samwha Paints Industrial Co., Ltd (Seoul, Korea) for impregnation. The composition of WPFR includes ammonium phosphate polymer, guanylurea phosphate, phosphoric acid, and additives. WPFR has a resin content of 25%, a specific gravity of 1.13, and a pH of 7.6. To visually identify the flame retardant penetration into the plywood, we mixed WPFR and water-soluble blue ink in a 30:1 ratio.

Impregnation Process

We applied the four-step WPFR impregnation process model, as shown in Fig 2. In Step 1, the specimen was placed inside a cylinder and subjected to depressurization at −0.098 MPa for 5 min using a vacuum pump to remove any air trapped inside the specimen. In Step 2, the cylinder was filled with WPFR while maintaining the reduced pressure. In Step 3, the pump was activated to pressurize the cylinder to 1.5 MPa. The pressurization duration was 30, 60, or 90 min. Finally, the cylinder was depressurized for 5 min at −0.098 MPa.

Visual Inspection

After the impregnation process, the specimens were dried in a laboratory oven at 100°C for 12 h.

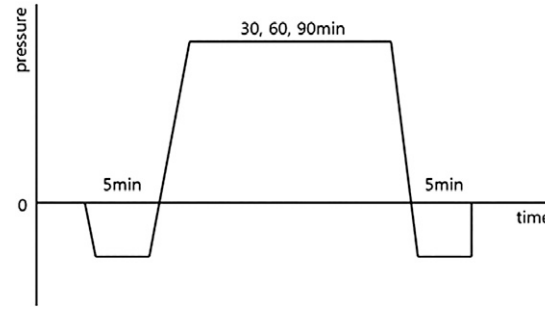

Figure 2. Water-soluble phosphate flame retardant impregnation.

The samples were cut through the center of the perforation to observe the surface.

Evaluation of WPFR Impregnation

We measured the mass of WPFR impregnation as the difference in weight of the specimen before and after impregnation (Eq 1) (Wang & Zhao 2022).

$$\text{WPFR impregnation } \left(\text{g/cm}^3\right) = \frac{M_a - M_b}{V} \quad (1)$$

where M_a is the mass of the specimen before impregnation (g), M_b is the mass of the specimen after impregnation (g), and V is the volume of the air-dried sample (cm^3).

Pearson correlation analysis was used to determine the influence of individual factors (impregnation time, perforation rate) on WPFR impregnation. In addition, we performed a multiple linear regression analysis to determine the combined effect of impregnation time and perforation rate on WPFR impregnation (Eq 2). This study used IBM SPSS Statistics 26 (Armonk, NY) for statistical analysis.

$$Y = \alpha_0 + \beta_1 X_1 + \beta_2 X_2 + \varepsilon \quad (2)$$

where Y is the WPFR impregnation, X_1 is the impregnation time, X_2 is the perforation rate, and ε is the residual (error term).

Combustion Test

A 45° angle combustion test was performed to evaluate the flammability of the samples (Nguyen et al 2012). The combustion test apparatus utilized a McClelland burner (SJTK-008-B, Sejin, Korea). The plywood panels were installed at a 45-degree angle, and the burner flame length was set to 65 mm for 2 min (KFIA 2017). Subsequently, the carbonized length and area of plywood were measured. This test was conducted on untreated plywood, Sample A, and Sample E.

RESULTS AND DISCUSSION

Visual Inspection

Figure 3 presents cross-sectional views of impregnated Hinoki plywood samples with varying impregnation rates and times. Overall, higher perforation frequencies and longer impregnation times result in improved penetration of the chemical solution.

Effect of Hole Spacing on Impregnation

Figure 4 provides the impregnation results for the perforated Hinoki plywood for different impregnation times and perforation rates. In nonperforated plywood (Sample A), the WPFR impregnation mass was 0.37 ± 0.01 g/cm^3 (± is standard deviation) after an impregnation time of 30 min. However, for the 1.7% perforated plywood (Sample E), the WPFR impregnation mass was 0.46 ± 0.01, indicating an approximately 1.2-fold increase in impregnation mass compared with the nonperforated condition. This difference was statistically significant ($p < 0.01$) based on Tukey's test using ANOVA.

For Sample A, the 60-min impregnation mass was 0.53 ± 0.01 g/cm^3, and the 90-min impregnation mass was 0.63 ± 0.01 g/cm^3. When perforated by 1.7%, the WPFR impregnation mass was improved by about 1.2 times compared with no perforation ($p < 0.01$). Further, after an impregnation time of 90 min, the impregnation mass of

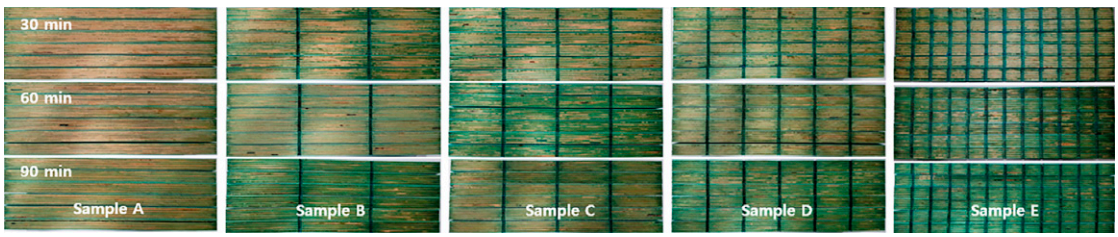

Figure 3. Photographs of impregnated Hinoki plywood with different perforation rates and impregnation times.

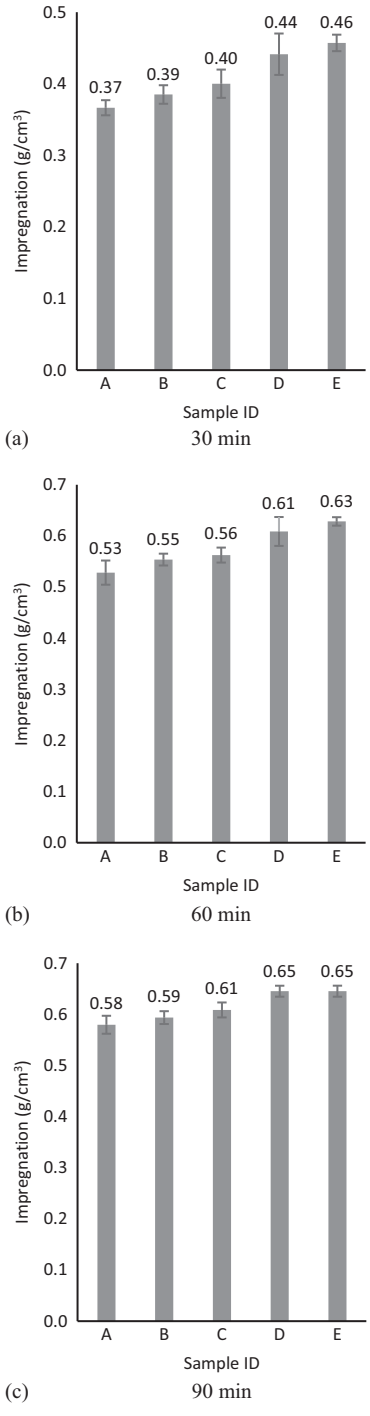

Figure 4. Impregnation-time- and perforation-rate-dependence of WPFR impregnation of perforated Hinoki plywood. (a) 30 min, (b) 60min, (c) 90 min.

Table 1. Pearson's coefficient correlation analysis.

	Impregnation time	Perforation rate
Impregnation mass	0.868[a]	0.261[a]

[a] Significant difference at the 1% level ($n = 90$).

Sample A was 1.1 times higher than that of Sample E. Consequently, perforations in the plywood contributed to enhancement in impregnation.

Table 1 presents the results of Pearson's coefficient correlation analysis that examined the effects of impregnation time and perforation rate on WPFR impregnation mass. Impregnation time was positively correlated to impregnation mass, as was perforation rate. The correlation coefficients between all coefficients were statistically significant at the 1% level. The absolute value of the correlation coefficient was greater for impregnation time than for perforation rate. Thus, it can be inferred that impregnation time has a more substantial impact on WPFR impregnation mass than does perforation rate.

Table 2 displays the results of the multiple linear regression analysis. Impregnation time (β_1) was positively significant at the 1% level, as was perforation rate (β_2). These results suggest that increases in impregnation time and perforation rate increase WPFR impregnation mass. All F-values were significant at the 1% level, indicating a good fit for the estimated regression results. The adjusted R^2 was 81.8%, indicating the high explanatory power of the regression model.

Table 2. Multiple linear regression analysis.

	$Y = \alpha_0 + \beta_1 X_1 + \beta_2 X_2 + \varepsilon$			
Variables	Coefficient	Standard coefficient	t-stat.	VIF
Intercept	0.312	—	26.306	—
X_1	0.003	0.868	19.203[a]	1.000
X_2	0.039	0.262	5.784[a]	1.000
Adjusted R^2		81.8%		
F-value		201.096		
p-value		<0.001		

[a] Significance at the 1% level ($n = 90$).

Y, impregnation mass; X_1, impregnation time; X_2, perforation ratio; ε, residuals (error term); VIF, variance inflation factors.

Standardized Pearson's coefficient values were used for each estimate, ensuring a uniform unit of measurement. These coefficients allow assessment of the relative significance of each independent variable, even in situations involving diverse units of measurement (Sreejesh et al 2014). Therefore, the standardized coefficient can identify which independent variable has the greatest influence on the dependent variable in a multiple regression model. In this multiple linear regression analysis, the standard coefficients were 0.868 for impregnation time and 0.262 for perforation rate. As the absolute value of the coefficient was greater for impregnation, impregnation time had a larger effect on improving impregnation mass than does the perforation rate. All variance inflation factors were less than 10, suggesting that multicollinearity is not significant (Jang et al 2020; Jang & Kang 2021).

Combustion Test

Figure 5 shows photographs of the samples after the 45° angle combustion test. According to the flame retardant performance standards of boards in Korea, the average carbonized area of untreated plywood must be less than 50 cm (KFIA 2017) under these tests. The carbonized area of untreated plywood was 56.30 cm^3, which fell short of this standard. However, the carbonized area of Sample A was 22.7 cm^3, which met the standard. Further, the carbonized area of Sample E was 19.1 cm^3, which shows approximately 15% better flame retardant performance than Sample A.

The level of flame retardant impregnation was related to longer impregnation time, which is consistent with previous studies (Jang & Kang 2023b, 2023a). Additionally, impregnation increased when the spacing between holes was narrower. The permeability of wood can be more accurately measured in a cross-sectional sample compared with radial and tangential sections. The perforation of plywood increases not only the overall specific surface area of the plywood but also the exposure of its cross section. It can be inferred that a higher perforation rate, resulting in high permeability, leads to a more pronounced impregnation effect. In addition, the high impregnation effect contributed to the improvement in flame retardant performance.

A limitation of this study was that the perforation rate was applied only up to 1.7%. In future research, we plan to evaluate impregnation by increasing the perforation rate as much as possible until there is no significant change in the physical properties of the plywood.

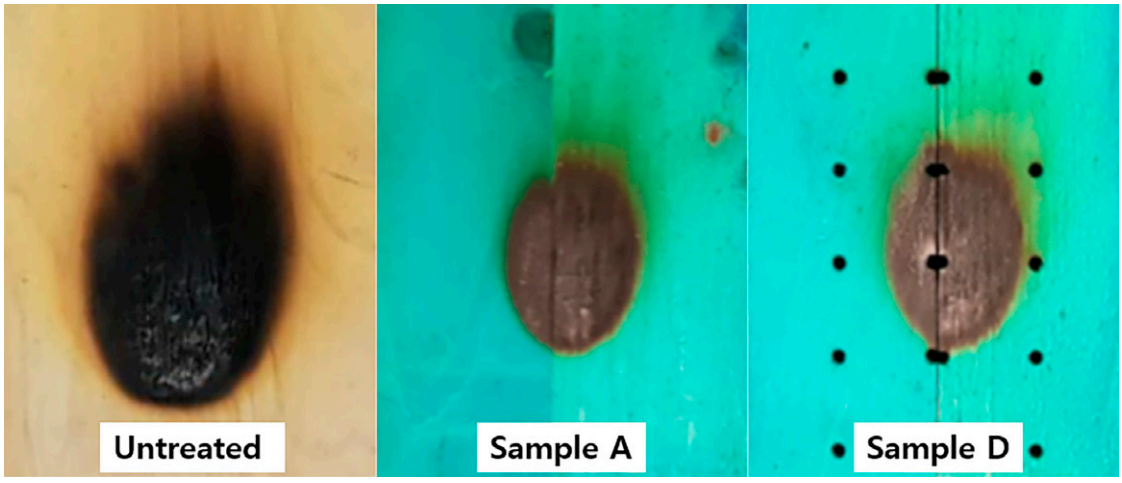

Figure 5. Photographs of samples after the 45° angle flammability test.

CONCLUSIONS

This study aimed to assess the impregnation of WPFR in perforated Hinoki plywood. Pearson correlation analysis revealed that perforation frequency and impregnation time had significant effects on WPFR impregnation. Furthermore, multiple linear regression analysis confirmed the significant positive influence of both variables on WPFR impregnation. Notably, in this study, impregnation time exhibited a greater impact on WPFR compared with perforation frequency. Depending on the impregnation capability, the flame retardant performance also improved. In future research, we intend to increase the perforation rate beyond 1.7% to examine whether the effect of the perforation rate on impregnation can be further enhanced.

ACKNOWLEDGMENTS

This research was supported by the Basic Science Research Program administered by the National Research Foundation of Korea (NRF), funded by the Ministry of Education (NRF-2019R1I1A3A02059471), and under the framework of an international cooperation program managed by the NRF of Korea (NRF-2020K2A9A2A08000181). Also, this research was funded by the R&D Program for Forest Science Technology in Korea (FTIS 2022457A00-2224-AC02, FTIS 2020223A00-2222-AC02). This paper was supported by research funds from Jeonbuk National University in 2023. This article was reconstructed by extracting data from Yong Woo-Jong's master's thesis at Jeonbuk National University.

REFERENCES

Andargie MS, Touchie M, O'Brien W (2021) Case study: A survey of perceived noise in Canadian multi-unit residential buildings to study long-term implications for widespread teleworking. Build Acoust 28(4):443-460.

Chen Z, Zhang S, Ding M, Wang M, Xu X (2021) Construction of a phytic acid–silica system in wood for highly efficient flame retardancy and smoke suppression. Materials 14(15):4164.

Chu T, Gao Y, Yi L, Fan C, Yan L, Ding C, Liu C, Huang Q, Wang Z (2022) Highly fire-retardant optical wood enabled by transparent fireproof coatings. Adv Compos Hybrid Mater 5(3):1821-1829.

Fekiač J, Gáborík J, Vojtkuliak M (2021) Properties of plywood made from perforated veneers. Forests 12(12): 1709.

Fu Q, Medina L, Li Y, Carosio F, Hajian A, Berglund LA (2017) Nanostructured wood hybrids for fire-retardancy prepared by clay impregnation into the cell wall. ACS Appl Mater Interfaces 9(41):36154-36163.

Howard C, Dymond CC, Griess VC, Tolkien-Spurr D, van Kooten GC (2021) Wood product carbon substitution benefits: A critical review of assumptions. Carbon Balance Manag 16(1):9.

Hu X, Sun Z (2021) Nano CaAlCO3-layered double hydroxide-doped intumescent fire-retardant coating for mitigating wood fire hazards. J Build Eng 44:102987.

Hughes M (2015) Plywood and other veneer-based products. Wood composites. Elsevier, Sawston, England. pp. 69-89.

Jang E-S (2022a) Experimental investigation of the sound absorption capability of wood pellets as an eco-friendly material. J Korean Wood Sci Technol 50(2):126-133.

Jang E-S (2022b) Investigation of sound absorption ability of Hinoki Cypress (*Chamaecyparis obtusa*) cubes. J Korean Wood Sci Technol 50(5):365-374.

Jang E-S (2022c) Use of pine (*Pinus densiflora*) pollen cones as an environmentally friendly sound-absorbing material. J Korean Wood Sci Technol 50(3):186-192.

Jang E-S (2023) Sound absorbing properties of selected green material—A review. Forests 14(7):1366.

Jang E-S, Kang C-W (2021) Delignification effects on Indonesian momala (*Homalium foetidum*) and Korean red toon (*Toona sinensis*) hardwood pore structure and sound absorption capabilities. Materials 14(18):5215.

Jang E-S, Kang C-W (2023a) Effect of steam explosion treatment on impregnation of three species of softwoods: North American spruce, Korean pine, and Japanese larch. BioResources 18(1):1454-1464.

Jang E-S, Kang C-W (2023b) Effects of pressure and temperature on wood impregnation—Focusing on larch (*Larix kaempferi*) and Korean pine (*Pinus koraiensis*). BioResources 18(2):3208-3216.

Jang E-S, Yuk J-H, Kang C-W (2020) An experimental study on change of gas permeability depending on pore structures in three species (hinoki, Douglas fir, and hemlock) of softwood. J Wood Sci 66(1):1-12.

KFIA (2017) Analysis of fire statistics and safety inspection results of special buildings. Korea Fire Insurance Association, Seoul, Korea.

Li L, Chen Z, Lu J, Wei M, Huang Y, Jiang P (2021) Combustion behavior and thermal degradation properties of wood impregnated with intumescent biomass flame retardants: Phytic acid, hydrolyzed collagen, and glycerol. ACS Omega 6(5):3921-3930.

Lu J, Huang Y, Jiang P, Chen Z, Bourbigot S, Fontaine G, Chang L, Zhang L, Pan F (2022) Universal circulating impregnation method for the fabrication of durable

flame-retardant plywood with low hygroscopicity and leaching resistance. Polym Degrad Stab 195:109799.

Mai C, Schmitt U, Niemz P (2022) A brief overview on the development of wood research. Holzforschung 76(2): 102-119.

Ncube M, Riffat S (2012) Developing an indoor environment quality tool for assessment of mechanically ventilated office buildings in the UK—A preliminary study. Build Environ 53:26-33.

Nguyen T-MD, Chang S, Condon B, Slopek R (2012) Synthesis of a novel flame retardant containing phosphorus-nitrogen and its comparison for cotton fabric. Fibers Polym 13(8):963-970.

Park S, Han Y, Son DW (2020) Flame retardancy of wood products by spreading concentration and impregnation time of flame retardant. J Korean Wood Sci Technol 48(4):417-430.

Peng L, Liu M, Wang D, Song B (2018) Sound absorption properties of wooden perforated plates. Wood Res 63: 559-572.

Shen J, Zhang X, Lian Z (2021) Gender differences in human psychological responses to wooden indoor environment. Eur J Wood Prod 79(1):217-226.

Song B, Peng L, Fu F, Liu M, Zhang H (2016) Experimental and theoretical analysis of sound absorption properties of finely perforated wooden panels. Materials 9(11):942.

Sreejesh S, Mohapatra S, Anusree M, Sreejesh S, Mohapatra S, Anusree M (2014) Multiple regression. Pages 195-206 *in* Business research methods: An applied orientation. Springer, Cham, Switzerland.

Vojta Š, Bečanová J, Melymuk L, Komprdová K, Kohoutek J, Kukučka P, Klánová J (2017) Screening for halogenated flame retardants in European consumer products, building materials and wastes. Chemosphere 168:457-466.

Wallenius MA (2004) The interaction of noise stress and personal project stress on subjective health. J Environ Psychol 24(2):167-177.

Wang H, Zhao Y (2022) Studies on pre-treatment by compression for wood impregnation III: Effects of the solid content of low-molecular-weight phenol formaldehyde resin on the impregnation. J Wood Sci 68(1):28.

Xiong X, Niu Y, Zhou Z, Ren J (2020) Development and application of a new flame-retardant adhesive. Polymers 12(9):2007.

COMPARISON OF GENETIC ALGORITHM OPTIMIZED AND PARTIAL LEAST SQUARES REGRESSION DENSITY MODELS FOR *ACACIA AURICULIFORMIS*

*Laurence R. Schimleck**†*
Professor
Department of Wood Science and Engineering
119 Richardson Hall
Oregon State University
Corvallis, OR 97331
E-mail: laurence.schimleck@oregonstate.edu

Tu X. Ho
Associate R&D Engineer
Simpson Strong-Tie
5956 W. Las Positas Blvd
Pleasanton, CA 94588
E-mail: tuho@strongtie.com

Doan Van Duong
Associate Professor
Thai Nguyen University of Agriculture and Forestry
Quyet Thang ward, Thai Nguyen city, Vietnam
E-mail: duongvandoan@tuaf.edu.vn

Arijit Sinha†
Professor
Department of Wood Science and Engineering
119 Richardson Hall
Oregon State University
Corvallis, OR 97331
E-mail: arijit.sinha@oregonstate.edu

Ighoyivwi Onakpoma†
PhD Candidate
Department of Wood Science and Engineering
119 Richardson Hall
Oregon State University
Corvallis, OR 97331
E-mail: ighoyivwi.onakpoma@oregonstate.edu

Galen Fox
Student
Department of Wood Science and Engineering
119 Richardson Hall
Oregon State University
Corvallis, OR 97331
E-mail: foxga@oregonstate.edu

(Received November 2023)

* Corresponding author
† SWST member

Wood and Fiber Science, 56(1), 2024, pp. 51-61
https://doi.org/10.22382/wfs-2024-05

Abstract. Partial least squares (PLS) regression models based on genetic algorithm (GA) representative near IR (NIR) wavelengths for estimating wood properties provide improved calibration and prediction statistics compared with PLS models based on all available NIR wavelengths. However, the utilization of predicted data, obtained from full NIR wavelength and GA-selected NIR wavelength models, in a practical application, has not been explored. Our application was to examine radial density variation in *Acacia auriculiformis* Cunn. Ex Benth. clones at a resolution of 10 mm. One hundred and forty *A. auriculiformis* samples representing seven clones and two radial positions (adjacent to pith and bark, respectively) had NIR hyperspectral images (wavelength range 931-1718 nm) collected from their transverse surface. Two PLS density models (all NIR wavelengths and GA representative NIR wavelengths) were developed using 134 NIR spectra extracted from the images. The models were then used to predict density in 10 mm increments of 144 radial samples from the same clones. A PLS density model using only 15 representative NIR wavelengths provided a mean (0.506 g/cm^3) that was not statistically significantly different from the measured density (0.503 g/cm^3), whereas the mean for the PLS model using all wavelengths was 0.522 g/cm^3. However, the PLS model with 15 representative NIR wavelengths had greater variation (standard deviation of 0.060) compared with measured data (0.052) and the full NIR wavelengths PLS model (0.047). Radial density variation was less than 0.09 g/cm^3 for six of the seven clones examined.

Keywords: *Acacia auriculiformis*, density, genetic algorithm, hyperspectral imaging, near infrared spectroscopy, partial least squares regression.

INTRODUCTION

Near IR (NIR) spectroscopy provides a rapid, nondestructive approach for the assessment of a variety of wood properties (Tsuchikawa and Kobori 2015; Schimleck and Tsuchikawa 2021). Several recent studies have reported the utilization of advanced modeling approaches (eg machine learning and genetic algorithm [GA]) for calibration development (Cogdill et al 2004; Mora and Schimleck 2010; Fernandes et al 2013; Li et al 2019; Nasir et al 2019, 2023; Ayanleye et al 2021; Ho et al 2021, 2022), however, the predictive performance of these models, and their practical significance in terms of an application, have not been assessed and compared with results obtained using predictive models obtained using partial least squares (PLS) regression, a modeling approach used for the large majority of NIR-wood related studies.

One advanced approach involves the utilization of GAs (Bangalore et al 1996; Villar et al 2014; De et al 2017) for model development. Recent papers have investigated the potential of PLS models based on GA-selected NIR wavelengths to estimate pulp yield of Tasmanian blue gum (*Eucalyptus globulus* Labill.) samples (Ho et al 2021) and the estimation of a variety of SilviScan (Evans 1994, 1999, 2006) measured by wood properties (density, microfibril angle, modulus of elasticity and tracheid coarseness, radial diameter, tangential diameter, and wall thickness) for loblolly pine (*Pinus taeda* L.) (Ho et al 2022). These studies demonstrate that PLS models based on GA-identified NIR wavelengths have improved calibration and prediction statistics. Moreover, band assignments for key wavelengths consistently arise from bond vibrations observed in lignin, cellulose, and hemicellulose, providing a strong fundamental basis for interpretation and explaining improved model performance. As noted, the utilization of predicted data in a practical application has not been explored, or compared with, the performance of predictions obtained using PLS regression models. Hence the aim of this study is to compare the performance of both model types in a practical application.

The application identified is the prediction of radial density variation in 10 mm increments in seven *Acacia auriculiformis* Cunn. Ex Benth. clones from a trial established in north central Vietnam. *A. auriculiformis* was introduced into Vietnam in the 1960s utilizing Australian, Papua New Guinean, and Indonesian provenances (Pinyopusarek et al 1991; Hai 2009) and owing to its fast growth and adaptability has become an important plantation species. It is a source of pulp wood (Jahan et al 2008), sawlogs (Hai et al 2008), and is also used for furniture (Hai 2009). *A. auriculiformis* tree improvement programs have been established with an emphasis on

growth, stem form, and disease resistance but little information is available regarding wood properties. For lumber production, in particular, radial variation in wood properties is important and research (Van Duong et al 2022) has aimed to investigate radial variation amongst clones, however only samples adjacent to the pith and bark were examined. To better understand radial patterns greater resolution is required and NIR-predicted density, obtained from PLS regression models based on all available NIR wavelengths and only those identified by GA, were utilized for this purpose.

MATERIALS AND METHODS

A. auriculiformis Wood Samples

Sample trees were harvested from an *A. auriculiformis* clonal trial established by the Vietnamese Academy of Forest Sciences to assess the growth rate and stem quality of different clones. The site is located in Cam Hieu commune, Cam Lo district, Quang Tri province, north central Vietnam (16°45′60″N and 107°01′12″E). The plantlets were propagated by tissue culture and planted at the site in December 2015 using a randomized complete block design with four replicates. Each plot comprised 36 ramets from a clone (6 lines × 6 ramets/line). The initial spacing between ramet was 3.0×3.0 m^2 (1100 trees/ha). Fertilizer application at planting was 100 g nitrogen (N), phosphate (P_2O_5), and potassium oxide (K_2O) (VADFCO, Hanoi, Vietnam) (elemental ratio 16:16:8) per ramet and 100 g NPK 1 yr later. There are seven clones considered in this study: Clt7, Clt18, Clt19, Clt25, Clt26, Clt57, and Clt43.

Sampling and Wood Property Assessment

A total of 35 ramets (5 per clone) were chosen based on straightness, branching, and absence of disease or pest symptoms in December 2020. Stress-wave velocity of standing tree was measured using a Fakopp Microsecond Timer for each tree (Serial No.: FN-12/2020; Fakopp Enterprise Bt., Fenyo u.26, Hungary). Prior to destructive sampling, stem diameter at a height of 1.3 m was measured, and the north and south sides were marked for selected ramets, and once felled, total height was measured.

A 1.0-m log was collected between 0.5 and 1.5 m from each sampled stem. Logs were dried in a room at ambient conditions for approximately 2 mo and after drying, eight 20 (radial) × 20 (tangential) × 300 (longitudinal) mm^3 small wood specimens adjacent to the pith and bark were cut from each log for additional stress wave measurements, gravimetric density determination and destructive evaluation of wood strength and stiffness (note – only the density data are used in this study). Four samples (2 adjacent to the pith and 2 adjacent to the bark) were available for each ramet, giving 140 samples in total for density PLS model development. More detail regarding these samples is reported in Van Duong et al (2022).

Samples to Test PLS and GA Density Models

From the sampled *A. auriculiformis* trees, a radial strip was also obtained from the 1.0-m log used to analyze density variation at a higher resolution and test the PLS models using all NIR wavelengths and NIR wavelengths identified by GA optimization. The radial strips were split into 10 mm increments to give 4-5 samples per radial strip (total 144 samples) and the density of these samples was determined gravimetrically. As the samples represented the complete radius of the sampled ramets they were distinct, but from the same population, as samples used for calibration that measured 20 mm in the radial direction. Hyperspectral images of examples of samples that formed the calibration and prediction sets are shown in Fig 1.

NIR-hyperspectral Imaging

NIR-hyperspectral imaging of all samples was done using a Specim FX17 camera (Specim; Spectral Imaging Ltd., Oulu, Finland) fitted with a Specim (OLET 17.5 F/2.1) focusing lens (wavelength range 931-1718 nm, 224 wavelengths). Six tungsten halogen lamps illuminated samples while sample motion and image acquisition (which included a dark current and white reference prior

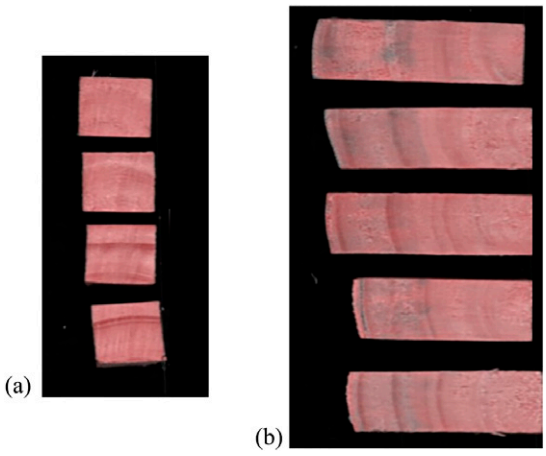

Figure 1. Hyperspectral images of a subset of the *Acacia auriculiformis* samples that formed the calibration and prediction sets. (a) Samples (20 mm radially × 20 mm tangentially) used for calibration and obtained from near the pith and from near the bark used for calibration. (b) Full radius samples (20 mm tangentially). After hyperspectral images were collected from the full radius samples they were split into sections (10 mm radially × 20 mm tangentially) and the 10 mm sections were used for density determination and formed the prediction set.

to collecting an image of each set of trays) were controlled using Lumo software supplied with the system. Samples were analyzed on a black background and care was taken to minimize exposure of the samples to the intense light of the lamps.

Relative reflectance values for each image were calibrated with the corresponding dark current and white reference data and then transformed to absorbance (A), $A = \log_{10} 1/R$. Regions of interest (ROI), corresponding to each 10 mm section for each radial strip, were identified in images of the samples and cropped to provide individual NIR spectra per section. ROI identification was completed using Matlab software (MathWorks, Natick, MA).

Six of the calibration samples had NIR spectra that were quite different from the others having high absorbance values in the region 931-1100 nm. Examination of a leverage plot (Fig 2) obtained from principal components analysis using Unscrambler (version 9.2) software (Camo, Oslo, Norway) indicated that these samples had an excessive influence on the data set and were excluded from further analysis. As a result, 134 spectra were used to develop PLS models for density using all available NIR wavelengths and only those identified by GA.

GA Model Optimization

The *A. auriculiformis* data set of 134 samples was separated into two subsets (108 samples in calibration set and 26 samples in prediction set) based on the DUPLEX selection method (Snee 1977). For each sample, the data consists of the NIR reflectance measurement of 224 wavelengths and density. PLS regression was adopted to develop predictive models for density using four cross-validation segments.

The GA was applied to determine the optimal wavelength set, number of wavelengths, N_{WvL}, and number of latent variables, N_{comp}, through optimizing the predictive performance of PLS models for the *A. auriculiformis* data set's mechanical properties. The optimal wavelengths were determined and varied from 10 to 50. The maximum number of latent variables was selected to be 40. To evaluate the predictive performance of PLS models, the *R*-squared of calibration and prediction sets were utilized. The objective function was defined for the optimization process as: $f_{\mathrm{obj}} = \alpha \times R_c^2 + \beta \times R_p^2$, in which α and β are weighted factors for R_c^2 and R_p^2, respectively. The summation of α and β equals one. In this study, α and β were selected to be 0.5.

The constraint conditions for the optimization problem are R_c^2 and R_p^2 values derived from the PLS models using all 224 wavelengths with N_{comp} up to 40 to obtain the best objective value. These conditions with their corresponding N_{comp} values are presented in Table 1. It is worth noting that PLS models using all wavelengths provide the best prediction performance with $N_{\mathrm{comp}} = 24$ for density. Higher values of N_{comp} caused overfitting on the calibration set which resulted in worse performance on the prediction set. More details on the establishment and optimization process using GAs can be found in Ho et al (2021, 2022).

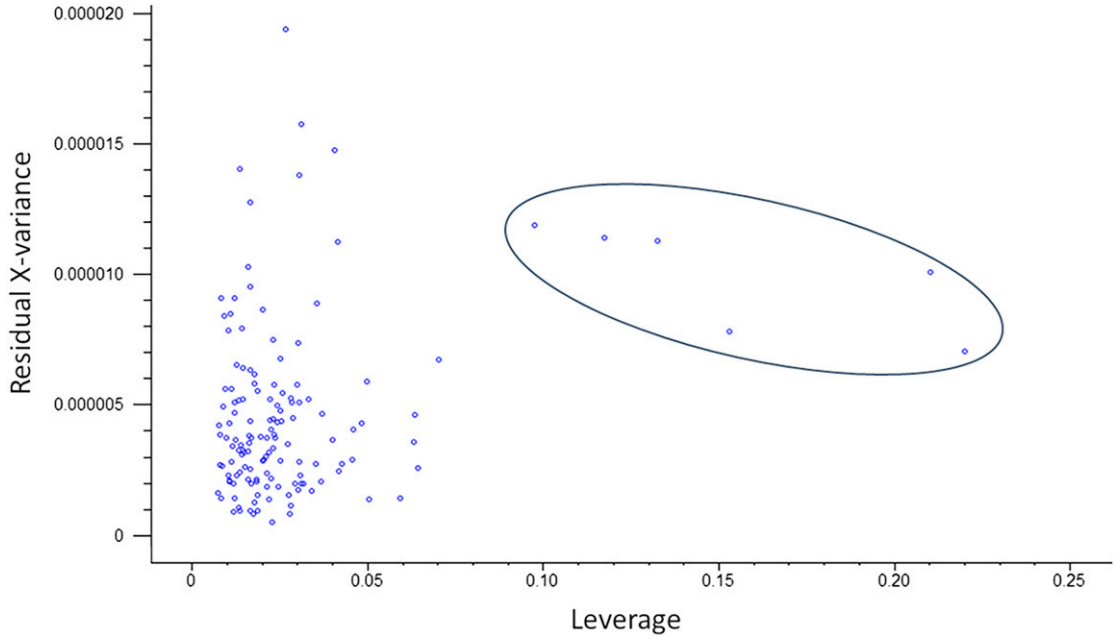

Figure 2. Plot of residual X-variance vs leverage for the 140 *Acacia auriculiformis* calibration samples. The six circled samples had excessive influence relative to the remaining samples and were excluded from genetic algorithm model development.

RESULTS AND DISCUSSION

GA Optimization Results for Density

The optimization was run three times which is a combination of density and a specific number of selected NIR wavelengths. The final result was determined as an average of the three optimizations.

Figure 3 shows predictive performance vs the number of wavelengths. The overall trend is that the objective value f_{obj} increases with N_{WvL}. When N_{WvL} is less than 20 for the density model, the predictive performance is weaker than the PLS density model using the full NIR wavelength range. When N_{WvL} approaches 50, f_{obj} is improved by about 8% for density, compared with that of the full NIR wavelength PLS model. However, *R*-squared of the calibration set, R_c^2 is not improved for the density model with all investigated N_{WvL}. R_c^2 of the density model drops to less than 0.8 when N_{WvL} is smaller than 20. In contrast, *R*-squared for the prediction set, R_p^2 improves more than 12% for the density model, even at a low N_{WvL} value of 10. As N_{WvL} increases, R_p^2 increases.

Table 1. Constraint conditions for the optimization problem.

Property	R_c^2	R_p^2	f_{obj}	N_{comp}
Density	0.9378	0.7958	0.8668	24

The optimization process also determines the optimal N_{comp} value to provide the best predictive performance corresponding to a specific N_{WvL}. The results of optimal N_{comp} are shown in Fig 4 and imply a steady increase in N_{comp} along with an increase of N_{WvL} to 25. Afterward, the optimal N_{comp} fluctuates considerably in the range of 21-38 for the density model. The optimal N_{comp} value of 40 appears only once and indicates that an upper limit of N_{comp} of 40 for the optimization process is reasonable.

In each combination of density and N_{WvL}, the optimization process results in a set of wavelengths that provide the best predictive performance. However, Ho et al (2021) observed that there were few common wavelengths among optimized sets, indicating that not all optimized

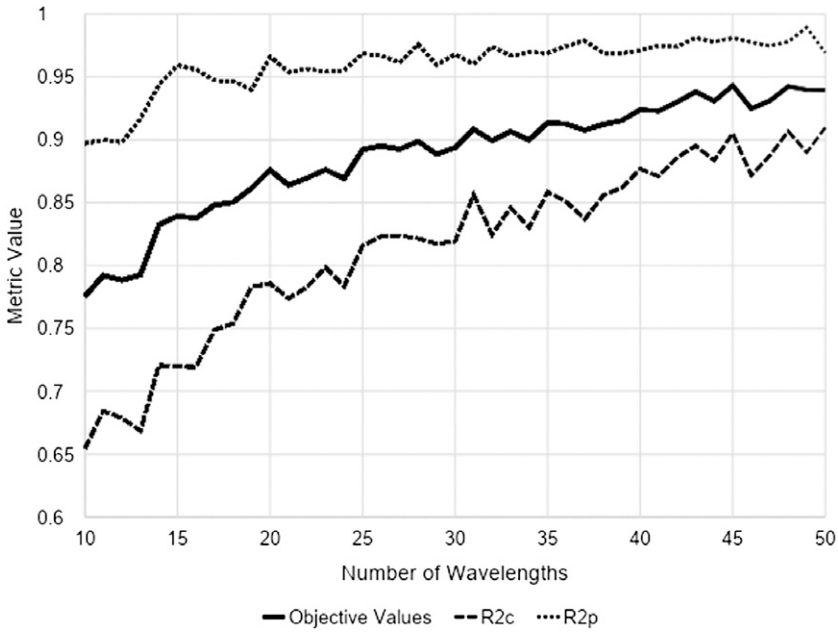

Figure 3. Predictive performance of partial least squares models for density based on an increasing number of genetic algorithm selected near IR wavelengths.

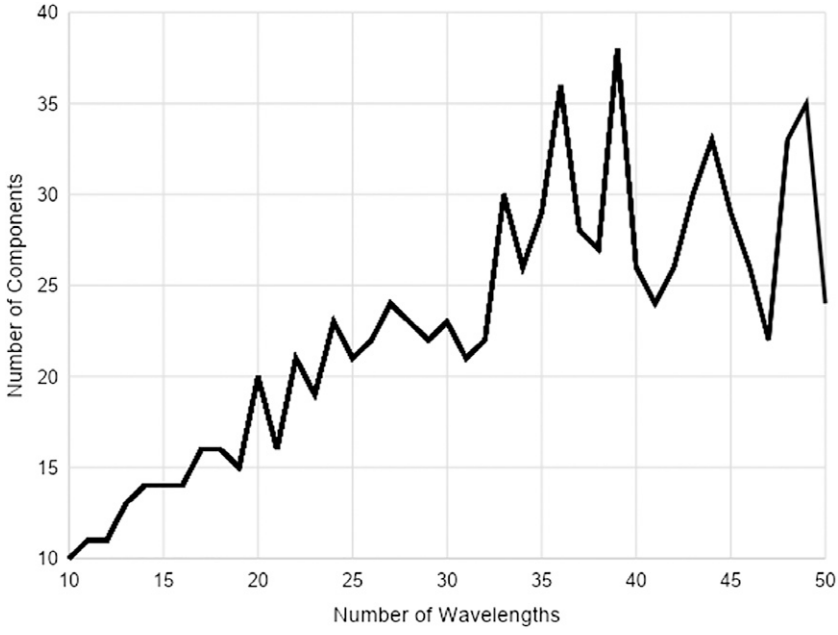

Figure 4. Optimal N_{comp} values for partial least squares density models based on an increasing number of genetic algorithm selected near IR wavelengths.

wavelengths contribute to global optimization and help to explain the relationship between wavelengths and wood components/properties. Ho et al (2021, 2022) utilized a statistical approach in which the most frequent wavelengths appearing in all optimized sets were considered the representative wavelengths. Band assignment was conducted, and strong agreement between representative wavelengths and specific wood components was observed. The same approach was applied in this study. The utilization of 224 wavelengths (average of three runs) from 931 to 1718 nm for density is shown in Fig 5. To simplify interpretation, the wavelengths are shown in intervals of 10 nm.

Band Assignments

Wavelengths in increments of 10 mm with an average frequency (determined from the three runs) greater than 20 are summarized for density (Table 2). Corresponding band locations, their bond vibrations, and specific wood component (if available) based on Schwanninger et al (2011) are also included. For nearly all wavelengths listed in Table 2, bond vibrations related to specific wood components. First overtone OH and first overtone CH stretch vibrations were consistently represented.

Performance of Density PLS Model Using Representative Wavelengths

To further investigate the application of representative NIR wavelengths identified in the GA optimization process, a PLS model for density was developed to predict the density of the samples cut from the *A. auriculiformis* radial strips. Only the most frequent wavelengths were used, and they varied from 10 to 77.

Figure 6 shows the mean and standard deviation of the measured density of 144 samples in comparison with those from PLS regression models using all wavelengths and GA representative wavelengths with the total number of 10-77 wavelengths. A t-test was implemented to compare the means between prediction models and measured data. There was no statistically significant difference in means between measured density and density predicted using models based on 61, 16, and 15 representative wavelengths (p-values of 0.135, 0.894, and 0.609, respectively). However, with 15 representative wavelengths, the PLS model provides the closest mean (0.506 g/cm^3) to that of measured data (0.503 g/cm^3), which is better than the PLS model using all wavelengths (0.522 g/cm^3). In addition, the PLS model with 15 representative wavelengths had the lowest variation (standard deviation = 0.060) compared with other prediction models using 61 and 16 representative wavelengths, though it was higher than that of measured density (0.052) and the PLS model based on all wavelengths (0.047).

For each clone, the average density of samples taken from different ramets, but the same radial position, were determined and plotted for six

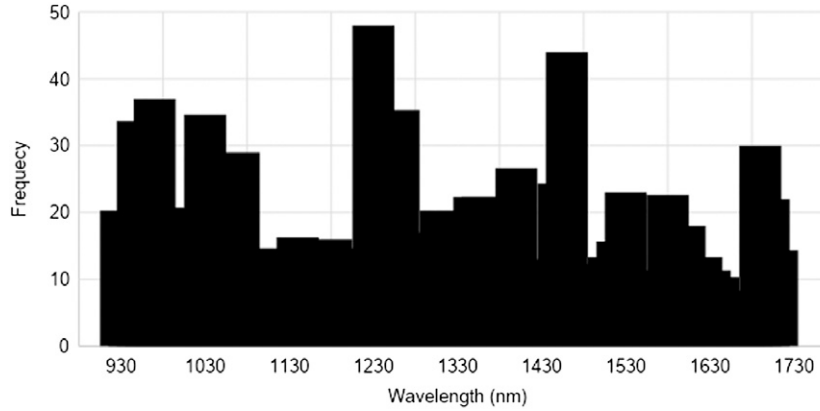

Figure 5. Frequency of optimized wavelengths (average of three runs) for density in increments of 10 mm.

Table 2. Band assignments for density optimization for NIR wavelengths with frequency greater than 20 (increments of 10 nm).

Identified wavelengths (nm)	Band location (nm)	Bond vibration	Wood component
930-950	938	3rd OT C-H str.	Not assigned
980, 1000	970-1000	2nd OT O-H str.	Starch (990 nm)
1030-1070	1037, 1053	2xC-H str.+ 2xC-H def.+$(CH_2)_n$	Not assigned
	1030, 1060	2nd OT N-H str.	Not assigned
1230-1240	1212-1225	2nd OT C-H str.	Cellulose
1260		Not assigned	
1310		Not assigned	
1350-1360	1350, 1360	1st OT C-H str. + C-H def.	Hemicellulose/all
1400	1410	1st OT O-H str.	Lignin/extractives
1450-1460	1447	1st OT O-H str.	Lignin/extractives
	1448	1st OT O-H str.	Lignin
1460	1471	1st OT O-H str.	Hemicellulose
	1473	1st OT O-H str.	Cellulose
1530	1534	1st OT O-H str.	Cellulose
1580	1579, 1580, 1586-1596	1st OT O-H str.	Cellulose
1690	1685	1st OT C_{ar}-H str.	Lignin
	1695	1st OT C-H str. CH_3 groups	Not assigned
	1698	1st OT C-H str.	Lignin
1700	1703	1st OT C-H str.	Cellulose
	1705	1st OT C-H str.	Hemicellulose

NIR, near IR; OT, overtone; str., stretching vibration; def., deformation vibration; +, combination band; ar, aromatic.

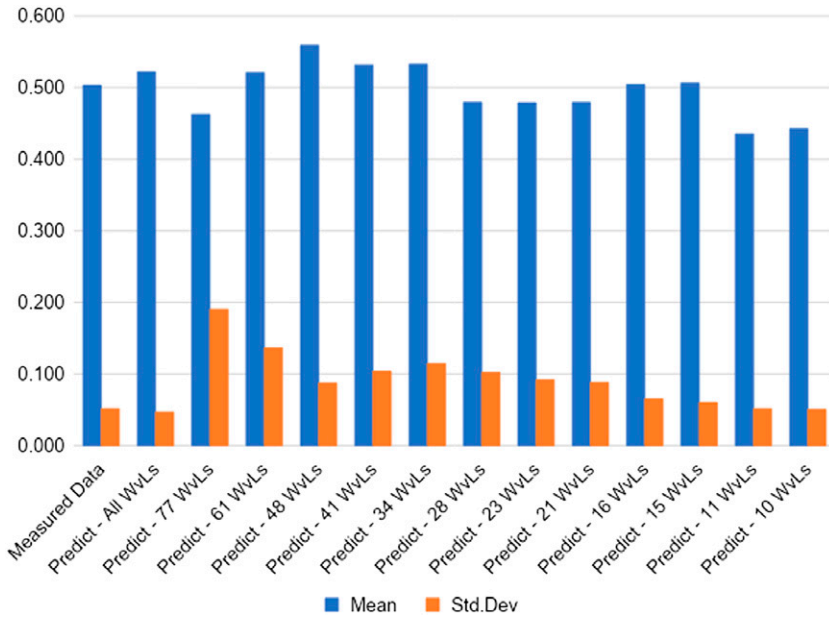

Figure 6. Comparison of mean and standard deviation from measured data, partial least squares prediction using all wavelengths and representative near IR wavelengths.

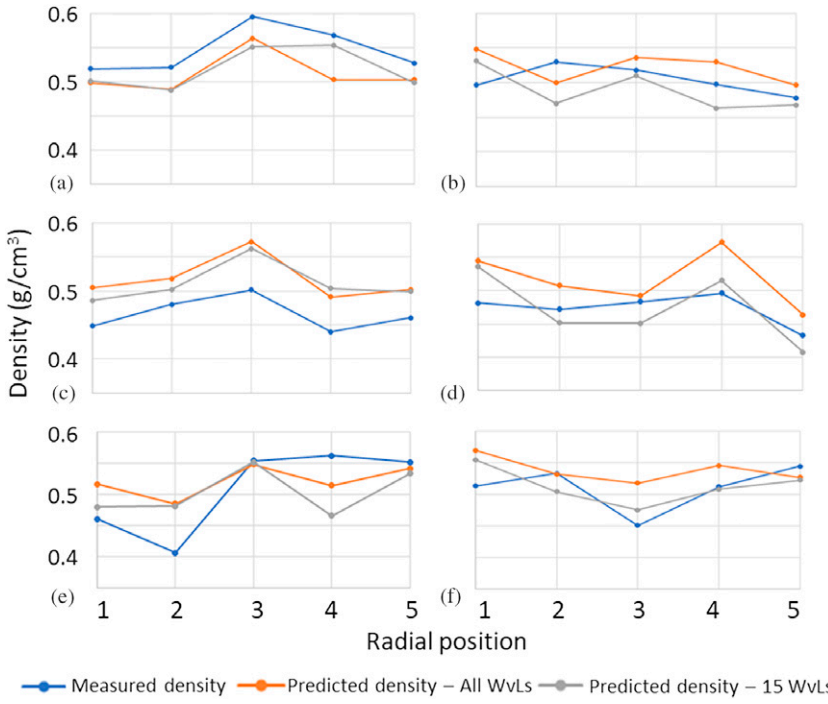

Figure 7. Density variation from pith to bark for six of the seven clones: (a) Clt18, (b) Clt19, (c) Clt25, (d) Clt26, (e) Clt43, and (f) Clt57. Radial density variation for Clt 7 was not plotted as it was missing one position.

clones in Fig 7. There are three density data series, including measured data, prediction data the from PLS model using all NIR wavelengths, and the PLS model using 15 representative NIR wavelengths. The radial location changes from pith (#1) to bark (#5).

Overall, the clones showed low radial density variation with six of the seven having a difference between maximum and minimum gravimetric densities of less than 0.09 g/cm^3. The exception was Clt43 with a range of 0.14 g/cm^3. Duc Viet et al (2020) showed a similar level of variation with density increasing from 0.47 to 0.54 g/cm^3 as did Hai et al (2010) with heartwood densities of 0.52 g/cm^3 and sapwood densities of 0.56 g/cm^3.

The narrow radial density variation made it difficult to detect a consistent trend in both measured and predicted values amongst *A. auriculiformis* clones. For some clones (Clt18, 19, 25, and 57), predicted densities from both PLS models displayed similar radial trends to measured values but for others, most notably Clt43, the models were not as successful.

CONCLUSIONS

To compare the performance of PLS regression models based on GA representative NIR wavelengths and full wavelength PLS models, radial density variation in seven *Acacia auriculiformis* Cunn. Ex Benth. clones at a resolution of 10 mm were examined. Overall, the clones showed low radial density variation with six of the seven having a difference between maximum and minimum measured densities of less than 0.09 g/cm^3. A PLS density model using only 15 representative NIR wavelengths provided a mean predicted density (0.506 g/cm^3) that was closest to the average measured density (0.503 g/cm^3) and there was no statistically significant difference in mean values between them based on t-tests. In comparison, the

mean density for the full NIR wavelength PLS model was 0.522 g/cm^3. The PLS model with 15 representative wavelengths also demonstrated greater variation (standard deviation of 0.060) compared with measured data (0.052) and the full wavelength PLS model (0.047).

Although the GA approach helped to identify representative NIR wavelengths for a PLS model for the density of *A. auriculiformis* clones, further studies should be conducted to generalize the findings in this study. This work should include comparing and validating the results from the GA approach with results from other optimization methods and determining the optimal number of representative NIR wavelengths to be used for the density prediction model regardless of clone.

ACKNOWLEDGMENT

This research is funded by the Vietnam National Foundation for Science and Technology Development (NAFOSTED), Grant No. 106.06-2019.319.

REFERENCES

Ayanleye S, Nasir V, Avramidis S, Cool J (2021) Effect of wood surface roughness on prediction of structural timber properties by infrared spectroscopy using ANFIS, ANN and PLS regression. Eur J Wood Wood Prod 79(1):101-115.

Bangalore AS, Shaffer RE, Small GW, Arnold MA (1996) Genetic algorithm-based method for selecting wavelengths and model size for use with partial least-squares regression: Application to near-infrared spectroscopy. Anal Chem 68(23):4200-4212.

Cogdill RP, Schimleck LR, Jones PD, Peter GF, Daniels RF, Clark A (2004) Estimation of the physical wood properties of *Pinus taeda* L. radial strips using least squares support vector machines. J Near Infrared Spectrosc 12(4):263-270.

De A, Chanda S, Tudu B, Bandyopadhyay RB, Hazarika AK, Sabhapondit S, Baruah BD, Tamuly P, Bhattachryya N (2017) Wavelength selection for prediction of polyphenol content in inward tea leaves using NIR. Pages 184-187 *in* IEEE 7th International Advance Computing Conference (IACC), January 5-7, 2017, Hyderabad, India.

Duc Viet D, Ma T, Inagaki T, Tu Kim N, Quynh Chi N, Tsuchikawa S (2020) Physical and mechanical properties of fast growing polyploid acacia hybrids (*A. auriculiformis* × *A. mangium*) from Vietnam. Forests 11:15.

Evans R (1994) Rapid measurement of the transverse dimensions of tracheids in radial wood sections from *Pinus radiata.* Holzforschung 48:168-172.

Evans R (1999) A variance approach to the X-ray diffractometric estimation of microfibril angle in wood. Appita J 52:283-289, 294.

Evans R (2006) Characterization of the cellulosic cell wall. Pages 138-146 DG Stokke and L Groom, eds. Blackwell Publishing, Ames, IA.

Fernandes A, Lousada J, Morais J, Xavier J, Pereira J, Melo-Pinto P (2013) Measurement of intra-ring wood density by means of imaging VIS/NIR spectroscopy (hyperspectral imaging). Holzforschung 67(1):59-65.

Hai PH (2009) Genetic improvement of plantation-grown *Acacia auriculiformis* for sawn timber production. PhD dissertation, Swedish University of Agricultural Sciences, Uppsala, Sweden.

Hai PH, Hannrup B, Harwood C, Jansson G, Ban DV (2010) Wood stiffness and strength as selection traits for sawn timber in *Acacia auriculiformis* A. Cunn. ex Benth. Can J Res 40(2):322-329.

Hai PH, Jansson G, Harwood C, Hannrup B, Ha TH (2008) Genetic variation in growth, stem straightness and branch thickness in clonal trials of *Acacia auriculiformis* at three contrasting sites in Vietnam. For Ecol Mgmt 255(1):156-167.

Ho TX, Schimleck LR, Sinha A (2021) Utilization of genetic algorithms to optimize *Eucalyptus globulus* pulp yield models based on NIR spectra. Wood Sci Technol 55(3):757-776.

Ho TX, Schimleck LR, Sinha A, Dahlen J (2022) Utilization of genetic algorithms to optimize loblolly pine wood property models based on NIR spectra and SilviScan data. Wood Sci Technol 56:1419-1437.

Jahan MS, Sabina R, Rubaiyat A (2008) Alkaline pulping and bleaching of *Acacia auriculiformis* grown in Bangladesh. Turk J Agric For 32(4):339-347.

Li Y, Via BK, Cheng Q, Zhao J, Li Y (2019) New pretreatment methods for visible–near-infrared calibration modeling of air-dry density of *Ulmus pumila* wood. Forest Prod J 69(3):188-194.

Mora C, Schimleck LR (2010) Kernel regression methods for the prediction of wood properties of *Pinus taeda* using near infrared (NIR) spectroscopy. Wood Sci Technol 44(4):561-578.

Nasir V, Danish Ali S, Mohammadpanah A, Raut S, Nabavi M, Dahlen J, Schimleck L (2023). Fiber quality prediction using NIR spectral data: tree-based ensemble learning vs. deep neural networks. Wood Fib Sci 55(1):100-115.

Nasir V, Nourian S, Zhou Z, Rahimi S, Avramidis S, Cool J (2019) Classification and characterization of thermally modified timber using visible and near-infrared spectroscopy and artificial neural networks: A comparative study on the performance of different NDE methods and ANNs. Wood Sci Technol 53(5): 1093-1109.

Pinyopusarek K, Williams E, Boland D (1991) Geographic-variation in seedling morphology of *Acacia auriculiformis* A. Cunn. ex Benth. Aust J Bot 39(3): 247-260.

Schimleck LR, Tsuchikawa S (2021) Application of NIR spectroscopy to wood and wood derived products (Chapter 37). Pages 759-780 *in* E Ciurczak, B Igne, J Workman, D Burns, eds. The Handbook of Near-Infrared Analysis, Fourth Edition. CRC Press, Boca Raton, FL.

Schwanninger M, Rodrigues JC, Fackler K (2011) A review of band assignments in near infrared spectra of wood and wood components. J Near Infrared Spectrosc 19:287-308.

Snee R (1977) Validation of regression models: Methods and examples. Technometrics 19:415-428.

Tsuchikawa S, Kobori H (2015) A review of recent application of near infrared spectroscopy to wood science and technology. J Wood Sci 61(3):213-220.

Van Duong D, Schimleck LR, Tran DL, Vo HD (2022) Radial and among-clonal variations of stress-wave velocity, wood density, and mechanical properties in 5-year-old *Acacia auriculiformis* clones. BioResources 17(2):2084-2096.

Villar A, Fernandez S, Gorritxategi E, Ciria JI, Fernandez LA (2014) Optimization of the multivariate calibration of a Vis-NIR sensor for the on-line monitoring of marine diesel engine lubricating oil by variable selection methods. Chemom Intell Lab Syst 130:68-75.